Application of finite element methods to the simulation of high temperature superconductors

A thesis accepted by the Faculty of Aerospace Engineering and Geodesy of the University of Stuttgart in partial fulfillment of the requirements for the degree of Doctor of Engineering Sciences (Dr.-Ing.)

by

Dipl.-Ing. Mojtaba Mashmool

born in Mashhad, Iran

main referee:	Prof. Dr.-Ing. Stefanos Fasoulas
co-referee:	Prof. Dr.-Ing. Jörg Wagner
Date of defence:	23.11.2017

Institute of Space Systems (IRS)

University of Stuttgart

2018

Contents

Acknowledgements

I would like to thank Prof. Dr. rer. nat. Hans-Peter Röser, Prof. Dr.-Ing. Stefanos Fasoulas and Prof. Dr.-Ing. Jörg Wagner for the opportunity they presented to me and their continued support and guidance.

My colleagues at the IRS, S. López, M. Stepper and F. Hetfleisch have also my gratitude for the many conversations and insights that helped me move this project along.

I am as well indebted to the Konrad-Adenauer-Stiftung, without whose patronage this work would not have been possible.

To my wife, thank you for encouraging me in all of my pursuits and inspiring me to follow my dreams.

I am especially grateful to my parents and to my brothers and my sisters, who supported me emotionally and financially.

Last but not least, many thanks to my niece; I hope that you always follow your dreams and work hard to achieve them.

Mojtaba Mashmool Stuttgart, 18.01.2018

Figures

Tables

Nomenclature

a	Lattice constants.
a_i	Fraction of an ion belonging to the unit cell.
a_k	Unknown constant.
$a_{\acute{k}}$	Unknown constant.
A	Amplitude of the vibration, potential parameters for an ionic pair.
Al	Aluminium.
Ba	Barium.
Bi	Bismuth.
Bi2212	$Bi_2Sr_2CaCu_2O_{8+\delta}$.
c	Speed of light.
c	Superconducting constant.
C	Potential parameters for an ionic pair.
Ca	Calcium.
C_{ij}	Elastic constants.
Cu	Copper.
C_V	Heat capacity.
d	Lattice constants.
$dr_{cs,i}$	Displacement between the core and the shell in the shell model.
$D(E_f)$	Density of states at Fermi level.
e	Elementary charge.
E	Energy near the Fermi level.
E_f	Fermi energy.
E_v	Energy of a vibration quantum state.
f	Frequency.
F	Coulomb force.
F_i	Coulomb force acting on ion i.
F_t	Impulse of an electron.
GULP	General Utility Lattice Program.
Hg	Mercury.
Hg1223	$HgBa_2Ca_2Cu_3O_{8+\delta}$.
HTSCs	High temperature superconductors.
k	Wave number, force constant.

$\vec{k}$	Wave vector.
k_{100}	Force constant in the [100] direction.
k_{110}	Force constant in the [110] direction.
k_{111}	Force constant in the [111] direction.
k_b	Boltzmann constant.
k_f	Fermi wave number.
k_i	Force constant between different ions in the unit cell.
K_i	Kinetic energy of each ion belonging to the unit cell.
l	Length of the deformation region after an electron fly-though.
La	Lanthanum.
LSCO	$La_{1.85}Sr_{0.15}CuO_4$
m_e	Mass of the electron.
m_{eff}	Electronic effective mass.
m_i	Mass of the i-th ion.
M	Mass of an ion.
n	Integer number of the charge of an ion.
N	Number of ions belonging to the unit cell.
Nb	Niobium.
O	Oxygen.
P_i	Potential energy of each ion belonging to the unit cell.
q_i	Charge of the four components of an ionic pair in the shell model.
q_j	Charge of the four components of an ionic pair in the shell model.
q_{shell}	Charge of the shell of an ion.
r	Distance between ion and moving electron.
r_0	Distance between two electron paths.
r_1	Local positions of two electrons.
r_2	Local positions of two electrons.
r_{eq}	Equilibrium distance between the two ions of an ionic pair.
r_{ij}	Distance between component i and component j.
r_l	Relative coordinate of two electrons.
R	Radius.
R_0	Center of mass of two electrons.
Ru	Ruthenium.

Sr	Strontium.
t	Time during which the Coulomb forces act on the ions.
T	Period of simple harmonic vibration.
T_c	Critical temperature.
v	Number of vibration quantum state, speed of sound.
v_e	Fermi velocity, electron velocity.
v_m	Maximum vibration velocity of an ion.
V	Volume of unit cell, interaction potential energy between two electrons.
V_0	Attractive potential energy.
V_{coul}	Coulomb interaction between atomic shells and cores.
$V_{k\acute{k}}$	Interaction potential energy.
V_{pol}	Potential energy of the spring constant for an ionic pair.
V_{short}	Short-range repulsive interaction.
V_{VW}	Van der Waals interaction.
x	x-coordinate in Cartesian system.
Y	Yttrium.
YBCO	$YBa_2Cu_3O_{7-\delta}$.
Z	Charge of an ion.
∂	Partial derivative.
∇	Laplacian operator.
Δ	Amount of energy below Fermi level or binding energy.
δ	Doping amount, small ionic displacement in y-direction.
ε	Energy above Fermi level.
ε_0	Permittivity of vacuum.
ϵ_0	Static dielectric constant.
ϵ_∞	Dynamic dielectric constant.
$\hbar$	Reduced Planck constant.
μ	Reduced mass between the atoms
ρ	Potential parameters for an ionic pair.
$\Phi(R)$	Plane wave function.
Ψ	Symmetric wave function of two electrons.
ω	Vibration frequency of an ion.
ω_D	Debye frequency.

Abstract

Superconductivity is an important physical phenomenon which has not yet been completely explained. There are two types of superconductors: conventional and unconventional (high temperature superconductors belong to the latter). The temperature at which electrical resistivity vanishes is called the critical temperature (T_c) and it is a characteristic of each superconductor. A physical explanation of superconductivity in the conventional superconductors is given by the BCS theory, with which critical temperatures can be calculated. This theory is based on the Coulomb interaction between Fermi electrons (free electrons) and atoms in the crystal structure of the material. Through this interaction, two electrons can be paired, building a so-called Cooper pair.

In this work, the finite element method has been used to simulate the BCS theory in conventional and unconventional superconductors (Al, Nb: conventional; Sr_2RuO_4, $La_{1.85}Sr_{0.15}CuO_4$, $Bi_2Sr_2CaCu_2O_{8+\delta}$, $HgBa_2Ca_2Cu_3O_{8+\delta}$ and $YBa_2Cu_3O_{7-\delta}$: unconventional). The corresponding Fermi velocity v_e (velocity of a free electron), density of states $D(E_f)$, force constants between atoms in the unit cell, and the symmetry of the unit cell are required for each simulation. The force constants can be measured by Raman spectroscopy or calculated with the potential theory.

With these parameters, the attractive potential energy V_0 caused by an electron moving through the unit cell can be simulated by the finite element method. This process has been carried out for the two conventional superconductors Al and Nb.

According to the BCS theory, the binding energy Δ of a Cooper pair depends on the density of states and the attractive potential energy according to the following equation:

$$\Delta \propto \exp\left(\frac{-2}{D(E_f)V_0}\right) .$$

Then, the critical temperature T_c can be found with the following equation where k_b is Boltzmann constant:

$$T_c = \frac{2\Delta}{3.53k_b} .$$

The results show that the Fermi velocity and the density of states play an important role regarding superconductivity. The lower the Fermi velocity v_e, the higher the attractive potential

energy V_0 and the lower the density of states $D(E_f)$. According to the first equation, this means that a reduction of the Fermi velocity yields an increase of the binding energy through increasing the attractive potential energy V_0. On the other hand, a reduction in the Fermi velocity yields to a reduction in the binding energy through reducing density of states. Because of these two dependencies, an optimal Fermi velocity must be found for which the binding energy reaches its maximum. Accordingly, and using the second equation, a maximum value is found for the critical temperature T_c.

For conventional superconductors the Fermi velocity can be approximated as a constant. Therefore, according to the two equations above, only a critical temperature can be calculated for these superconductors. For high temperature superconductor cuprates (which belong to the unconventional superconductors and are doped with different concentrations of foreign atoms or oxygen vacancies), the Fermi velocity changes linearly with the doping amount δ. Thus, different critical temperatures exist for different doping amounts.

The phase diagrams of high temperature superconductors (T_c vs. doping amount δ) show a dome with a maximum critical temperature at an optimal doping. Because the Fermi velocity depends linearly on the doping amount δ, the latter can be replaced in the phase diagram by the Fermi velocity and so an optimal Fermi velocity can be used instead of an optimal doping.

A linear relationship of $2\Delta = 2.865T_c$ for some unconventional and conventional superconductors has also been found in this work, which is in good agreement with the experimentally determined linear relationship of C. Panagopoulos and T. Xiang ($2\Delta = 2.214T_c$).

Kurzfassung

Die Supraleitung ist eins der wichtigen physikalischen Phänomene, die bis jetzt nicht vollständig physikalisch aufgeklärt wurden. Es gibt zwei Arten von Supraleitern: konventionelle und unkonventionelle Supraleiter (Hochtemperatursupraleiter gehören zu der letzteren Art). Die Temperatur, bei der der elektrische Widerstand verschwindet, wird kritische Temperatur (T_c) genannt und ist eine charakteristische Größe von jedem Supraleiter. Die Supraleitung in den konventionellen Supraleitern kann durch die BCS-Theorie beschrieben werden. Mit Hilfe dieser Theorie kann die kritische Temperatur berechnet werden. Diese Theorie basiert auf der Coulomb-Wechselwirkung zwischen Fermi Elektronen und Atomen in der Kristallstruktur von Supraleitern. Durch diese Wechselwirkung werden zwei Elektronen miteinander gepaart; somit bilden diese ein sogenanntes Cooper-Paar. Bis jetzt wurde keine etablierte Theorie entwickelt, mit der die Supraleitung in Hochtemperatursupraleitern (HTSCs) entsprechend beschrieben werden kann.

In dieser Arbeit wurde die finite Elemente Methode zur Simulation der BCS-Theorie in konventionellen und unkonventionellen Supraleitern (Al, Nb: konventionell; Sr_2RuO_4, $La_{1.85}Sr_{0.15}CuO_4$, $Bi_2Sr_2CaCu_2O_{8+\delta}$, $HgBa_2Ca_2Cu_3O_{8+\delta}$ und $YBa_2Cu_3O_{7-\delta}$: unkonventionell) verwendet. Dafür wird die Fermi-Geschwindigkeit v_e (Geschwindigkeit eines freien Elektrons), die Zustandsdichte $D(E_f)$, die Kraftkonstanten zwischen Atomen in der Elementarzelle und die Symmetrie der Elementarzelle benötigt. Die Kraftkonstanten können entweder durch Ramanspektroskopie gemessen oder durch die Potentialtheorie berechnet werden. Mit diesen Parametern kann die attraktive potentielle Energie V_0, die durch ein bewegliches Elektron in der Elementarzelle verursacht wird, durch die finite Elemente Methode simuliert werden. Dieses Verfahren wurde anhand der zwei konventionellen Supraleiter Al und Nb validiert.

Die Bindungsenergie Δ eines Cooper-Paars ist abhängig von der Zustandsdichte und der attraktiven potentiellen Energie. Diese Abhängigkeit wird durch folgende Gleichung beschrieben:

$$\Delta \propto \exp\left(\frac{-2}{D(E_f)V_0}\right) .$$

Danach kann die kritische Temperatur T_c durch folgende Gleichung berechnet werden, wobei k_b die Boltzmann-Konstante ist:

$$T_c = \frac{2\Delta}{3.53k_b} .$$

Die Ergebnisse zeigen, dass die Fermi-Geschwindigkeit und die Zustandsdichte eine sehr wichtige Rolle bezüglich der Supraleitung spielen. Einerseits, je kleiner die Fermi-Geschwindigkeit ist, desto größer ist die attraktive potentielle Energie. Andererseits reduziert sich die Zustandsdichte mit der Abnahme der Fermi-Geschwindigkeit. Aufgrund dieser zwei Abhängigkeiten muss eine optimale Fermi-Geschwindigkeit existieren, bei der die Bindungsenergie maximal ist. Mit dieser maximalen Bindungsenergie und der zweiten Gleichung kann die maximale kritische Temperatur berechnet werden.

Für die konventionellen Supraleiter ist die Fermi-Geschwindigkeit ungefähr konstant. Deshalb kann nur eine kritische Temperatur durch die zwei obigen Gleichungen ermittelt werden. Für Hochtemperatursupraleiter-Kuprate, die zu den unkonventionellen Supraleitern gehören, ändert sich die Fermi-Geschwindigkeit linear mit dem Dotierungsanteil, da diese Supraleiter mit unterschiedlichen Anteilen von fremden Atomen bzw. Sauerstoffleerstellen dotiert werden. Es gibt daher verschiedene kritische Temperaturen für die unterschiedliche Dotierungsanteile δ.

Die Phasendiagrame von Hochtemperatursupraleitern (T_c vs. Dotierungsanteil δ) weisen eine Glockenkurve auf, mit einem Maximum für die kritische Temperatur bei einem optimalen Dotierungsanteil. Es ist physikalisch bekannt dass die Fermi-Geschwindigkeit vom Dotierungsanteil δ abhängt. Aufgrund dieser Abhängigkeit kann der Dotierungsanteil im Phasendiagram mit der Fermi-Geschwindigkeit ersetzt werden. Daher wird eine optimale Fermi-Geschwindigkeit statt des optimalen Dotierungsanteils verwendet.

Eine lineare Beziehung von $2\Delta = 2.865T_c$ für einige unkonventionelle und konventionelle Supraleiter wurde in dieser Arbeit gefunden, die nahe an der experimentell bestimmten linearen Beziehung von C. Panagopoulos und T. Xiang ($2\Delta = 2.214T_c$) liegt.

1 Introduction

Superconductivity is a very important phenomenon in Physics due to the special electrical and magnetic properties associated with it. In 1911, the Dutch physicist Heike Kamerlingh Onnes discovered superconductivity in mercury while measuring its electrical resistance at low temperatures. Superconductivity appears in some materials below a certain temperature called the critical temperature T_c; in this regime, the electrical resistivity disappears and external magnetic fields are expelled from the bulk of the superconducting material (Meissner-Ochsenfeld effect).

In conventional superconductors, superconductivity can be explained by the BCS theory which relies on a pairing of electrons into so-called Cooper pairs. With the discovery of superconductivity in doped La_2CuO_4, another group of superconductors has been found, called unconventional superconductors. The application of the BCS theory to unconventional superconductors has been investigated by some researchers. Many researchers believe that a second mechanism must be available for the electron pairing in these superconductors.

In particle physics, a fermion is a particle with half-integer spin (1/2, 3/2 and so forth) and a boson one with integer spin (0, 1, 2 and so forth). Electrons are fermions due to their half-integer spin (1/2 or -1/2). By considering the direction of an electron spin, paired electrons can have a total spin of 0 or 1 and, therefore, they are a boson. The momentum of a Cooper pair is equal to zero, because the momenta of its constituting electrons have the same magnitude but opposite directions.

In the BCS theory, two electrons can be paired through the lattice deformation caused by Coulomb forces between moving electrons and the atoms in the lattice. In this work, the energy of this deformation is designated as the attractive potential energy V_0.

For the calculation of the electronic band structure of materials only electrons (fermions) are considered. When electron pairing occurs, an energy gap, called the superconducting gap, can be found in the electronic band structure of superconductors, because the electron pairs are bosons and are not used for the calculation of the electronic band structure.

There are different experimental and theoretical ways to determine the superconducting gap. Using scanning tunneling microscope (STM), the width 2Δ (Δ: binding energy) of the superconducting gap can be measured. Through the BCS theory, this width can be mathematically found using the attractive potential energy V_0, the density of states $D(E_f)$ and the Debye frequency ω_D of the material. The calculation of the superconducting gap width is complicated for superconductors with complex unit cells due to the difficulty involved in the calculation of their attractive potential energies. Finite element methods can be used to calculate

this energy for superconductors with complex unit cells. The influence of the electrical properties on the width of the superconducting gap can be investigated by these methods.

1.1 Motivation

At the Institute of Space Systems of the University of Stuttgart a lot of theoretical work for superconductors has been performed. The main subject of research concerns the development of a correlation between the critical temperature and some physical properties for unconventional superconductors. In 2007, Prof. Hans-Peter-Röser proposed a correlation between critical temperature and doping distance in high temperature superconductors (HTSCs). He assumed that the doping atoms or vacancies are distributed evenly in the crystal structure of superconductors. With this assumption the distance between the doping atoms can be mathematically determined. It has also been found that for A_3C_{60} fullerides superconductors, the ionization energy is linearly correlated with critical temperature.

The application of the BCS theory to explain the superconductivity in HTSCs has been performed by some researchers. Until now, there are no direct mathematical calculations of attractive potential energy V_0 for HTSCs due to their complex unit cells. The finite element method (FEM) could provide a good methodology to calculate this energy. This method is used in different engineering and scientific fields. Complex resonance problems of classical mechanical structures can be solved using this method. Another important application lies in solving the Schrödinger equation in quantum mechanics [1]: the time independent Schrödinger equation can be numerically solved by FEM using an explicit method, and the time-dependent Schrödinger equation can be discretized and also numerically solved [2]. This method is applied to quantum mechanical problems for superconductivity as well. Qiang Du has used a finite element code to solve the time-dependent Ginzburg-Landau equations of superconductivity. The code is based on the fully discrete backward Euler scheme of a two-dimensional square box [3].

The attractive potential energy caused by a moving Fermi electron through a two-dimensional single atomic unit cell can be calculated by analytical methods. But for the three-dimensional unit cell of superconductors this method cannot be used since the unit cell consists of different ions and force constants in different space directions. Using a finite element code, the value of this energy can be found and used to calculate the binding energy Δ according to the BCS theory.

If the symmetry of the unit cell, force constants in the unit cell, Fermi velocity, density of states and Debye frequency of a superconductor were available, this code would help to determine the binding energy without any experiment performed by scanning tunneling microscopy. The code is able to determine which physical property has the major influence on superconductivity. There are superconductors that have different Fermi electrons and, therefore, different Fermi velocities. Using this code, it can be determined at which Fermi velocity the binding energy reaches its maximum value.

High temperature superconductors that belong to the unconventional superconductors, are usually doped with oxygen vacancies or foreign atoms. The amount of doping is very important because only at a certain level (called the optimal doping amount) the critical temperature and the binding energy reach their maximum values.

The Fermi velocity depends directly on the doping amount. Due to this dependence, the trend of the binding energy against the doping amount can be determined by performing a parameter study for the Fermi velocity. Furthermore, the optimal doping amount can be determined from the Fermi velocity at which the binding energy is maximal.

1.2 Objective

The attractive potential energy of some conventional and unconventional superconductors must be calculated. First of all, a two-dimensional model must be considered for the analytical calculation. The calculated attractive potential energy must be used to determine the binding energy Δ according to the BCS theory. The diagram $\log \Delta$ vs. $\log T_c$ for the analytical results must be determined.

In order to obtain more accurate results, a special finite element code has to be prepared and implemented. Using this code, the attractive potential energy for the three-dimensional unit cell of the considered superconductors can be simulated and the corresponding binding energy Δ determined. At first, the code must be evaluated for the conventional superconductors, because it has been proven that the BCS theory is valid for these. The diagram 2Δ vs. T_c must be drawn and a line has to be fit to the results. The function of the line has to be compared with the experimentally determined function in [4].

As it is known from BCS theory, the value of the binding energy depends on the attractive potential energy, the density of states and the Debye frequency. The Fermi velocity is also one of the important parameters which indirectly influences the value of the binding energy through

the attractive potential energy. The influence of these parameters on the binding energy must be investigated in this work.

It must be determined for superconductors with different Fermi electrons at which Fermi velocity the maximum value of the binding energy appears. There are two binding energies for some superconductors; the appearance of two binding energies must be investigated by the code.

The unit cell must be constructed. To perform this, the mass of the ions, the force constants between the ions within the unit cell and the symmetry of the unit cell are required. The force constants can be calculated by the potential theory, or determined using Raman spectroscopy through the eigenfrequencies of ionic pairs within the unit cell. The time-dependent Coulomb forces between the ions in the unit cell and the moving Fermi electron can be calculated by means of the Fermi velocity. By having all these parameters and available values, the finite element code can be applied to calculate the attractive potential energy and the corresponding binding energy.

Here follows a brief explanation of the contents of this work. In chapter 2, the theory of superconductivity is explained; calculations of the binding energy and the critical temperature of superconductors are introduced; and two ways are discussed to determine the force constants between ions inside a unit cell. Chapter 3 explores the theory of the finite element method and the finite element model used in this work. Three different codes are prepared for the simulation described in chapter 4. The analytical method and results for the calculation of the attractive potential energy of some superconductors are discussed in chapter 5, which justify the motivation of this work for using finite element methods. The finite element results are discussed for the same superconductors in chapter 6. Finally, Chapter 7 gives a summary of the results obtained.

2 Theory

2.1 Fundementals of Electron Theory

2.1.1 Electron Model

There are different models to describe the electron properties in an atom. In 1911, Rutherford proposed a model in which electrons orbit a core consisting entirely of neutrons and protons (figure 1). But according to classical mechanics and electromagnetic theory, if a charged particle (as is, for instance, an electron) moves on a curved path, it emits electromagnetic radiation. Therefore, the electron loses its energy and after some revolutions it falls into the core. Hence, this model is unstable. To remedy this instability, Bohr proposed a model in 1913 according to which the electron moves in orbits with fixed radius and energy (figure 2). The energy of the electron depends directly on the radius of its orbit. The smaller the radius, the lower the energy. Radiation is only possible if the electron changes its orbit by jumping into another orbit.

The Bohr model is not a final model with which the electron properties in an atom can be described. This model cannot explain the wave nature of the electron. Another limitation is that it predicts a definite momentum of an electron moving on an orbit with a definite radius, which is not possible according to the uncertainty principle. Due to the uncertainty principle, the position and momentum of a particle cannot be simultaneously determined.

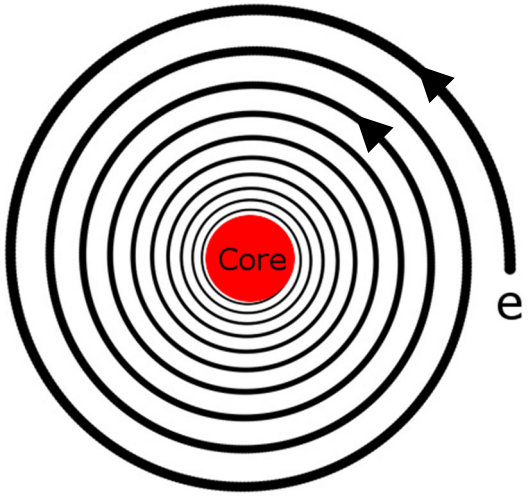

Figure 1: Rutherford model.

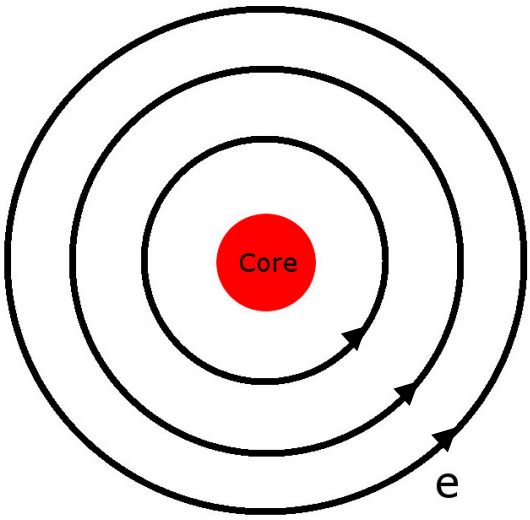

Figure 2: Bohr model.

2.1.2 Wave-Particle Duality

In the Bohr and Rutherford models, the electron is considered as a particle. But none of them can explain the wave nature of the electron as evidenced by the double slit experiment. The double slit experiment can be used to prove the wave behaviour of light. In this experiment, the light waves passing through two parallel slits on a screen interfere with each other, producing a light and dark pattern on the wall behind the slits (figure 3). In 1928 Davisson and Germer used this method for an electron beam directed at a crystal. The gaps between the atoms in the crystal act like the slits on the screen. They found a light and dark pattern on the other side of the crystal as well. This can only be explained by the wave behaviour of the electron.

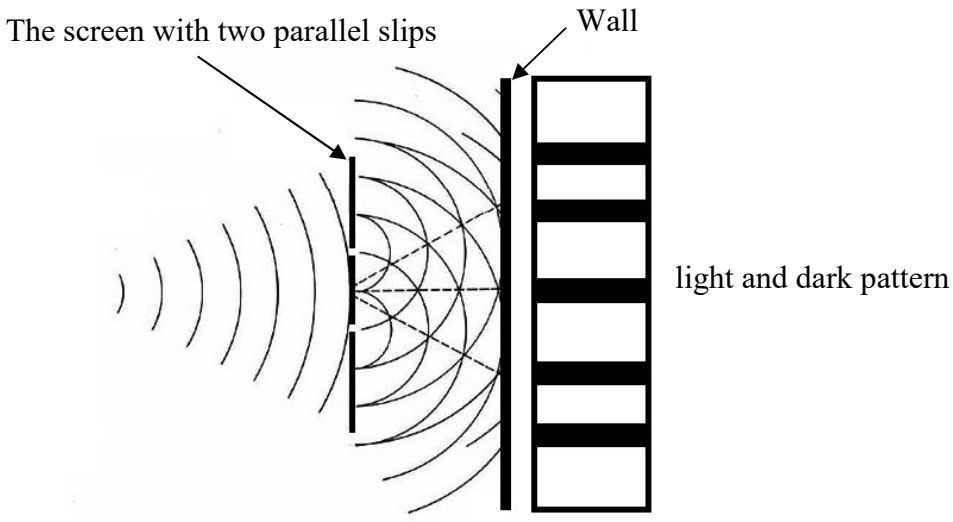

Figure 3: The double slit experiment.

In 1928, de Broglie proposed that all matter can exhibit wave-like behaviour. According to the de Broglie theory, the wavelength λ of an object can be calculated by

$$\lambda = -\frac{h}{\mathrm{mv}} \ , \tag{2.1}$$

where m is the mass, v the velocity of the object and h the Planck constant. For objects of everyday experiences the calculated wavelength according to equation 2.1 is much smaller than that of atomic particles, so their wave properties have never been detected; these objects exhibit only particle behaviour. It is only for the subatomic scale that the wave-like behavior of a particle must be considered. Having the mass and the velocity of an electron, its wavelength can be calculated using the equation above.

To describe the wave property of subatomic particles in quantum mechanics, the Schrödinger equation is required. This equation describes how the quantum state of a physical system changes in time.

2.1.3 Schrödinger Equation

In 1926, Erwin Schrödinger derived a partial differential equation with which the quantum mechanical behaviour of a system can be described. The Schrödinger equation has two forms, one of them is time-dependent and the other one is time-independent [5].

The time-independent Schrödinger equation is used to describe the properties of atomic systems in stationary conditions (stationary condition means that the properties of the system do not change with time), which is the case for most applications. The time-independent Schrödinger equation for an electron can be written as follows [5]:

$$-\frac{\hbar^2}{2\mathrm{m_e}}\nabla^2\Psi - (\mathrm{E}-\mathrm{V})\Psi = 0 \ , \tag{2.2}$$

where $\mathrm{m_e}$ is the mass of the electron, $\hbar$ the reduced Planck constant, ∇^2 the Laplacian (a differential operator $\nabla^2 = \frac{\partial^2}{\partial \mathrm{x}^2} + \frac{\partial^2}{\partial \mathrm{y}^2} + \frac{\partial^2}{\partial \mathrm{z}^2}$), Ψ the wave function, E the energy of the electron and V the potential barrier. Assuming that the potential barrier V depends only on space, the time-independent Schrödinger equation is an equation for a vibration. Therefore, the wave function Ψ is a function of space and can be rewritten as [5]:

$$\Psi = \Psi(\mathrm{x},\mathrm{y},\mathrm{z}) \ . \tag{2.3}$$

The solution of the time-dependent Schrödinger equation is a wave function due to its dependence on time and space ($\Psi(x, y, z, t)$). The following equation is the time-dependent Schrödinger equation with $i = \sqrt{-1}$ [5]:

$$-\frac{\hbar^2}{2m_e}\nabla^2\Psi - i\frac{\partial\Psi}{\partial t} + V\Psi = 0 \ . \qquad (2.4)$$

2.2 Superconductors

For superconducting materials, there is a critical temperature T_c below which the electrical resistance disappears. In a broad sense, these materials can be classified in two groups: conventional and unconventional superconductors. The first can be described by the BCS theory, which is based on bound pairs of electrons (Cooper pairs) that carry the electrical current below the critical temperature and cannot be scattered by the atoms in the crystal structure. For the second, which includes the high temperature superconductors (HTSCs), there is so far no generally accepted mathematical and physical description. The maximum critical temperature belongs to the high temperature superconductor $HgBa_2Ca_2Cu_3O_{8+\delta}$ with 134 K (in the case of a chemical formula, δ represents the doping amount).

HTSCs comprise different material families, the main ones being cuprates (copper-oxygen compounds) and iron pnictides. Depending on their chemical formula, all cuprates possess at least one CuO_2 plane (figure 4). To obtain the superconducting phase for cuprates, they must be doped either with foreign atoms or oxygen vacancies. The doped carriers are located in the CuO_2 plane.

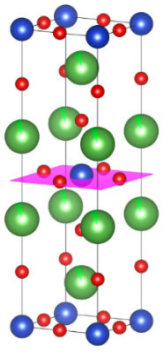

Figure 4: The unit cell of the high temperature superconductor $La_{1.85}Sr_{0.15}CuO_4$. It consists of two chemical formulas. The red atoms are oxygen, the blue copper and the green lanthanum. The pink plane represents a CuO_2 plane.

2.3 Cooper Pair

Due to the change in the electrical conductivity and the magnetic properties after the appearance of superconductivity, one can guess that the superconducting property can be described by ordering processes of the conductive electrons. The energy of a conductive electron is, however, of the order of some eV (one eV corresponds to a thermal energy of 1100 K). The transition from the normal state to superconducting state takes place at very low temperatures [6].

There are different interactions between the conductive electrons in metals. The Coulomb interaction could be a reason for the three-dimensional order of electrons in the crystal lattice. Another interaction could be the magnetic field built by the motion of the electrons with energies near the Fermi level. These interactions alone are not sufficient to explain the superconductivity phenomenon, until the formulation of a new interaction between the electrons through the lattice deformation. Using this interaction, Bardeen, Cooper and Schrieffer were able to propose a microscopic theory: the BCS theory of superconductivity [6].

To understand this interaction one can imagine an elastic membrane with a ball on each of its two corers (figure 5). The membrane represents the ion lattice of the superconductor, and the balls, its conduction electrons. Due to the weight of the balls, the membrane is deformed (figure 5 (a)). To reduce the total energy (reducing the potential energy) of the complete system, both balls tend to move towards each other until they get together in the middle of the membrane (figure 5 (b) and (c)). In this case, the elasticity deformation of the membrane represents the attraction interaction between both balls, which results in a new state for both balls and bonds them together in the middle of the membrane (figure 5 (c)) [6].

In the case of a crystal structure, the lattice with all ions has a certain elasticity that can be described by springs between ions in the lattice. The ions are not stiffly bound to their sites in the lattice but they vibrate around their equilibrium positions. The average vibration amplitude and frequency vary according to the temperature.

The electrons deform the lattice due to the Coulomb interaction with ions and create a deformation area around each of ions (figure 6 (a)) The deformation due to an electron can be felt by another electron giving rise to a net attractive interaction between the two. Both electrons tend to pair to reduce the total energy of the system despite the repulsive Coulomb interaction between them, just as the balls do on the elastic membrane. In other words, an electron moving through the lattice leaves a polarization wake behind itself (figure 6 (b)). This polarization wake can be spread out over the entire lattice in the form of a so-called phonon wave and can interact with a second electron, effectively creating an attractive interaction between both electrons. This is called electron pairing through the electron-phonon interaction [6].

(a) (b) (c)

Figure 5: (a) a ball on an elastic membrane, (b) the unstable situation for two balls moving towards each other on the elastic membrane and (c) the stable situation for the two balls on the elastic membrane.

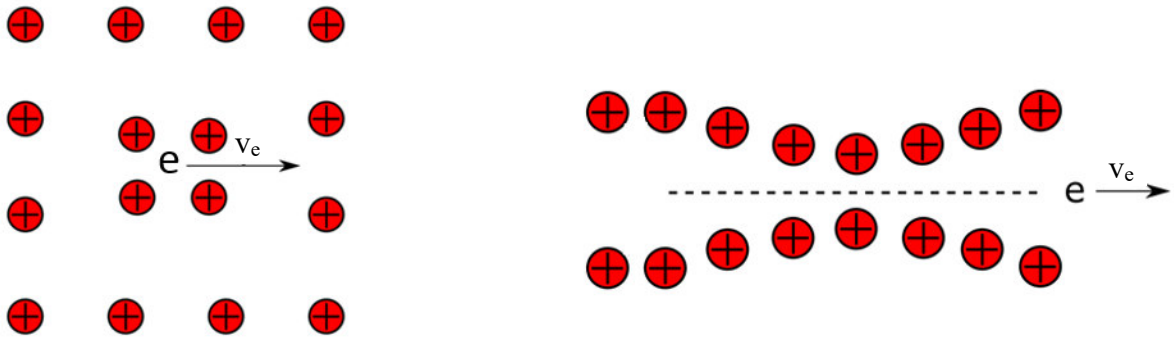

(a) (b)

Figure 6: (a) deformation of the lattice due to Coulomb forces between an electron and the ions and (b) polarization wake behind an electron with Fermi velocity v_e.

The polarization strength depends on the velocity of the electron, the mass of the ions and the force constants between ions. For example, in the case of different isotopes (isotopes are variants of a chemical element with different neutron number), the heavier the isotope, the smaller the polarization strength and also the attractive interaction for the electron pairing [6]. Regarding momentum, there are two possibilities for electron pairing. The first is that the absolute value of the momentum and the propagation direction of both electrons are the same, $\vec{p}_1 = \vec{p}_2 = \hbar\vec{k}$ ($\vec{k}$ is the wave vector of an electron). The second is that the absolute value is the same but the propagation direction is inverted, $\vec{p}_1 = \hbar\vec{k}$ and $\vec{p}_2 = -\hbar\vec{k}$. The total momentum of the pair in this second case is equal to zero. The pair with zero total momentum is called a Cooper-pair, since Cooper was the first who proved that this mechanism leads to a reduction of the total energy of the system [6].

2.3.1 Normal Conductivity

In quantum mechanics, the density of states is the number of states per energy interval for a certain energy. Due to Pauli's principle each state can normally be occupied with only two electrons, one spin up and the other spin down. The electrical conductivity in metals can be explained by free electrons in the conductive band. In figure 7, the dependence of the density of states on the energy within a partially occupied conductive band for a metal can be seen. According to quantum mechanics, the electrical conductivity is caused by the electrons with energies close to the Fermi level (Fermi level is the level with energy E_f), because these electrons are the first to fill the unoccupied energy states when enough voltage is applied (figure 7). These electron are called Fermi electrons. If voltage is applied on a metal, electrons will be accelerated and scattered by the lattice atoms or among themselves and, therefore, electrical resistance will appear. The electrical resistance R can be calculated by Ohm's law (equation 2.5), where V is the voltage and I the electrical current.

$$R = \frac{V}{I} \ . \tag{2.5}$$

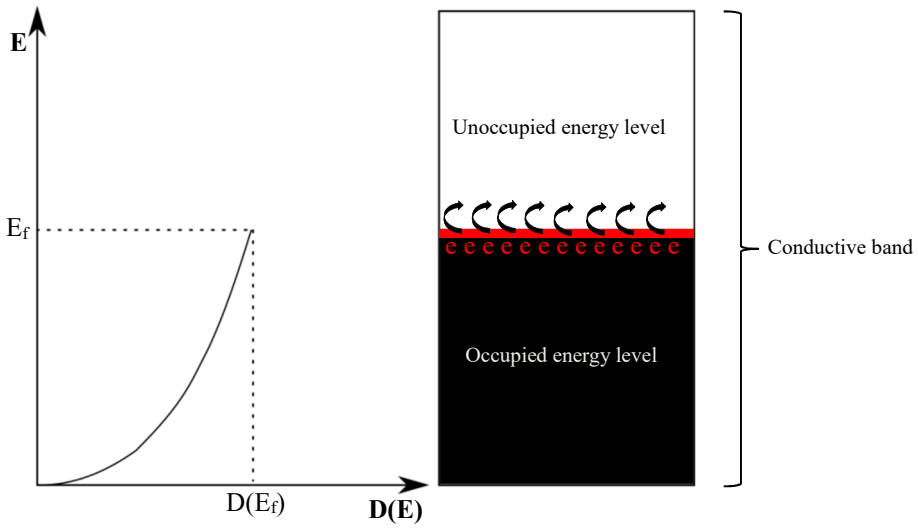

Figure 7: Energy E vs. density of states D(E) within a partially filled conduction band of a metal. E_f is the Fermi energy, $D(E_f)$ is the density of states at the Fermi energy and e are the Fermi electrons. ↻ shows Fermi electron jumps into unoccupied energy level.

2.3.2 Superconductivity

The formation of Cooper pairs occurs, according to the BCS theory, at a very low temperature (called the critical temperature T_c). The binding energy Δ of a Cooper pair is very small (meV). Therefore, if the temperature is higher than the critical temperature ($T > T_c$), the thermal fluctuations will be enough to break the Cooper pairs and so superconductivity disappears.
For bosons (particles with integer spin) Pauli's principle doesn't apply, therefore, the same energy state can be occupied by any number of bosons. Because the spin of the Cooper pair for the conventional superconductors is an integer number (the spin of an electron is 1/2 and the other one is -1/2 and, therefore, the total spin of a Cooper pair is zero which is an integer number), a Cooper pair is considered a boson. Therefore, a large number of Cooper pairs can occupy the same energy state at the same time and so a collective state can be built.
In superconductors, the electrical current is carried by Cooper pairs below the critical temperature. According to quantum mechanics, scattering of a particle by the lattice atoms induces a change in its energy state. Due to the fact that all Cooper pairs build a collective and occupy the same state, it is not energetically favorable to scatter all of them at once. The electrical resistance is then zero as long as the temperature is lower than the critical temperature.

2.3.3 Mathematical Description of Cooper Pairing

To calculate the deformation of the lattice due to the motion of a Fermi electron, a lattice structure with a simple cubic unit cell has been considered. This lattice structure can be built from two-dimensional planes of positive ions (figure 8) [7]. If a Fermi electron passes through this two-dimensional lattice, the Coulomb interaction between the electron and the positive ions causes the ions to be attracted to the electron. This attraction moves the positive ions closer to each other in some areas and so a local deformation of the lattice appears (figure 9). Equation 2.6 gives the Coulomb force between a positive ion and a Fermi electron [7]:

$$F(r) = -\frac{ne^2}{4\pi\varepsilon_0 r^2} \quad , \tag{2.6}$$

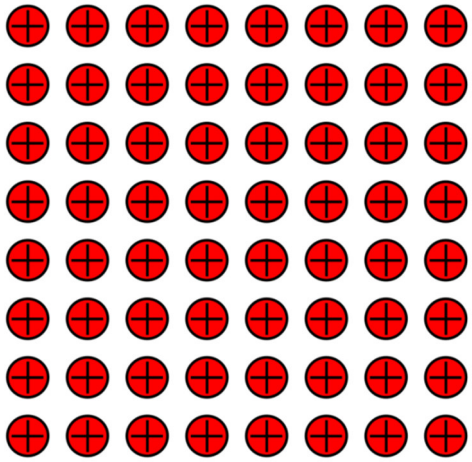

Figure 8: Two-dimensional lattice structure of the positive ions.

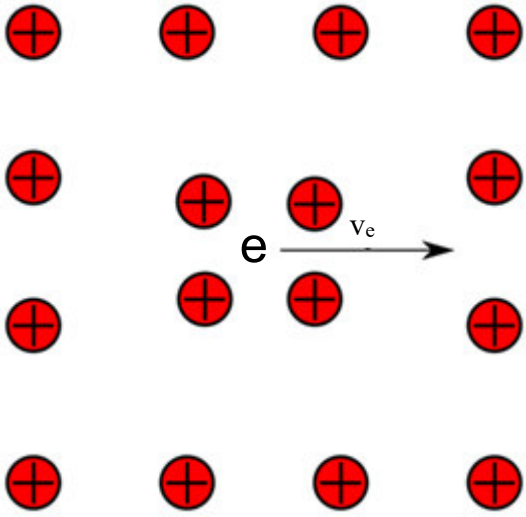

Figure 9: The deformation of the lattice due to the Coulomb interaction between the Fermi electron and positive ions.

where e is the elementary charge, n is an integer number for the charge of an ion, ε_0 is the permittivity in vacuum, r is the distance between the electron and the nearest ion and the minus sign is to indicate that the force is attractive. It is assumed that the Coulomb force is just active over a distance equal to the lattice constant d. For paths with lengths larger than d, the Coulomb force is very small because of its inverse square dependence on the distance r. Because the velocity of the Fermi electron is very high, the time during which the Coulomb forces act on the positive ions is very small. Therefore, the displacement of an ion δ in the y direction (figure 10) is very small relative to the lattice constant d ($\delta = 10^{-3}$-10^{-2} Å and d = 1-5 Å). Due to the small displacement δ, the distance r between the ion and the Fermi electron can be approximated by equation 2.7 (figure 10) [7]:

$$r = \sqrt{\left(\frac{d}{2} - \delta\right)^2 + \left(\frac{d}{2} - x\right)^2} \quad \overset{d>>\delta}{\Longrightarrow} \quad r \approx \sqrt{\left(\frac{d}{2}\right)^2 + \left(\frac{d}{2} - x\right)^2} \ . \tag{2.7}$$

Here, d is the lattice constant, δ is the small displacement of the ion in the y direction, and x is the coordinate of the Fermi electron relative to the middle of the neighbour cell (figure 10). The change in the attractive potential energy of an ion ∂V_0 caused by the movement of a Fermi electron through the lattice can be approximated using the Coulomb potential energy as follows [7]:

$$U = -\frac{ne^2}{4\pi\varepsilon_0 r} \ , \tag{2.8}$$

$$\partial V_0 = \frac{dU}{dr}\partial r \ . \tag{2.9}$$

The Coulomb force in the x direction before the electron surpasses the ion is compensated by the same force afterwards. Because of this, and using the small change approximation, the displacement ∂r can be approximated by the displacement in the y direction $\partial r_y = \delta$ [7]. Here both displaced ions (upper and lower in figure 10) are considered. By setting $\partial r = y$ and the derivative of equation 2.8 in equation 2.9, the attractive potential energy of an ion V_0 can be found [7]:

$$V_0 = \frac{ne^2}{2\pi\varepsilon_0 r^2}\delta \ , \tag{2.10}$$

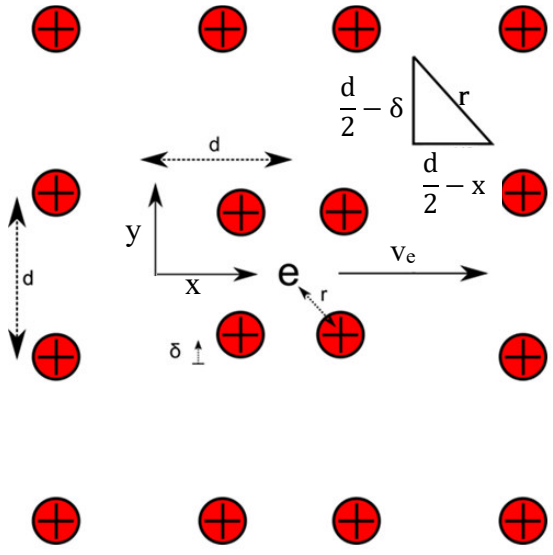

Figure 10: The lattice distortion due to the movement of a Fermi electron.

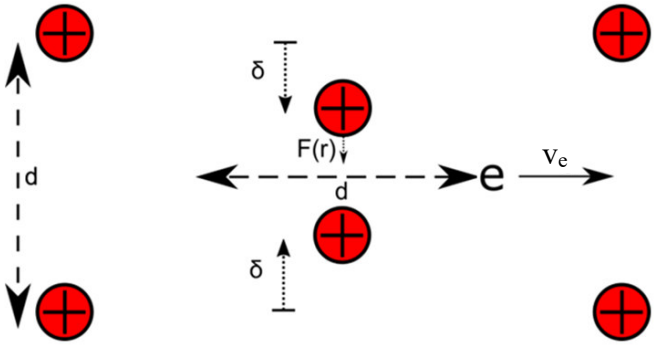

Figure 11: Fermi electron path of length d for calculations.

The displacement δ must then be calculated in order to find the value of the attractive potential energy V_0. The acting time of the Coulomb forces on the ions when the Fermi electron moves over a distance d (figure 11) can be calculated approximately by equation 2.11 where v_e is the Fermi velocity [7]. The Fermi velocity can be obtained from the Fermi energy E_f and the electron mass m_e (equation 2.12). The Coulomb force itself is given by equation 2.6.

$$t = \frac{d}{v_e}\,, \tag{2.11}$$

$$v_e = \sqrt{2\frac{E_f}{m_e}}\,. \tag{2.12}$$

The momentum can be calculated by integrating the Coulomb force with respect to time (equation 2.13). By plugging equation 2.7 into equation 2.6 and replacing x by $v_e t$, the time-dependent Coulomb force can be found by equation 2.14. By integrating the Coulomb force with respect to time, equation 2.15 is obtained, which gives the momentum transferred to the ion [7].

$$p(t) = -\int_0^t F(r)dt = \int_0^t \frac{ne^2}{4\pi\varepsilon_0 r^2}dt\,, \tag{2.13}$$

$$F(r) = -\frac{ne^2}{4\pi\varepsilon_0\left(\left(\frac{d}{2}\right)^2 + \left(\frac{d}{2} - v_e t\right)^2\right)}\,, \tag{2.14}$$

$$p = -\frac{ne^2}{8\pi\varepsilon_0 d}\frac{\pi}{v_e}\,. \tag{2.15}$$

The vibration of the ions after the electron passes is approximated as simple harmonic due to their small displacements. For a simple harmonic vibration the maximum velocity of an ion is reached at half of its vibration period $T/2$. This can be calculated by the following equation [7]:

$$v_m = A\omega = \delta\omega \ , \tag{2.16}$$

where A is the amplitude of the vibration (corresponding to the small displacement δ) and ω is its frequency. Furthermore, the maximum vibration velocity can also be found from the momentum p, dividing by the ionic mass M [7]:

$$v_m = \frac{p}{M} \ . \tag{2.17}$$

For a unit cell consisting of different ions, there are different frequencies. The frequency for the ion i in the unit cell can be determined from the force constant belonging to the ion k_i and the mass of the ion m_i (equation 2.18). The required frequency for a single atomic crystal structure is the Debye frequency $\omega = \omega_D$, which can be calculated by equation 2.19 [7]:

$$\omega_i = \sqrt{\frac{k_i}{m_i}} \ , \tag{2.18}$$

$$\omega_D = \left(\frac{6N\,\pi^2 {v_s}^3}{V}\right)^{1/3} \ . \tag{2.19}$$

Here, N is the number of ions belonging to the unit cell, v_s is the speed of sound and V is the volume of the unit cell. By equating equations 2.17 and 2.16, the displacement δ can be derived [7] as follows:

$$\delta = \frac{p}{M\,\omega} \ . \tag{2.20}$$

Setting equation 2.15 for the momentum and the Debye frequency of the single atomic structure into equation 2.20, the following equation for the displacement δ can be determined:

$$\delta = -\frac{ne^2}{8\pi\varepsilon_0 d}\frac{\pi}{v_e}\frac{1}{M}\frac{1}{\omega_D} \ . \tag{2.21}$$

By plugging equation 2.21 of the displacement into equation 2.10, the attractive potential energy V_0 can be found [7]:

$$V_0 = \frac{ne^2}{2\pi\varepsilon_0 d^2}\left(-\frac{ne^2}{8\pi\varepsilon_0 d}\frac{\pi}{v_e}\frac{1}{M}\frac{1}{\omega_D}\right) . \tag{2.22}$$

The ions will go back through their starting position after a time equal to half the period of the simple harmonic vibration [7]:

$$T = \frac{1}{2}\frac{2\pi}{\omega_D} = \frac{\pi}{\omega_D} . \tag{2.23}$$

During this time the Fermi electron covers a distance l given by

$$l = v_e T = \frac{v_e \pi}{\omega_D} , \tag{2.24}$$

which is assumed to be roughly the length of the deformation trail that the electron leaves in its wake (figure 12) [7]. This deformation region can attract another Fermi electron moving in the opposite direction to the first one if the distance r_0 between the paths of the two electrons satisfies the condition $r_0 < l$ (figure 13) [7]. Therefore, the attractive potential energy of two paired electrons is then defined by the following equation, where r_0 is the distance between both electrons [7]:

$$V(r) = \begin{cases} -V_0 & r_0 < l \\ 0 & r_0 > l \end{cases} . \tag{2.25}$$

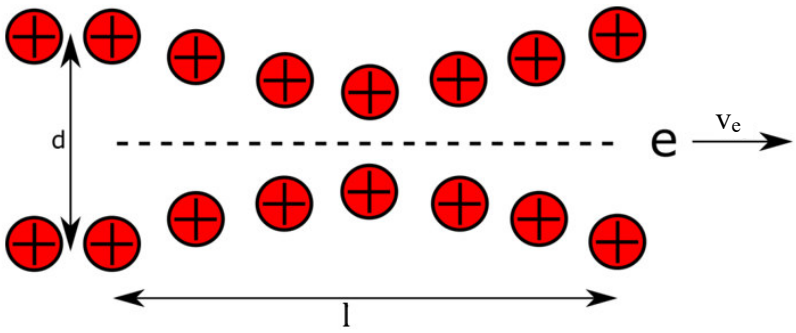

Figure 12: The length l of the polarization region in the electron's wake.

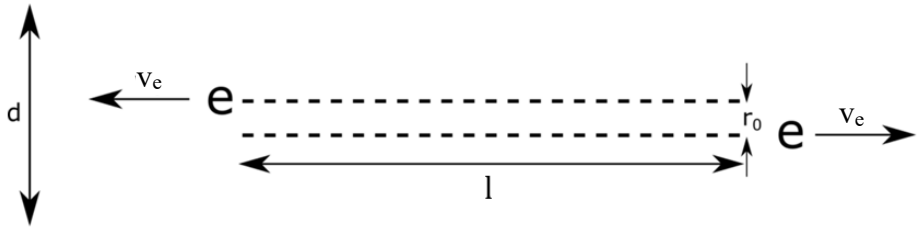

Figure 13: The attraction of the second Fermi electron due to the lattice deformation caused by the first Fermi electron.

2.3.4 Schrödinger Equation for an Electron Pair

To describe the quantum mechanical phenomenon of electron pairing, one has to write the Schrödinger equation for two particles (here two electrons) interacting via the potential energy $V(r_1 - r_2)$ [8]:

$$\left[-\frac{\hbar^2}{2m_e}(\nabla_1^2 + \nabla_2^2) + V(r_1 - r_2)\right]\Psi(r_1, r_2) = E\Psi(r_1, r_2) \ , \tag{2.26}$$

where $\hbar$ is the reduced Planck constant, m_e the mass of an electron, V the interacting potential energy, E the energy, Ψ the symmetric wave function of the two electrons, ∇ the Laplacian operator and r_1 and r_2 are the local coordinate of the electrons. Since the conducting electrons are located near the Fermi level (Fermi level is the level with energy E_f), the value of the energy E in the Schrödinger equation should be close to the Fermi energy. To simplify the Schrödinger equation, the center of mass R_0, the relative coordinate of both electrons r_l, the reduced mass μ and the wave number K must be defined as follows [8]:

$$R_0 = \frac{1}{2}(r_1 + r_2) \ , \tag{2.27}$$

$$r_l = r_1 - r_2 \ , \tag{2.28}$$

$$\mu = \frac{m_e m_e}{m_e + m_e} = \frac{m_e}{2} \ , \tag{2.29}$$

$$K = k_1 + k_2 \ . \tag{2.30}$$

The wave number of an electron k can be related to the momentum of the electron p by the following equation:

$$k = \frac{p}{\hbar} \quad \Rightarrow \quad k_1 = \frac{p_1}{\hbar}, k_2 = \frac{p_2}{\hbar} \ . \tag{2.31}$$

Due to the fact that the momentum of the two electrons have the same magnitude but opposite sign, the total momentum of the pair P is equal to zero and, therefore, the wave number of the pair K is zero as well [8].

$$p_1 = -p_2 \quad \Rightarrow \quad P = p_1 + p_2 = 0 \quad \xrightarrow{\text{equation 2.30 and 2.31}} \quad K = 0 \ . \tag{2.32}$$

Using these new coordinates R_0 and r_l, the reduced mass μ and $\nabla_1^2 + \nabla_2^2 = \left(\nabla_{R_0}^2/4 + \nabla_{r_l}^2\right)$ the Schrödinger equation can be rewritten as follows [8]:

$$-\frac{\hbar^2}{2\mu}\left(\frac{\nabla_{R_0}^2}{4} + \nabla_{r_l}^2\right)\Psi(R_0, r_l) + V(r_l)\Psi(R_0, r_l) = E\Psi(R_0, r_l) \ . \tag{2.33}$$

The wave function can be separated and be described by the following equation [8]:

$$\Psi(R_0, r_l) = \Phi(R_0)\psi(r_l) \ . \tag{2.34}$$

$\Phi(R_0)$ is simply a plane wave function which is defined as [8]:

$$\Phi(R_0) = e^{iKR_0} \ . \tag{2.35}$$

By setting equation 2.34 into equation 2.33 and using the reduced mass $\mu = m_e/2$ and $K = 0$, the Schrödinger equation can be further simplified [8]:

$$\left[-\frac{\hbar^2}{m_e}\nabla_{r_l}^2 + V(r_l)\right]\psi(r_l) = E\psi(r_l) \ . \tag{2.36}$$

One can try a solution in the form of a sum of sinus functions for $\psi(r_l)$:

$$\psi(r_l) = \sum_{k'} a_{k'} \sin(k' r_l) \ , \tag{2.37}$$

where $a_{k'}$ are unknown constants and k' is the wave number. The prime symbol for the wave number k' stands for the new state of the electron after the electron pairing. It is well known

that k and k′ are quantized values by solving the Schrödinger equation for the electrons in metals. Due to the spherical symmetry in this case, a sphere of radius R must be used. The relation between the quantized wave number k and R are given as [7, 8]:

$$k = \frac{n\pi}{R} \ . \tag{2.38}$$

After the substitution of equation 2.37 into equation 2.36, the Schrödinger equation can be rewritten as follows [7]:

$$\sum_{k'} a_{k'}\left(\frac{\hbar^2 k'^2}{m_e} - E\right)\sin(k'r_l) = -V(r_l)\sum_{k'} a_{k'}\sin(k'r) \ . \tag{2.39}$$

Taking into account that

$$\int_0^R \sin(kr)\sin(k'r)\,dr = \begin{cases} \frac{R}{2} & \text{for } k = k' \\ 0 & \text{otherwise} \end{cases} , \tag{2.40}$$

multiplying equation 2.39 with $\sin(kr_l)$ and integrate

$$\sum_{k'} a_{k'}\left(\frac{\hbar^2 k'^2}{m_e} - E\right)\int_0^R \sin(k'r_l)\sin(kr_l)dr_l = -\sum_{k'} a_{k'}\int_0^R V(r_l)\sin(k'r)\sin(kr_l)\,dr_l \ . \tag{2.41}$$

Using equation 2.40, the left integral of above equation will be zero for $k \neq k'$ and equal to $R/2$ for $k = k'$. Using equation 2.25 for the value of $V(r_l)$, the integral on the right side of equation 2.41 can be rewritten as follows:

$$\begin{cases} V_0\int_0^R \sin(k'r)\sin(kr_l)dr_l & r_l < l \\ 0 & r_l > l \end{cases} . \tag{2.42}$$

Because the value of this equation for $r_l > l$ is zero, the upper limit of the integral has to be set to l. The following equation can then be defined:

$$V_{kk'} = V_0\int_0^l \sin(kr_l)\sin(k'r_l)dr_l \ . \tag{2.43}$$

If $|k - k'| < \pi/l$, and k and k' are nearly equal, then $l \approx R$. Therefore, the integral in equation 2.43 is approximately equal to $V_0 R/2$; otherwise it is equal to zero. Using $l = \pi v_e/\omega_D$ in $|k - k'| < \pi/l$, a new function for the interaction potential energy $V_{kk'}$ can be calculated as follows [7]:

$$V_{kk'} = \begin{cases} \frac{R}{2} V_0 & \text{for } |k - k'| < \omega_D/v_e \\ 0 & \text{for } |k - k'| > \omega_D/v_e \end{cases} . \tag{2.44}$$

Using equation 2.43 and the value of $R/2$ for the left integral calculated by equation 2.40, equation 2.41 can be simplified as follows:

$$\frac{R}{2} a_k \left(\frac{\hbar^2 k^2}{m_e} - E \right) = - \sum_{k'} a_{k'} V_{kk'} . \tag{2.45}$$

With the following definitions for ε and Δ [7]:

$$\varepsilon = \frac{\hbar^2 k^2}{2 m_e} - E_f , \tag{2.46}$$

$$\Delta = E_f - \frac{E}{2} , \tag{2.47}$$

equations 2.44 and 2.45 can then be rewritten for $|k - k'| < \omega_D/v_e$ as follows [7]:

$$\frac{R}{2} a_k (2\varepsilon + 2\Delta) = - \frac{R}{2} V_0 \sum_{k'} a_{k'} . \tag{2.48}$$

A new integral for $\sum_{k'} a_{k'}$ must be defined. To do that, the density of states at Fermi energy $D(E_f)$ is needed. Then the new integral can be defined with ε' as integration variable [7]:

$$\sum_{k'} a_{k'} \approx \int a_{\varepsilon'} D(E_f) d\varepsilon' . \tag{2.49}$$

Because only the electrons close to the Fermi level can build Cooper pairs, therefore, the lower limit of this integral is equal to the Fermi energy. If all energies are taken relative to E_f, one can set $E_f = 0$ and, therefore, the lower limit of the integral in equation 2.49 is also zero. To define

the upper limit of the integral one recalls equation 2.44 which indicates that $V_{kk'}$ is not zero if $|k - k'| < \omega_D/v_e$ or $\partial k < \omega_D/v_e$ [7]. By differentiation of equation 2.46 with respect to k:

$$\partial\varepsilon = \frac{2\hbar^2 k\,\partial k}{2m_e} = \hbar v_e\,\partial k\ , \tag{2.50}$$

$$\partial k < \frac{\omega_D}{v_e} \qquad \Rightarrow \qquad \partial\varepsilon < \hbar\omega_D\ . \tag{2.51}$$

According to $\partial\varepsilon = |\varepsilon - \varepsilon'|$ and $\partial\varepsilon < \hbar\omega_D$, if $\varepsilon = 0$, then $\varepsilon' < \hbar\omega_D$. Then, the upper limit of the integral is $\hbar\omega_D$, the upper limit must be approximated as $\hbar\omega_D$. Because the $D(E_f)$ is always a constant value, the equation 2.48 can be simplified as follows:

$$a_\varepsilon(2\varepsilon + 2\Delta) = -D(E_f)(V_0)\int_0^{\hbar\omega_D} a_{\varepsilon'}\,d\varepsilon'\ . \tag{2.52}$$

The right side of equation 2.52 is constant. Therefore, this equation can be rewritten as follows:

$$a_\varepsilon = \frac{C}{(2\varepsilon + 2\Delta)}\ , \tag{2.53}$$

where C is a constant. Using equation 2.53 in equation 2.52 and integrate [7]:

$$C = -D(E_f)V_0\int_0^{\hbar\omega_D} \frac{C}{(2\varepsilon' + 2\Delta)}\,d\varepsilon'\ , \tag{2.54}$$

$$1 = -\frac{1}{2}D(E_f)V_0 \ln 2(\varepsilon' + \Delta)|_0^{\hbar\omega_D}\ , \tag{2.55}$$

$$1 = -\frac{1}{2}D(E_f)V_0 \ln\left(\frac{\hbar\omega_D + \Delta}{\Delta}\right)\ . \tag{2.56}$$

Because $\hbar\omega_D$ is 100 times larger than Δ then:

$$\Delta = \hbar\omega_D \exp\left(\frac{-2}{D(E_f)V_0}\right)\ . \tag{2.57}$$

If the superconductor has different types of Fermi electrons (with different Fermi velocities and different densities of states), the influence of each type i for the binding energy Δ must be calculated. Therefore, a sum is needed for the calculation over all types:

$$\sum_{i}^{n} D_i(E_f)V_{0_i} \qquad \Rightarrow \qquad \Delta = \hbar\omega_D \exp\left(\frac{-2}{\sum_i^n D_i(E_f)V_{0_i}}\right), \tag{2.58}$$

where n is the number of the Fermi electron types. At temperatures above the critical temperature T_c, the thermal energy is large enough to break the Cooper pairs. A mathematical relationship between the thermal energy and the binding energy at T_c has been found (equation 2.59). The constant c has a theoretical value of 3.53 and it's called the "superconducting constant". In practice, it varies depending on the superconductor according to experimental results [8]:

$$ck_B T_c = 2\Delta \ . \tag{2.59}$$

Cooper pairs, which are bosons, form after the pairing of electrons (fermions) near the Fermi level. Because bosons are not considered in the calculation of the electronic band structure and the electrons near the Fermi level, which are paired together, have vanished from the electronic band structure, a gap will appear in the latter. This gap is called the "superconducting gap" and has a width of 2Δ. The number 2 behind the binding energy Δ is due to the two electrons.

2.4 Potential Theory

2.4.1 Shell Model

To calculate the force constant for an ionic pair using the shell model, it has been assumed that each ion consists of a core and a shell which are connected by a spring with the constant k (figure 14). The total charge of an ion is the sum of the charges of these two components ($Z = q_{shell} + q_{core}$). There are different interactions between these, due to which an equilibrium with a given distance between each two components can be achieved. The shell and the core of an ion are displaced relative to each other, causing a polarization of the ion arises. Shell and core want to go back to their initial positions. To account for this, a spring of constant k for an ion is considered (k_A for ion A and k_B for ion B). The spring of constant K has been assumed

between two whole ions of an ionic pair. The equilibrium is represented in figure 14 by these three spring constants k_A, k_B and K.

The interactions for an ionic pair can be described by four potentials: the Coulomb interaction between the shells and the cores V_{coul}, the van der Waals interaction V_{VW}, the short-range repulsive interaction V_{short} and the potential energy of the inner springs (polarization energy) V_{pol}.

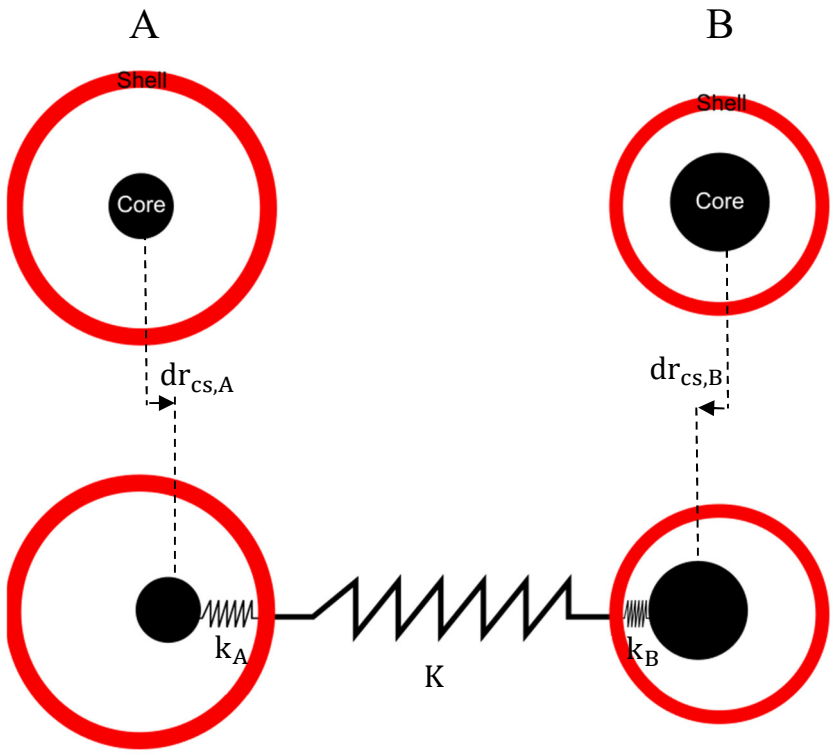

Figure 14: Shells and cores of two ions A, B, the springs with constants K, k_A and k_B, and the relative displacements between shell and core of the ions A and B ($dr_{cs,A}$ and $dr_{cs,B}$).

The Coulomb interaction between the shells and the cores is given by equation 2.60, where q stands for the charge of a component of the ionic pair (the shells and the cores), and r_{ij} is the distance between component i and component j.

$$V_{coul} = \frac{1}{2}\sum_{j=1}^{4}\sum_{i=1}^{4}\frac{q_i q_j}{4\pi\varepsilon_0 r_{ij}} \qquad i \neq j \ , \tag{2.60}$$

$i, j = 1$: The core of the ion A ,
$i, j = 2$: The shell of the ion A ,
$i, j = 3$: The core of the ion B ,
$i, j = 4$: The shell of the ion B .

The van der Waals interaction and the short-range repulsive interaction can be calculated respectively by the following equations, where C, A and ρ are potential parameters for the ionic pair:

$$V_{VW} = \frac{1}{2}\sum_{j=1}^{4}\sum_{i=1}^{4} -C r_{ij}^{-6} \qquad i \neq j \ , \tag{2.61}$$

$$V_{short} = \frac{1}{2}\sum_{j=1}^{4}\sum_{i=1}^{4} A \exp\left(-\frac{r_{ij}}{\rho}\right) \qquad i \neq j \ . \tag{2.62}$$

Due to the relative displacements $dr_{cs,A}$ and $dr_{cs,B}$ between core and shell of the ion A and B (polarization), the potential energy of the inner springs with constants k_A and k_B must also be considered:

$$V_{pol} = \frac{1}{2}k_A dr_{cs,A}^2 + \frac{1}{2}k_B dr_{cs,B}^2 \ . \tag{2.63}$$

The total potential interaction for an ionic pair is the sum of the four preceding potentials:

$$V_{tot} = V_{coul} + V_{VW} + V_{short} + V_{pol} \ . \tag{2.64}$$

As it is known, the second derivative of the total potential interaction at the equilibrium distances $r_{ij,eq}$ and the equilibrium displacement $dr_{cs,A}$ and $dr_{cs,B}$ is equal to the force constant between the two ions:

$$K = \sum \frac{\partial^2 V_{tot}}{\partial^2 r_{ij}} \left(r_{ij,eq}, dr_{cs,A}, dr_{cs,B}\right) , \tag{2.65}$$

$$r_{ij,eq} = \left\{r_{12,eq}, r_{13,eq}, r_{14,eq}, r_{23,eq}, r_{24,eq}, r_{34,eq}\right\} .$$

2.5 Raman and Infrared Spectroscopy

2.5.1 Infrared Spectroscopy

If a diatomic molecule or a crystal lattice composed of two kinds of atoms is irradiated by infrared light, the atoms are excited from the ground vibration state $v = 0$ to the next state, $v = 1$. The energy of a vibration state v can be found by equation 2.66 according to quantum mechanics, where k is the force constant between the atoms, μ is the reduced mass of atoms with masses m_1 and m_2, and v is the vibration quantum number [9].

$$E_v = \hbar \left(v + \frac{1}{2}\right) \sqrt{\frac{k}{\mu}} , \tag{2.66}$$

$$\mu = \frac{m_1 + m_2}{m_1 m_2} . \tag{2.67}$$

In the measured infrared spectrum, the frequency of each peak corresponds to a vibration mode. By getting the peak frequency, the force constant between two atoms for the vibration mode can be calculated by the following equation, where c is the speed of light and f the frequency [9].

$$f = \frac{1}{2\pi c} \sqrt{\frac{k}{\mu}} . \tag{2.68}$$

2.5.2 Raman Spectroscopy

If a molecule or a crystal lattice is exposed to monochromatic light, the atoms would be excited by a photon from the ground state to a virtual energy state. The atoms can relax and return back to the ground state by emission of a photon. Depending on the frequency of the scattered photon, there are three different scattering types. If the scattered frequency is equal to the frequency of the incident radiation, it is called as Rayleigh scattering, if it is lower, it is called Stokes shift.

Otherwise it is named anti-Stockes-shift (figure 15). As described for the infrared spectrum, the force constant can be calculated from the peak frequency in Raman spectra for a vibration mode by equation 2.68 [9].

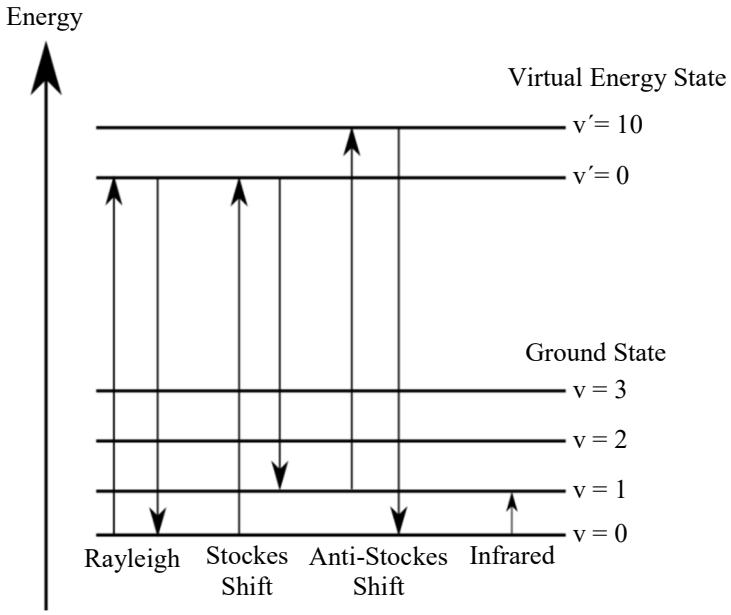

Figure 15: Energy level diagram for the atom vibrations **[9]**.

3 Finite Element Method

The finite element method (FEM) is a numerical method for solving problems in engineering and mathematical physics which are described mathematically by partial differential equations. This method is useful e.g. for structural problems with complicated geometries, loads and material properties, where analytical methods cannot be applied to obtain a solution. It can also be used especially to solve problems in solid mechanics, fluid mechanics, heat transfer and vibrations. For this method, a structure is divided into several finite elements. These elements are connected at nodes. As such, a discretized finite element problem with unknown nodal values describes a continuous physical problem. Considering a static linear problem, a system of linear algebraic equations should be solved and the nodal values of each element can be determined. The main steps of the finite element solution procedure are:

1. Discretization of continuum. In this first step the domain is divided into a finite number of elements. This is called the meshing process which is performed by a preprocessor program. There are different types of finite elements: one-dimensional (spring, beam, pipe, truss, etc.), two-dimensional (membrane, shell, plate, etc.), and three-dimensional.
2. Selection of interpolation functions. A field quantity is interpolated by a polynomial over an element. The degree of the polynomial depends on the number of nodes assigned to the element.
3. Determination of element properties. The matrix equation for the finite element should be established. This relates the nodal values of the unknown function to other parameters.
4. Assemble the element equations. All element equations must be assembled to find the global equation system for the whole solution region. The boundary conditions must be defined before solving.
5. Solving the global equation system. The finite element global equation system can be sparse, symmetric and positive definite. Direct and iterative methods can be applied for solving the problem. As a result of the solution the nodal values are determined.
6. Computation of additional results. In many cases additional parameters are needed to evaluate the results. For example, strains and stresses are of interest in addition to displacements, which are calculated after the solution of the global equation system. [10]

3.1 Pre-Processing, Processing and Post-Processing

The attractive potential energy (the deformation energy), caused by the Coulomb forces between a moving Fermi electron and the ions in the crystal structure, is required to calculate the critical temperature using the BCS theory. Due to the complex unit cell structure of high temperature superconductors, the finite element method must be applied to calculate this energy.

A finite element simulation consists of three different stages; pre-processing, processing, and post-processing. In the pre-processing stage, the finite element mesh is prepared, material properties are assigned and boundary conditions in the form of restraints and loads are applied. In the processing or solution stage, the differential equations are converted into matrix form and are solved numerically. The processing depends on the type of analysis (static or dynamic), and element types and properties, material properties and boundary conditions. In the post-processing stage, the results are prepared. Typically, the deformation, mode shapes, temperature, energy, strain and stress distribution are shown at this stage. In the following paragraphs, the pre- and post-processing of the simulation are explained. In this work, ANSYS is used as a finite element program for the three stages. [10]

3.2 Pre-Processing

3.2.1 Finite Element Domain

The unit cell must be defined as a finite element domain for the simulation. The equilibrium coordinates of each ion can be determined from the symmetry of the unit cell and the lattice parameters. By treating the ions as nodes and using the coordinates of each ion in the global coordinate system, a three-dimensional arrangement of nodes can be generated. For the simulation, one-dimensional elements - spring and point mass elements - can be used: the ions belonging to the unit cell are considered as nodes with mass; the bonds between them are spring elements connecting two nodes. This provides a three-dimensional finite element domain. The real constants for the elements (the values of mass and spring constants) must be defined for the simulation. The mass of each ion can be found in the periodic table and the value of spring constants (force constants) can be taken from published results of Raman spectroscopy or determined by the potential theory. [10]

3.2.2 Boundary Condition

Since a structural node holds at most six degrees of freedom (three translations and three rotations), every single movement can be fixed separately, i.e. set to zero. All degrees of freedom of the nodes representing the ions inside the neighbouring unit cells are fixed. Due to the time-dependent Coulomb forces the simulation must be transient. Therefore, a time-dependent step must be defined. The calculated time-dependent Coulomb forces are applied on the nodes which represent the ions belonging to the unit cell under consideration. [11]

3.2.2.1 Mass Element

For the simulation in ANSYS, the mass element MASS21 is added to the all nodes. This is a one-dimensional point element that has six degrees of freedom: three translation and three rotations. Different masses and rotational inertias can be assigned to each coordinate direction. Due to the linear motion of the ions in the crystal structure, the rotational inertia has been excluded from the simulation. If a three-dimensional mass without rotational inertia is added to a node, then only one value for the mass is needed for the simulation. [11]

3.2.2.2 Spring Element

For the simulation in ANSYS, the spring element COMBIN14 is considered between two nodes that represents a bond between two ions in the unit cell. This element has longitudinal or torsional properties and no mass. The mass of this element can be considered by the mass element MASS21. The longitudinal spring-damper is a uniaxial tension-compression element with three translational degrees of freedom at its belonging nodes. In this case no bending or torsion is considered. To simplify, it is assumed that the spring-damper element is longitudinal and no damping effect exists between ions in an ionic pair. Therefore, the damping constant is set to zero for the simulation. [11]

3.3 Post-Processing

After reaching a solution, the kinetic and the potential energies of all masses and spring elements belonging to the unit cell under consideration must be summed up to determine the attractive potential energy of the unit cell.

4 Codes

Three different codes must be prepared to simulate the attractive potential energies and the binding energy of superconductors.

4.1 First Code

A code (called first code) has to be prepared to construct the unit cell. The mass and coordinates of the ions of the unit cell are required to construct it. Because two neighbour ions in the unit cell are elastically tied, a spring between both ions can be used to consider this behaviour. Therefore, for the construction of the unit cell, springs between the ions are needed as well; the spring constant (force constant) can be calculated by Raman spectroscopy or the potential theory.

It is important to keep in mind that only certain neighbour ions within the unit cell are bound. Two bound ions together build together an ionic pair. Each ionic pair can be designated by the distance between its ions. The springs can only be used for the ionic pairs, because their ions are bound. The distance for each ionic pair is an additional input for the first code. As such, the code only considers a spring between the two bound ions of each ionic pair.

The code takes the coordinates of ions and assumes a node with the same coordinates for each ion. A mass element (MASS21) is defined for each node and its value is equal to the given mass of the corresponding ion. A linear spring element (COMBIN14) can be considered between two nodes (two ions of an ionic pair), because the displacement of ions (10^{-3}-10^{-2}Å) due to the Coulomb forces are very small compared to the distance between ions of an ionic pair (1-5Å).

The pertinent spring constants for the ionic pairs in a unit cell of a superconductor have been determined using Raman spectroscopy or the potential theory. The code must define the linear spring elements between bound nodes (each two nodes with a spring element represents an ionic pair). To find out which nodes are bound (according to the information available from Raman spectroscopy or the potential theory), the code calculates the distances between all neighbour nodes and compares these with all distances between the ions of the ionic pairs for which the spring constants are known. If the code finds two neighbour nodes whose distance is exactly the same as the distance between two ions of an ionic pair, then it assumes a linear spring element for the corresponding two neighbour nodes; if not, then the two nodes are not bound and, therefore, no spring element is considered for those nodes. The code performs this process for all neighbour nodes, until all bound nodes are found and so that all spring elements can be defined (figure 16).

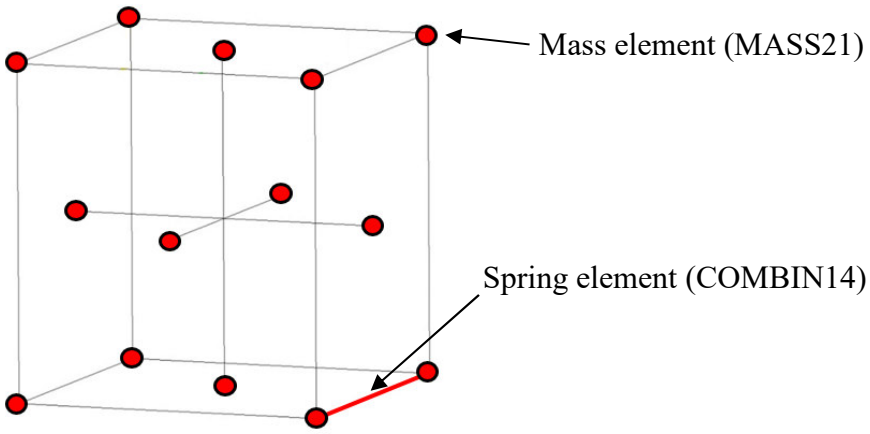

Figure 16: The FE-Model of the unit cell of aluminium.

4.2 Second Code

The Fermi velocity and the coordinates of the ions within the unit cell are required for the calculation of the time-dependent Coulomb forces between the ions and the moving Fermi electron. The coordinates of the ions are taken from the first code; the Fermi velocity is taken from different references given in (table 2, 3 and 4) or calculated and must be given by the user before running this code. The direction of the electron movement depends on superconductors. It is assumed that the Fermi electron starts its movement 30 unit cells away from the one being considered and travels through 60 unit cells. The time required for the Fermi electron to move on this path is calculated from the Fermi velocity and the corresponding distance involved. After that, this time is discretized. With the help of the Fermi velocity v_e, the time-dependent coordinate $r(t)$ of the Fermi electron relative to the unit cell under consideration can be calculated at each discretized time t_i with $r(t) = v_e t_i$.

From this coordinate and the coordinates of each ion, the time-dependent distance between the electron and each ion is determined. Using this distance and the charge of each ion, the time-dependent Coulomb force acting on each ion is calculated and saved as a table in a text file containing two columns: one for the discretized time and one for the calculated Coulomb forces acting on the corresponding ion.

4.3 Major FE-Code

A major FE-code (finite element code) has been prepared, which calculates the attractive potential energy, the binding energy and the superconducting constant of superconductors. This code takes the results of the first and second codes as input, since the unit cell as a finite element

domain and the time-dependent Coulomb forces as loads are required for the calculation of the attractive potential energy. A transient simulation is considered and two steps are defined for it. In both the first and second steps all degrees of freedom of the nodes belonging to neighbouring unit cells are fixed. In the second step, the time-dependent Coulomb forces saved in a text file by the second code, are loaded and made to act on the nodes, which belong to the unit cell under consideration. The time for the second step must be set for the simulation. The formula for this time is given in chapter 4.2. After reaching a solution, the kinetic and the potential energies of all masses and spring elements belonging to the unit cell under consideration are summed up to determine the attractive potential energy. Using equations 2.58 and 2.59, this code calculates the binding energy and the superconducting constant of superconductors.

5 Analytical Method and Results

The equation 2.22 can be used only for monoatomic unit cells. The unit cells of HTSC cuprates and the unconventional superconductor Sr_2RuO_4 are very complex. Therefore, it is not possible to use this equation to calculate the attractive potential energy V_0 of the unit cell for these superconductors. Furthermore, it has been shown that the superconductivity in HTSC cuprates comes from the doped charged carriers in the CuO_2 plane, whereas for Sr_2RuO_4, it has been assumed that the movement of the charged carrier on the RuO_2 plane causes the superconductivity [8]. Therefore, to calculate the attractive potential energy, the Fermi electrons are assumed to move on these planes. The first difference between the two types of planes is that the charge of Ru ions is 4+ and the charge of Cu ions 2+. The second one is that the masses of Ru and Cu ions are different.

The distance between a moving Fermi electron and ions in the CuO_2 or RuO_2 planes is much smaller than that of other planes in the unit cell. Therefore, the corresponding Coulomb forces are much larger than those in other planes in the unit cell, which causes a larger attractive potential energy. So it can be assumed that the attractive potential energy of the unit cell can be approximated by the attractive potential energy of the CuO_2 or RuO_2 plane, the calculation of which can be performed as described mathematically in the preceding chapters, the difference being that it must be calculated for O, Cu and Ru ions separately. Therefore, the frequency of each ion must be calculated, which is not equal to the Debye frequency.

To calculate the frequency ω_i of every ion in equation 2.18, the force constants between ions in the two planes are required. It has been assumed that there are two force constants between the ions: k_1 for the Cu-O / Ru-O bond and k_2 for the O-O bond (figure 17). These force constants can be calculated with the potential theory or measured by Raman spectroscopy.

Here, the total force constant in the y direction is needed, because for the calculation of the attractive potential energy of an ion in both planes, the small displacement δ used is a displacement in this direction. Due to the angle of 45°, one can take the effective amount of the force constant k_2 in y direction as $(\sqrt{2}/2)k_2$. Now from figure 17, the total force constant for oxygen, cupper and ruthenium ion in y direction can be calculated as follows:

O1: $$k_{O1,y} = 4\left(\frac{\sqrt{2}}{2}\right)k_2 + 2k_1 \ , \tag{5.1}$$

O2: $$k_{O2,y} = 4\left(\frac{\sqrt{2}}{2}\right)k_2 \ , \tag{5.2}$$

O3: $$k_{O3,y} = 4\left(\frac{\sqrt{2}}{2}\right)k_2 + 2k_1 \ , \tag{5.3}$$

Cu/Ru: $$k_{Cu/Ru,y} = 2k_1 \ . \tag{5.4}$$

Now, the frequency ω_i can be calculated by equation 2.18. The oxygen ions must be treated separately, not only because of the different frequencies but also because in this case the charge carrier must move between the Cu or Ru and the O1 ion (figure 17). There are thus different distances between the carrier and each ion, r_{o1}, r_{o2}, r_{o3} and $r_{Cu/Ru}$, which yields the different Coulomb forces for the ions. If x is the horizontal coordinate of the Fermi electron, then:

$$r_{o1} = \sqrt{\left(\frac{a}{4}\right)^2 + \left(\frac{a}{2} - x\right)^2} \ , \tag{5.5}$$

$$r_{o2} = \sqrt{(\frac{a}{4})^2 + (\frac{a}{2} - x)^2} \ , \tag{5.6}$$

$$r_{o3} = \sqrt{(\frac{3a}{4})^2 + (\frac{a}{2} - x)^2} \ , \tag{5.7}$$

$$r_{Cu/Ru} = \sqrt{(\frac{a}{4})^2 + (\frac{a}{2} - x)^2} \ . \tag{5.8}$$

Equation 2.22 can be rewritten for each ion as follows:

$$V_{0,i} = \frac{n_i e^2}{2\pi\varepsilon_0 {r_i}^2}\left(-\frac{n_i e^2}{8\pi\varepsilon_0 r_i}\frac{\pi}{v_e}\frac{1}{M_i}\frac{1}{\omega_{D,i}}\right) \ , \tag{5.9}$$

where e is the elementary charge, n_i is an integer number for the charge of ion i, ε_0 is the permittivity in vacuum, r_i is the distance between the electron and the nearest ion, v_e is the Fermi velocity, M_i is the mass of ion and $\omega_{D,i}$ is the Debye frequency related to ion i. Using the equation 5.9, the equation of the attractive potential energy for each ion in both planes can be determined as follows:

$$V_{0,O1} = -\frac{n_o^2 e^4}{a^3 \varepsilon_0^2 v_e} \frac{0.0897}{M_O \omega_{O1}} , \tag{5.10}$$

$$V_{0,O2} = -\frac{n_o^2 e^4}{a^3 \varepsilon_0^2 v_e} \frac{0.0897}{M_O \omega_{O2}} , \tag{5.11}$$

$$V_{0,O3} = -\frac{n_o^2 e^4}{a^3 \varepsilon_0^2 v_e} \frac{0.00061}{M_O \omega_{O3}} , \tag{5.12}$$

$$V_{0,Cu/Ru} = -\frac{n_{Cu/Ru}^2 e^4}{a^3 \varepsilon_0^2 v_e} \frac{0.0897}{M_{Cu} \omega_{Cu/Ru}} . \tag{5.13}$$

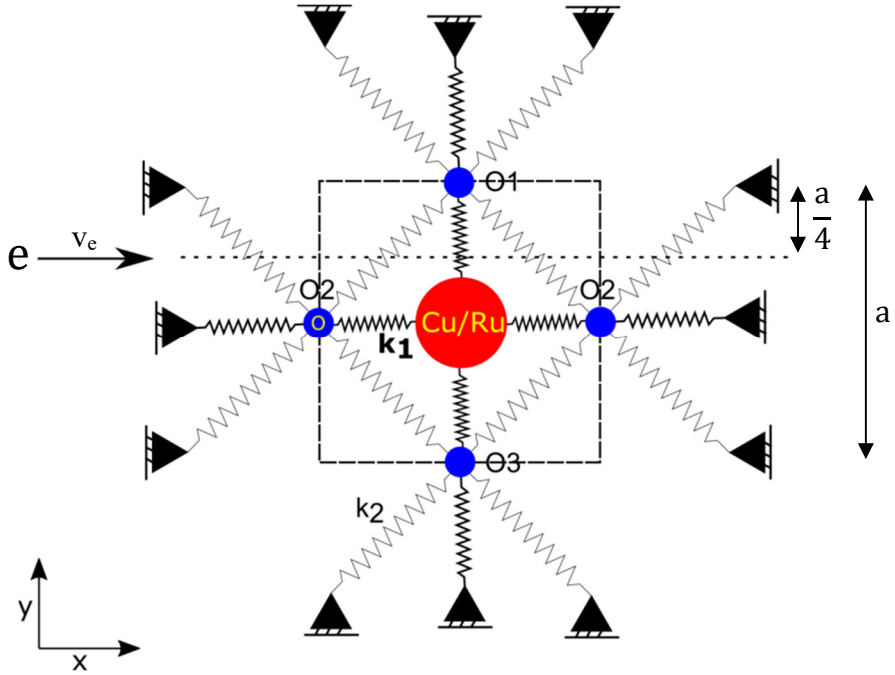

Figure 17: Force constants and different ions in the CuO_2 plane and path of the electron. The dashed square presents CuO_2 or RuO_2 Plane. The distance a is a lattice parameter.

It can be seen from figure 17 that for the calculation of the total attractive potential energy only half of the attractive potential energy of the O1 and O3 ions must be considered, because half of them belongs to CuO_2 or RuO_2 plane. Due to the fact that there are in total one O2 ion and one Cu/Ru ion in the plane, their attractive potential energies of O2 and Cu/Ru enter whole in the calculation of the total attractive potential energy of the plane.

$$V_0 = 0.5\, V_{0,O1} + 0.5\, V_{0,O3} + V_{0,O2} + V_{0,Cu/Ru} \ . \qquad (5.14)$$

5.1 Conventional, Unconventional and High Temperature Superconductors

The calculation of the attractive potential energy has been performed for the two conventional superconductors Al and Nb, four different high temperature superconductors (cuprates) and the unconventional superconductor Sr_2RuO_4 (table 1). Their unit cell structures can be seen in figure 18 and 19.

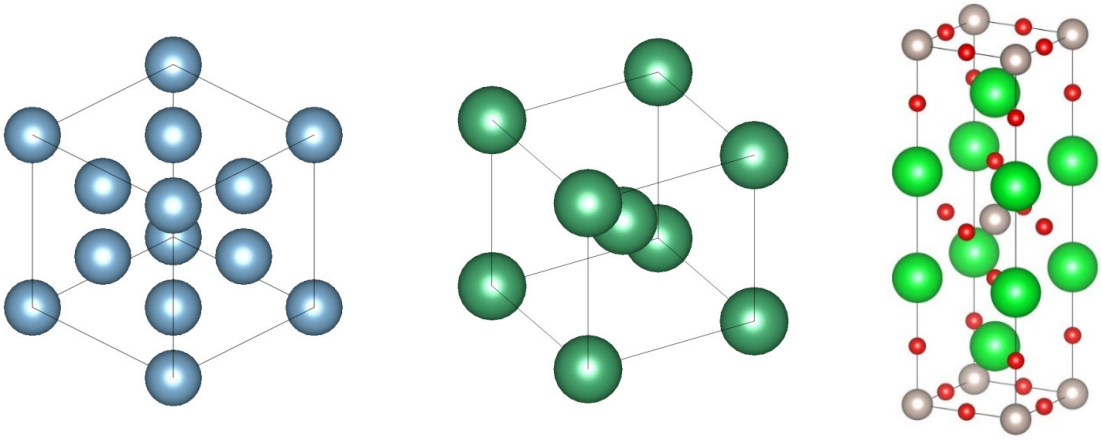

Al

Nb

Sr_2RuO_4
Sr: Green
O: Red
Ru: Light Braun

Figure 18: Unit cells of Al, Nb and Sr_2RuO_4.

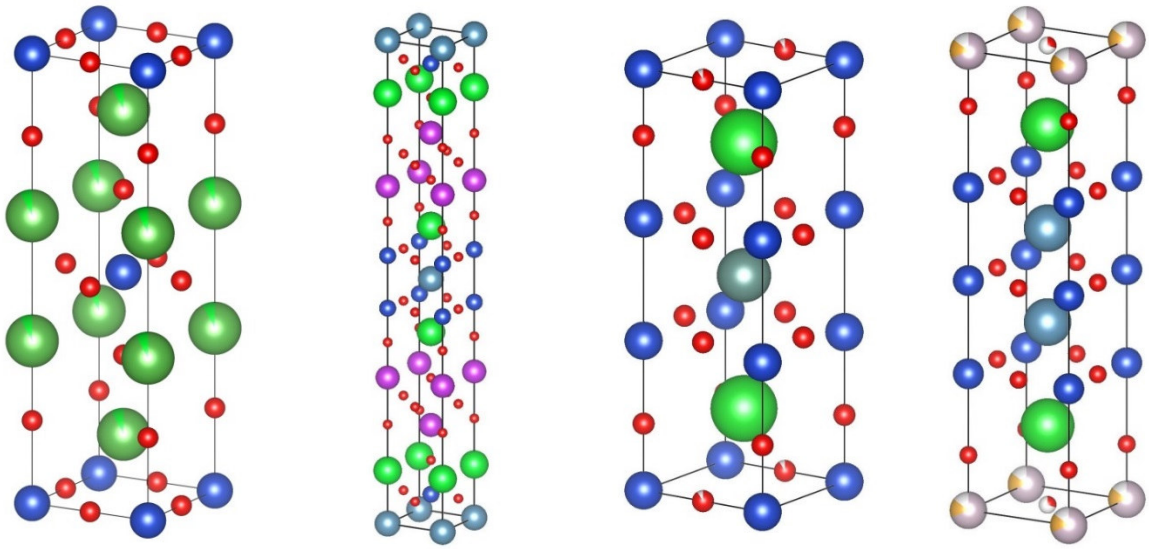

$La_{1.85}Sr_{0.15}CuO_4$	$Bi_2Sr_2CaCu_2O_{8+\delta}$	$YBa_2Cu_3O_{6.9}$	$HgBa_2Ca_2Cu_3O_{8+\delta}$
La: Green	Bi: Violet	Y: Dark Green	Hg: Light Violet
Cu: Blue	Sr: Green	Ba: Green	Ca: Dark Green
O: Red	Ca: Light Blue	Cu: Blue	Ba: Green
	Cu: Blue	O: Red	Cu: Blue
	O: Red		O: Red

Figure 19: Unit cells of $La_{1.85}Sr_{0.15}CuO_4$, $Bi_2Sr_2CaCu_2O_{8+\delta}$, $YBa_2Cu_3O_{6.9}$ and $HgBa_2Ca_2Cu_3O_{8+\delta}$.

5.2 Calculation of the Debye Frequency for the Single Atomic Superconductors Al and Nb

According to equation 2.22 and 2.57, the Debye frequency ω_D is required to calculate the attractive potential energy V_0 and the binding energy Δ of the Cooper pairs. For single atomic superconductors (Al and Nb), the Debye frequency can be calculated by the following equation, where k_B is the Boltzmann constant and T_D is the Debye temperature [5]

$$\omega_D = \frac{k_B T_D}{\hbar} . \qquad (5.15)$$

5.3 Calculation of the Debye Temperature for the High Temperature Superconductor $HgBa_2Ca_2Cu_3O_{8+\delta}$

The Debye temperature for $HgBa_2Ca_2Cu_3O_{8+\delta}$ must be calculated from the heat capacity C_V at a given temperature by [5]

$$C_V(T) = 16\,\frac{12\pi^4}{5}\left(\frac{T}{T_D}\right)k_B\,. \qquad (5.16)$$

The heat capacity $C_V(T)$ can either be determined by a quantum mechanical calculation with the program Gulp [12] ($C_V(134) = 0.002762$ J/K) or taken from Ref. [8] ($C_V(134) = 0.00367$ J/K). Now, using equation 5.16, the Debye temperature can be calculated from the heat capacity. These calculated values for the Debye temperature are given in table 1. Debye temperatures for other superconductors have been taken from different references. According to equation 5.15, the Debye frequencies for all superconductors can be calculated with Debye temperatures from table 1.

5.4 Calculation of Two Dimensional Density of States D_{2D} and Fermi Velocities v_e for Different Types of Fermi Electrons in Sr_2RuO_4

There are three different types of Fermi electrons (α, β and γ) with different Fermi velocities and densities of states in the unconventional superconductor Sr_2RuO_4. Due to its quasi-two-dimensional band structure, the two-dimensional density of states D_{2D} must be used. The two-dimensional density of states D_{2D} and the Fermi velocity v_e for each type of Fermi electron must be calculated from the wave number k_f (wave number for the Fermi electron wave) and the effective electron mass m_{eff} (the effective electron mass is usually stated in units of the true mass of an electron, $m_e = 9.11 \times 10^{-31}$kg) in the following equations. The values for the wave numbers, the effective electron masses, the volume fractions, the calculated Fermi velocities and the calculated two-dimensional density of states of each type of Femi electrons are given in table 2. For other superconductors, $D(E_f)$ and v_e are directly taken from published data (table 3 and 4).

$$D_{2D} = \frac{m_{eff}}{\pi\hbar^2}a^2\ , \qquad (5.17)$$

$$v_e = \frac{\hbar k_f}{m_{eff}}\ . \qquad (5.18)$$

Superconductors	T_c [K]	T_D [K]	Symmetry	a (Å)	b (Å)	c (Å)	n
Al	1.18	423 [8]	fcc	4.05 [8]	4.05 [8]	4.05 [8]	Al^{3+}
Sr_2RuO_4	1.15	312 [13]	I4/m m m	3.87 [14]	3.87 [14]	12.7 [14]	Ru^{4+}/O^{2-}
Nb	9.26	277 [8]	bcc	3.30 [8]	3.30 [8]	3.30 [8]	Nb^{1+}
$La_{1.85}Sr_{0.15}CuO_4$	38	360 [8]	I4/m m m	3.78 [15]	3.78 [15]	13.2 [15]	Cu^{4+}/O^{2-}
$Bi_2Sr_2CaCu_2O_{8+\delta}$	83	250 [8]	I4/m m m	3.81 [16]	3.81 [16]	30.5 [16]	Cu^{4+}/O^{2-}
$YBa_2Cu_3O_{6.9}$	93	437 [17]		3.83 [8]	3.88 [8]	11.68 [8]	Cu^{4+}/O^{2-}
$HgBa_2Ca_2Cu_3O_{8+\delta}$	134	592 calc. from [8] 654 calc. by Gulp [12]	P 4/m m m	3.85 [18]	3.85 [18]	16.1 [18]	Cu^{4+}/O^{2-}

Table 1: Electrical properties and lattice parameters. The numbers in square brackets give the corresponding references.

Sr_2RuO_4	$k_f(Å^{-1})$	m_{eff}/m_e	Vol_{frac}	$v_e\left[\frac{m}{s}\right]/10^6$	$D_{2D}(E_f)[\frac{1}{eV}]$
α-type	0.302	1.1	0.108	0.318	0.69
β-type	0.621	2	0.457	0.359	1.24
γ-type	0.75	2.9	0.667	0.299	1.80

Table 2: Three types of the Fermi electrons α, β and γ and their electrical properties in Sr_2RuO_4 **[26]**.

Superconductors	$v_e\left[\frac{m}{s}\right]/10^6$	$D(E_f)[\frac{1}{eV}]$	m_{eff}/m_e	Ref.
Al	1.097	1.64	1.4	[8], [19]
Nb	0.273	6.62		[20]
$La_{1.85}Sr_{0.15}CuO_4$	0.314	2.09		[21]
$Bi_2Sr_2CaCu_2O_{8+\delta}$	0.274	2.63		[22], [23]
$YBa_2Cu_3O_{6.9}$	0.250	4.19		[24], [25]

Table 3: Fermi velocity, density of states and effective electron mass.

$HgBa_2Ca_2Cu_3O_{8+\delta}$	$v_e\left[\frac{m}{s}\right]/10^6$	$D(E_f)[\frac{1}{eV}]$
1-type	0.198	0.75
2-type	0.189	0.84
3-type	0.177	1.75

Table 4: Three types of the Fermi electrons and their electrical properties in $HgBa_2Ca_2Cu_3O_{8+\delta}$ **[27]**.

5.5 Force Constants within the CuO_2 and RuO_2 Planes and for the Single Atomic Superconductors Al and Nb

The force constants k_1 and k_2 within the CuO_2 plane for the cuprates are taken from Ref. [8]. The calculation of all force constants in the unit cell of Sr_2RuO_4 will be shown in chapter 6.3.1, which contains the force constants in RuO_2. For the calculation of the frequency by equation 2.18, the effective amount of the force constants in the y direction is required, which is calculated from equations 5.1, 5.2, 5.3 and 5.4. The force constants and the effective amount of the force constants in the y direction are given in table 5 and the calculated frequencies are listed in table 6. For Al and Nb, due to their single atomic structure, the calculation of the force constants is not required, because the Debye frequency can be directly used to calculate the attractive potential energy using equation 2.22.

Superconductors	k_1 (Cu-O/Ru-O)	k_2 (O-O)	$k_{O1,y}$	$k_{O2,y}$	$k_{O3,y}$	$k_{Cu,y}$ / $k_{Ru,y}$
Sr_2RuO_4	172 calc. with PT	57 calc. with PT	505	161	505	344
$La_{1.85}Sr_{0.15}CuO_4$	85 Ref. [28]	20 Ref. [28]	226	56	226	170
$Bi_2Sr_2CaCu_2O_{8+\delta}$	85 Ref. [29]	20 Ref. [29]	226	56	226	170
$YBa_2Cu_3O_{6.9}$	152 Ref. [8]	20 Ref. [8]	360	56	360	304
$HgBa_2Ca_2Cu_3O_{8+\delta}$	111 calc. with PT	20 calc. with PT	278	56	278	222

Table 5: Force constants for oxygen, copper and ruthenium-ion in [N/m]. PT: Potential theory.

Superconductors	ω_D	$\omega_{O1,y}$	$\omega_{O2,y}$	$\omega_{O3,y}$	$\omega_{Cu,y}/\omega_{Ru,y}$
Al	5.54				
Sr_2RuO_4		13.4	7.79	13.4	4.53
Nb	3.63				
$La_{1.85}Sr_{0.15}CuO_4$		9.23	4.61	9.23	4.01
$Bi_2Sr_2CaCu_2O_{8+\delta}$		9.23	4.61	9.23	4.01
$YBa_2Cu_3O_{6.9}$		11.6	4.61	11.6	5.37
$HgBa_2Ca_2Cu_3O_{8+\delta}$		10.2	4.61	10.2	4.59

Table 6: Frequencies for each ion calculated from equation 2.18 and the Debye frequency for the single atomic superconductors Al and Nb calculated from Debye temperature by equation 5.15. All values in 1/s and divided by 10^3.

5.6 Calculation of the Attractive potential Energy V_0 and the Binding Energy Δ

Using equations 5.9, 5.10, 5.11 and 5.12, the attractive potential energy of each ion $V_{0,ion}$ belonging to CuO_2–plane for cuprates (or RuO_2–plane for Sr_2RuO_4) can be calculated. The corresponding total attractive potential V_0 is determined by equation 5.14. For Al and Nb, only equation 2.22 is required for calculation of V_0.

The binding energy Δ of Al, Nb, $La_{1.85}Sr_{0.15}CuO_4$, $Bi_2Sr_2CaCu_2O_{8+\delta}$ and $YBa_2Cu_3O_{6.9}$ can be calculated by equation 2.57. For each of the two superconductors Sr_2RuO_4 and $HgBa_2Ca_2Cu_3O_{8+\delta}$, three types of Fermi electrons have been found [26, 27]. Therefore, equation 2.58 must be applied to determine the binding energy of these two superconductors.

For Sr_2RuO_4, the volume fractions of the three types are also found in the literature. This fraction must be multiplied with the attractive potential energy for each ion $V_{0,i}$ to calculate its contribution to the total attractive potential energy V_0. In Ref. [27] the fraction of each Fermi electron in the unit cell of $HgBa_2Ca_2Cu_3O_{8+\delta}$ has been assumed to be equal to 1 to calculate density of states and Fermi velocity. In the following tables 7 to 12, the calculated values of V_0, $D(E_f)V_0$, $\sum D(E_f)V_0$ and Δ are given for these two superconductors ($HgBa_2Ca_2Cu_3O_{8+\delta}$, Sr_2RuO_4).

Superconductor	$V_{0,ion}$					
Sr_2RuO_4	$V_{0,O1}[eV]$	$V_{0,O2}[eV]$	$V_{0,O3}[eV]$	$V_{0,Ru}[eV]$	Vol_{frac}	$V_0[eV]$
α-type	0.003	0.006	0.004	0.028	0.108	0.041
β-type	0.006	0.012	0.008	0.024	0.457	0.051
γ-type	0.007	0.015	0.010	0.029	0.667	0.061

Table 7: The attractive potential energy of each ion within the RuO_2 plane for each type of Fermi electron α, β and γ in Sr_2RuO_4.

Sr_2RuO_4	$Vol_{frac}V_0[eV]$	$D_{2D}(E_f)[\frac{1}{eV}]$	$D_{2D}(E_f)V_0$	$\sum D_{2D}(E_f)V_0$	Δ [meV]
α-type	0.004	0.69	0.003	0.105	2.44×10^{-7}
β-type	0.023	1.24	0.029		
γ-type	0.041	1.80	0.073		

Table 8: The total attractive potential energy for each type of Fermi electron α, β and γ used for the calculation of the binding energy Δ of the Cooper pairs in Sr_2RuO_4.

Superconductor	$V_{0,ion}$ [eV]				
$HgBa_2Ca_2Cu_3O_{8+\delta}$	$V_{0,O1}[eV]$	$V_{0,O2}[eV]$	$V_{0,O3}[eV]$	$V_{0,Cu}[eV]$	$V_0[eV]$
1-type	0.032	0.063	0.022	0.036	0.041
2-type	0.032	0.064	0.022	0.036	0.051
3-type	0.034	0.068	0.023	0.038	0.061

Table 9: The attractive potential energy of each ion within the RuO_2 plane for each sheet (type) of Fermi electrons in $HgBa_2Ca_2Cu_3O_{8+\delta}$.

$HgBa_2Ca_2Cu_3O_{8+\delta}$	$D(E_f)[\frac{1}{eV}]$	$D(E_f)V_0$	$\sum D(E_f)V_0$	Δ [meV]
1-type	0.75	0.114	0.530	2.66
2-type	0.84	0.129		
3-type	1.75	0.288		

Table 10: The total potential energy for each sheet (type) of Fermi electrons used for the calculation of the binding energy Δ of the Cooper pairs in $HgBa_2Ca_2Cu_3O_{8+\delta}$.

	$V_{0,ion}$ [eV]						
Superconductors	$V_{0,O1}$[eV]	$V_{0,O2}$[eV]	$V_{0,O3}$[eV]	$V_{0,Cu/Ru}$[eV]	V_0[eV]	$D(E_f)[\frac{1}{eV}]$	Δ [meV]
Al					0.052	1.64	4.69×10^{-9}
Nb					0.030	6.62	1.83×10^{-3}
$La_{1.85}Sr_{0.15}CuO_4$	0.022	0.045	0.015	0.026	0.108	2.09	8.61×10^{-3}
$Bi_2Sr_2CaCu_2O_{8+\delta}$	0.025	0.050	0.017	0.029	0.122	2.63	8.65×10^{-3}
$YBa_2Cu_3O_{6.9}$	0.021	0.042	0.014	0.023	0.101	4.19	4.52×10^{-1}

Table 11: The attractive potential energy of each ion within the CuO_2 plane for other cuprates and the single atomic superconductors Al and Nb and their calculated binding energy Δ.

Superconductors	Δ [meV]
Al	4.69×10^{-9}
Sr_2RuO_4	2.44×10^{-7}
Nb	1.83×10^{-3}
$La_{1.85}Sr_{0.15}CuO_4$	8.61×10^{-3}
$Bi_2Sr_2CaCu_2O_{8+\delta}$	8.65×10^{-3}
$YBa_2Cu_3O_{6.9}$	4.52×10^{-1}
$HgBa_2Ca_2Cu_3O_{8+\delta}$	2.66

Table 12: The calculated binding energy Δ.

5.7 Results

There are some simplifications underlying the calculation of the binding energy Δ. Therefore, the calculated values of the binding energy Δ are different from the experimental data. For cuprates and Sr_2RuO_4, it has been assumed that the total attractive potential energy in the unit cell comes only from the CuO_2 and RuO_2 planes which cannot be the case for a large unit cell. It has also been assumed that the ions in the neighbouring cells are fixed; but in reality they are not fixed and, therefore, the attractive potential energy should be different. Furthermore, only the effective force constants in the y direction have been used (equations 5.1, 5.2, 5.3 and 5.4) to determine the frequency of each ion in the planes, by which the attractive potential energy is achieved. In reality, however, the force constants in the x and z direction must also be

considered to determine the exact value of the attractive potential energy and these haven't been taken into account in this simplification.

Consequently, a plot of log(Δ) vs. log(T_c) has been made to show the current trend. From table 12 and figure 20, it can be seen that the larger Δ is, the larger T_c. This trend is what one would expect. This is, then, a motivation to calculate the attractive potential energy by finite element methods, which do not require the simplifications of the theoretical method and, therefore, are more exact.

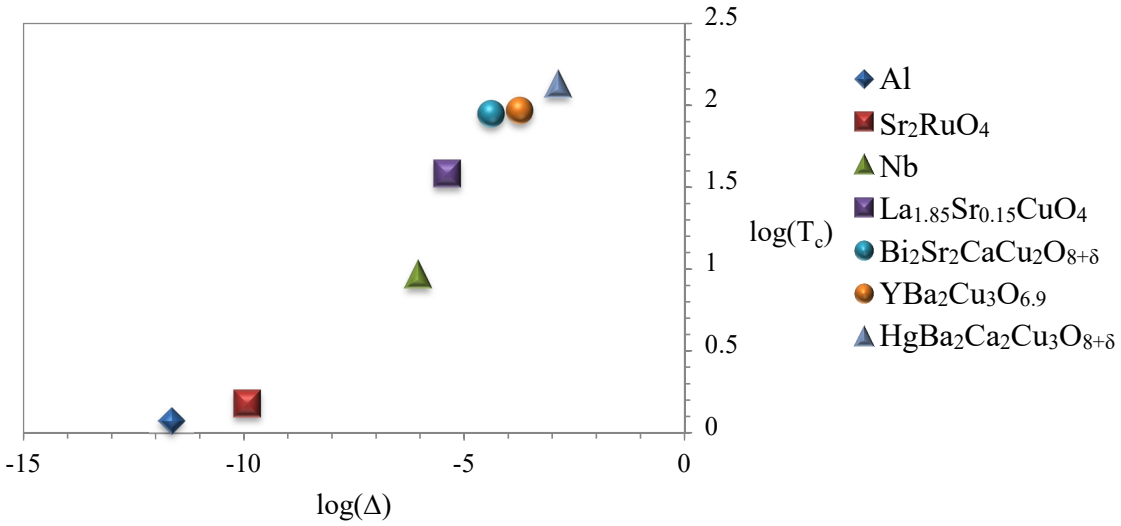

Figure 20: log(T_c) vs. log(Δ) for all superconductors studied.

6 Finite Element Results

As described in the previous chapter, the calculation of the attractive potential energy must be done by another method to find more exact values of the binding energy Δ. To reach this goal, the major FE-code is used to simulate the attractive potential energy V_0 (chapter 4.3). Using the first code, the unit cell of superconductors can be constructed for the simulation (chapter 4.1). This requires knowing the force constants, the mass of the ions in the chemical formula and the coordinates of the ions within the unit cell for each superconductor. The force constants can be calculated with the potential theory or measured by Raman spectroscopy. As described previously, Raman spectroscopy is based on the frequency of the ions in a pair that vibrates about their equilibrium position, whereas in the potential theory the force constants can be calculated from the interactions between the ions in a pair.

The distance between an ion and the Fermi electron changes with time because the Fermi electron moves toward the unit cell. This time-dependent distance can be calculated using the Fermi velocity. Due to the dependence of the Coulomb force on this distance, the Coulomb force depends on the Fermi velocity as well and it is also time-dependent. Furthermore, it is dependent on the charge of the ions. If the Coulomb force between the Fermi electron and an ion is plotted against time, a peak can be seen; the faster the electron, the narrower the peak. The time-dependent Coulomb forces between the Fermi electron and each ion can be calculated with the second code (chapter 4.2).

For validation, it is needed to simulate the attractive potential energy V_0 and calculate the binding energy Δ for the two conventional superconductors Al and Nb because, as it is known, these two superconductors are very well explained by the BCS theory. If the results of the simulation coincide with the experimental results, then the simulation can be used for other superconductors. To calculate these values, the major FE-code must be used, which needs the first and second code.

6.1 Aluminium

Aluminium is a metal element from group 3 in the periodic table, with electron configuration $[Ne]3s^2 3p^1$. Its atomic mass is 26.98u (u = 1.66×10^{-27} kg) and it has three Fermi electrons per atom in its unit cell. The crystal structure of aluminium is fcc (four atoms in the unit cell, figure 18), with the lattice parameter a = 4.05 Å (Ref. [8]). Because there are four aluminium atoms in the unit cell and three Fermi electrons exist for each atom in the unit cell, there are twelve Fermi electrons in the unit cell. Aluminium becomes superconducting at T_c =1.18 K.

6.1.1 Calculation of Force Constants

There are three main directions in the unit cell of the fcc structure: [100], [110] and [111]. The force constants for the three directions can be calculated from Ref. [30]. In this reference, the calculated x, y and z contributions of the force constants for the different directions in the unit cell are given:

Force constant	[N/m]
k_{100}	2.452
$k_{110,x}$ and $k_{110,y}$	10.107
$k_{110,xy}$	11.444
$k_{111,x}$, $k_{111,y}$ and $k_{111,z}$	0.142

Table 13: Force constants for aluminium **[30]**.

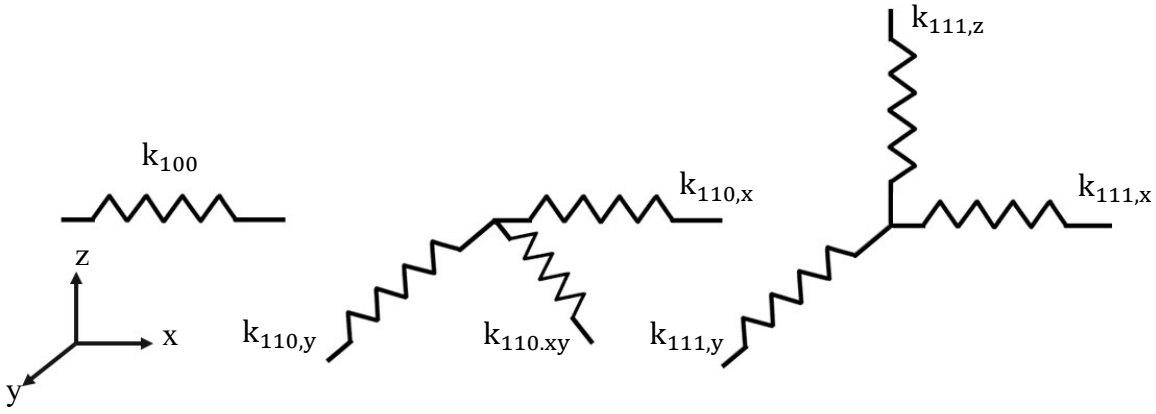

Figure 21: Spring elements of aluminium in different directions.

For the calculation of the total force constant in [110] direction, the values of $k_{110,x}$ and $k_{110,y}$ must be projected onto the [110] direction. This is accomplished by multiplying with $\sqrt{2}/2$. After the projection, the two new force constants are connected in series with each other; the resulting force constant can then be calculated as follows:

$$k_{110,x} \text{ projected in [110] direction} \quad \rightarrow \quad \frac{\sqrt{2}k_{110,x}}{2}\,, \tag{6.1}$$

$$k_{110,y} \text{ projected in [110] direction} \quad \rightarrow \quad \frac{\sqrt{2}k_{110,y}}{2}\,, \tag{6.2}$$

$$k_{110}^{*} = \left(\left(\frac{\sqrt{2}k_{110,x}}{2}\right)^{-1} + \left(\frac{\sqrt{2}k_{110,y}}{2}\right)^{-1}\right)^{-1}\,. \tag{6.3}$$

This has to be added with the given $k_{110,xy}$ from table 13, since together they build a parallel system:

$$k_{110,total} = k_{110}^{*} + k_{110,xy}\,. \tag{6.4}$$

The total force constant for the [111] direction can be calculated by the projection of the three force constants $k_{111,x}$, $k_{111,y}$ and $k_{111,z}$ onto the [111] direction. The three resulting force constants are connected in series. The total force constant can, therefore, be calculated as follows:

$$k_{111,x} \text{ projected in [111] direction} \quad \rightarrow \quad \frac{\sqrt{3}k_{111,x}}{3}\,, \tag{6.5}$$

$$k_{111,y} \text{ projected in [111] direction} \quad \rightarrow \quad \frac{\sqrt{3}k_{111,y}}{3}\,, \tag{6.6}$$

$$k_{111,z} \text{ projected in [111] direction} \quad \rightarrow \quad \frac{\sqrt{3}k_{111,z}}{3}\,, \tag{6.7}$$

$$k_{111} = \left(\left(\frac{\sqrt{3}k_{111,x}}{3}\right)^{-1} + \left(\frac{\sqrt{3}k_{111,y}}{3}\right)^{-1} + \left(\frac{\sqrt{3}k_{111,z}}{3}\right)^{-1}\right)^{-1}\,. \tag{6.8}$$

The calculated force constants are given in the following table.

Force constant	[N/m]
k_{100}	2.452
k_{110}	15.017
k_{111}	0.027

Table 14: The calculated force constants for aluminium.

6.1.2 Calculation of Coulomb Forces

The Coulomb force acting on the aluminium ions in the unit cell must be calculated. Thus, it is important to choose a direction for the movement of the electron. For the purpose of the simulations performed in this work, the [100] direction is taken (equivalent to [010] and [001]). The paths for the movement of four electrons in the (001) plane in the unit cell of aluminium are shown in figure 22. For the calculation of Coulomb forces, it is assumed that all electrons start 30 units cells away from the one being analyzed. For example, for two electrons e_1 and e_2 moving on the plane (001) in the [100] direction in figure 22, the coordinates $\mathbf{r_{e,1}}(t)$ and $\mathbf{r_{e,2}}(t)$ of both electrons can be calculated using equations 6.9 and 6.10 below, where v_e is the Fermi velocity, t is the time and a is the lattice parameter. There are four paths for every four electrons in each plane of the unit cell (figure 22). Because the unit cell consists of 6 planes and there are 4 electrons on each plane, there are 24 electrons in all planes of the unit cell. But because only half of all electrons on each plane belongs to the unit cell, there are in total twelve electrons in the unit cell (figure 22), which come from the four Al ions in the cell. Table 15 lists the coordinates of all electrons in the different planes and directions.

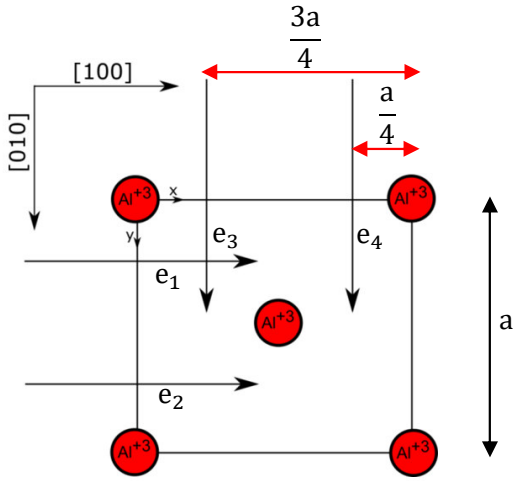

Figure 22: Paths of electrons moving in the (100) plane in the unit cell of aluminium (movement in the [100] and [010] directions).

$$\mathbf{r_{e,1}}(t) = \left(30a - tv_e\,, \frac{a}{4}\,, 0\right)\,, \tag{6.9}$$

$$\mathbf{r_{e,2}}(t) = \left(30a - tv_e\,, \frac{3a}{4}, 0\right)\,. \tag{6.10}$$

$\mathbf{r_{e,j}}(t)$	Coordinate	plane direction	$\mathbf{r_{e,j}}(t)$	Coordinate	plane direction
$\mathbf{r_{e,1}}(t)$	$(30a - tv_e\,, \frac{a}{4}\,, 0)$	(001) [100]	$\mathbf{r_{e,13}}(t)$	$(30a - tv_e, a, \frac{a}{4})$	(020) [100]
$\mathbf{r_{e,2}}(t)$	$(30a - tv_e\,, \frac{3a}{4}\,, 0)$	(001) [100]	$\mathbf{r_{e,14}}(t)$	$(30a - tv_e, a, \frac{3a}{4})$	(020) [100]
$\mathbf{r_{e,3}}(t)$	$(\frac{a}{4}\,, 30a - tv_e\,, 0)$	(001) [010]	$\mathbf{r_{e,15}}(t)$	$(\frac{a}{4}, a, 30a - tv_e)$	(020) [001]
$\mathbf{r_{e,4}}(t)$	$(\frac{3a}{4}\,, 30a - tv_e\,, 0)$	(001) [010]	$\mathbf{r_{e,16}}(t)$	$(\frac{3a}{4}, a, 30a - tv_e)$	(020) [001]
$\mathbf{r_{e,5}}(t)$	$(30a - tv_e\,, \frac{a}{4}\,, a)$	(002) [100]	$\mathbf{r_{e,17}}(t)$	$(0, \frac{a}{4}, 30a - tv_e)$	(100) [001]
$\mathbf{r_{e,6}}(t)$	$(30a - tv_e\,, \frac{3a}{4}\,, a)$	(002) [100]	$\mathbf{r_{e,18}}(t)$	$(0, \frac{3a}{4}, 30a - tv_e)$	(100) [001]
$\mathbf{r_{e,7}}(t)$	$(\frac{a}{4}\,, 30a - tv_e\,, a)$	(002) [010]	$\mathbf{r_{e,19}}(t)$	$(0, 30a - tv_e, \frac{a}{4})$	(100) [001]
$\mathbf{r_{e,8}}(t)$	$(\frac{3a}{4}\,, 30a - tv_e\,, a)$	(002) [010]	$\mathbf{r_{e,20}}(t)$	$(0, 30a - tv_e, \frac{3a}{4})$	(100) [001]
$\mathbf{r_{e,9}}(t)$	$(30a - tv_e, 0, \frac{a}{4})$	(010) [100]	$\mathbf{r_{e,21}}(t)$	$(a, \frac{a}{4}, 30a - tv_e)$	(200) [001]
$\mathbf{r_{e,10}}(t)$	$(30a - tv_e, 0, \frac{3a}{4})$	(010) [100]	$\mathbf{r_{e,22}}(t)$	$(a, \frac{3a}{4}, 30a - tv_e)$	(200) [001]
$\mathbf{r_{e,11}}(t)$	$(\frac{a}{4}, 0, 30a - tv_e)$	(010) [001]	$\mathbf{r_{e,23}}(t)$	$(a, 30a - tv_e, \frac{a}{4})$	(200) [001]
$\mathbf{r_{e,12}}(t)$	$(\frac{3a}{4}, 0, 30a - tv_e)$	(010) [001]	$\mathbf{r_{e,24}}(t)$	$(a, 30a - tv_e, \frac{3a}{4})$	(200) [001]

Table 15: Coordinates of electrons in the different planes and directions for aluminium.

The distance between the ion i in the unit cell and the electron j can be determined by the following equation, where $\mathbf{r_i}$ is the coordinate of the ion i.

$$|\mathbf{r_i} - \mathbf{r_{e,j}}|(t) = \sqrt{(x_i - x_{e,j})^2 + (y_i - y_{e,j})^2 + (z_i - z_{e,j})^2}\,. \qquad (6.11)$$

Now, the Coulomb force between the ion i and the electron j can be calculated with equation 6.12. To calculate the total Coulomb force exerted by all electrons acting on the ion i, a sum must be used (equation 6.13). This mathematically complex process of finding the Coulomb forces for each ion has been performed with the second code described in chapter 4.2. Figure 23 shows the curve of the calculated Coulomb force as a function of time for a certain aluminium ion. As seen from figure 23, the Coulomb force is only effective when the electron is located very close to the unit cell. This is because of the inverse dependence of the Coulomb force on $|\mathbf{r_i} - \mathbf{r_{e,j}}|^2$. The Coulomb force in figure 23 is not symmetric because it comes from 24 electrons moving on different electron paths.

$$F_{i,j} = \frac{3e^2}{4\pi\varepsilon_0 |\mathbf{r_i} - \mathbf{r_{e,j}}|^2}\,, \qquad (6.12)$$

$$F_i = \sum_{j=1}^{24} F_{i,j}\,. \qquad (6.13)$$

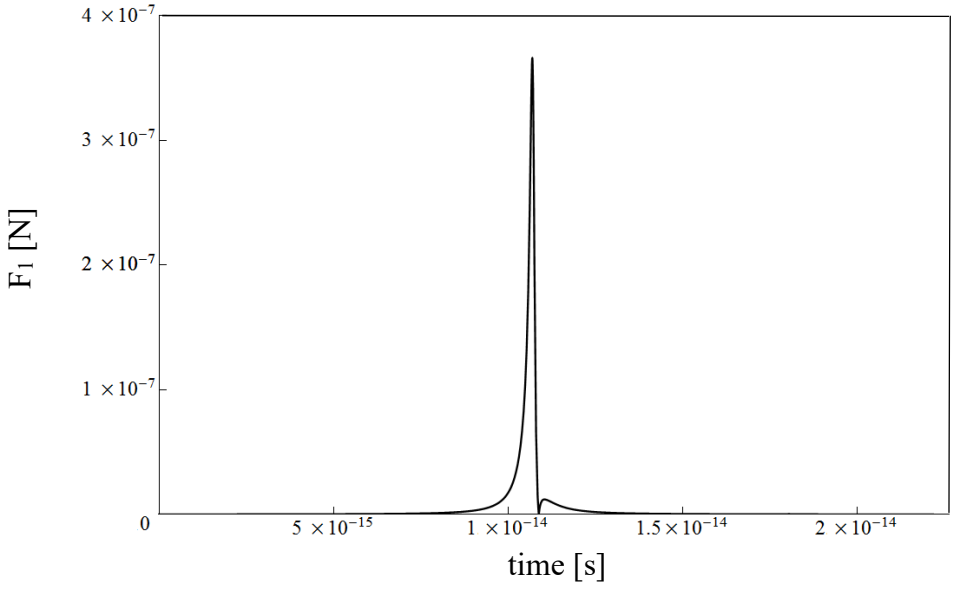

Figure 23: The Coulomb force between an aluminium ion and all considered moving electrons in the unit cell for the time it takes for an electron to move through 60 unit cells with the Fermi velocity.

6.1.3 Simulation of the Attractive Potential Energy V_0 and the Binding Energy Δ

Once the force constants for aluminium have been calculated, the unit cell is constructed by first code (chapter 4.1) according to the crystal symmetry, the mass of the ions and the force constants. After calculating the Coulomb forces by the second code, the major FE-code can be used to calculate the attractive potential energy. The attractive potential energy $V_{0,i}$ for each ion is the sum of the simulated kinetic energy K_i and the simulated potential energy P_i of each ion at each time (equation 6.14). For the ions located on the corners of the unit cell, 1/8 amount of their attractive potential energy must be considered because only 1/8 of each of these ions belongs to the unit cell. For the ions which are located in the planes of the unit cell, only 1/2 ion belongs to the unit cell, therefore, 1/2 amount of their attractive potential energy must be considered for the total attractive potential energy V_0 in the unit cell. There are eight ions in the corner and six ions in the middle of the planes of the unit cell. Therefore, the total attractive potential energy can be calculated with equation 6.15, where a_i stands for the amount of each ion belonging to the unit cell.

$$V_{0,i} = P_i + K_i \ , \tag{6.14}$$

$$V_0 = \sum_{i=1}^{14} a_i V_{0,i} \qquad a_i = \frac{1}{2} \text{ or } \frac{1}{8} \ . \tag{6.15}$$

As the electron moves through the unit cell, the ions in the unit cell begin to vibrate; since damping is not being considered in the simulation, this vibration doesn't stop. The total vibration energy of all the ions involved in the simulation is, thus, a constant once the electron has left the area of interest. But only the energy of those ions belonging to the unit cell has been considered to calculate the total attractive potential energy V_0 (equation 6.15). This is not a constant value, since there is a transfer of energy between the ions in the considered cell and the ones surrounding it in neighboring unit cell and this amount of transfer energy has not been considered for the total attractive potential energy. For the following calculation, therefore, the mean value of the total attractive potential energy for all ions in the unit cell under consideration is used.

The obtained simulated potential energy P, kinetic energy K and total attractive potential energy V_0 of the unit cell are shown in figure 24 as a function of time. The mean value of the total attractive potential energy can be found by extrapolating the fitted dotted line in figure 24 until

it intersects the axis and is $V_0 = 5.093$ eV. The slight slope of the line is attributed to numerical error. An example for the displacement of the ions at a given time can be seen in figure 25.

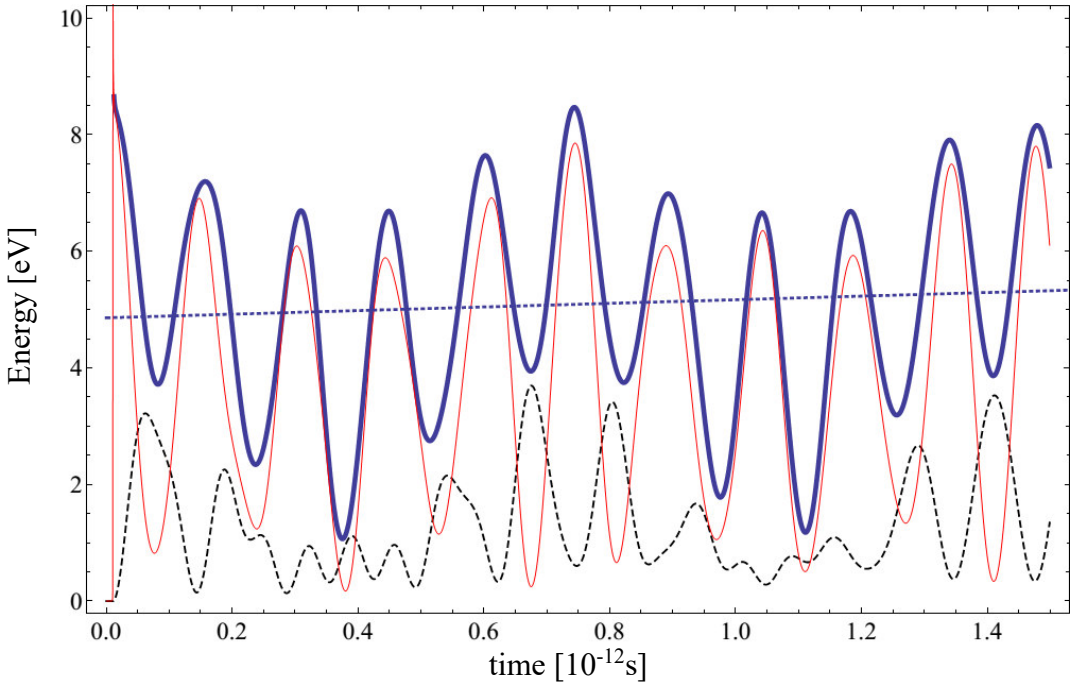

Figure 24: Energy of the ions belonging to the considered unit cell. Blue curve: attractive potential energy V_0; red curve: kinetic energy K; dashed curve: potential energy P. The dotted line shows the mean value.

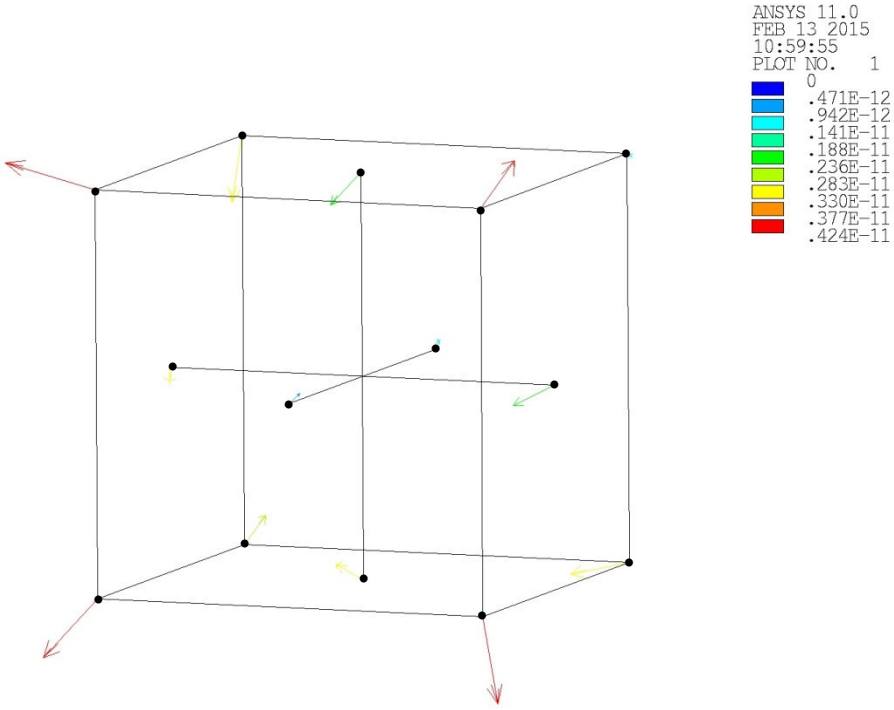

Figure 25: Vector plot of the displacement of the ions in the unit cell at a given time. • stands for aluminium ions.

As previously explained, there are 24 electrons in the unit cell of aluminium. For the calculation of the binding energy Δ with equation 2.57, the attractive potential energy caused by only one electron must be used. Therefore, the total attractive potential energy V_0 = 5.093 eV must be divided by 24 which yields a value of 0.2121 eV because, for the calculation of the binding energy Δ, only the total attractive potential energy V_0 per one electron is required. The superconducting constant c can then be calculated with equation 2.59. The results are given in table 16.

The calculated values for the binding energy Δ and the superconducting constant c are about half of those given in Ref. [8]. This can be partly attributed to the simplified model used for the simulation, but also to the fact that the simulation of the attractive potential energy V_0 is based on theoretical values of the force constants. Their real values can be different, therefore, introducing additional inaccuracies when comparing calculated results with the real, measured ones.

			calculated		Ref. [8]	
Superconductor	$D(E_f)[\frac{1}{eV}]$	$V_0[eV]$	Δ [meV]	c	Δ [meV]	c
Al	1.64	0.2121	0.09	1.695	0.35	3.4

Table 16: Density of states $D(E_f)$, attractive potential energy V_0, binding energy Δ and superconducting constant c for aluminium. The density of states is taken from Ref. **[19]**.

6.2 Niobium

Niobium is a transition metal from group VA in the periodic table with electronic configuration [Kr]$4d^4 5p^1$ and atomic mass 92.91u. According to the orbital theory, it has one Fermi electron per atom in the unit cell. The crystal structure of niobium has a bcc structure with lattice parameter a = 3.30 Å (Ref. [8]), with two niobium atoms belonging to the unit cell (figure 18). Because there are in total two atoms in the unit cell and each of them possesses only one Fermi electron, there are two Fermi electrons in the unit cell in total. For niobium there are different references giving different types of Fermi electrons with different values of the Fermi velocities and the density of states (table 17 and 18). Niobium becomes superconducting at 9.26 K. [8]

Ref. [20]	$v_e \left[\frac{m}{s}\right] / 10^6$	$D(E_f)[\frac{1}{eV}]$
avg.	0.273	6.62

Table 17: Average Fermi velocity and density of states of the Fermi electrons in niobium.

Ref. [31]	$v_e \left[\frac{m}{s}\right] / 10^6$	$D(E_f)[\frac{1}{eV}]$
ELL	0.35	2.5
OCT	0.81	1.09
Jung	0.28	3.15

Table 18: Three types of Fermi electrons for niobium, their Fermi velocities and densities of states.

6.2.1 Calculation of Force Constants

As for the fcc structure of aluminium, the three directions [100], [110], and [111] are used as the main directions for the bcc structure. To calculate the force constants, the amount of each force constant calculated with the potential theory from Ref. [32] is required. The results are shown in table 19.

Force constant	[N/m]
k_{100}	13.330
$k_{110,x}$ and $k_{110,y}$	2.505
$k_{110,xy}$	1.241
$k_{111,xy}$	9.951
$k_{111,x}$, $k_{111,y}$ and $k_{111,z}$	13.182

Table 19: Force constants for niobium **[32]**.

Like aluminium, the projections of the force constants $k_{110,x}$ and $k_{110,y}$ in the [110] direction are needed. The two new projections are connected in series with each other which results in a new force constant k^*_{110}, connected in parallel to $k_{110,xy}$. Then, the total force constant k_{110} is calculated using the following equations:

$$k_{110,x} \text{ projected in [110] direction} \quad \rightarrow \quad \frac{\sqrt{2}k_{110,x}}{2}\,, \tag{6.16}$$

$$k_{110,y} \text{ projected in [110] direction} \quad \rightarrow \quad \frac{\sqrt{2}k_{110,y}}{2}\,, \tag{6.17}$$

$$k^*_{110} = \left(\left(\frac{\sqrt{2}k_{110,x}}{2}\right)^{-1} + \left(\frac{\sqrt{2}k_{110,y}}{2}\right)^{-1}\right)^{-1}\,, \tag{6.18}$$

$$k_{110} = k^*_{110} + k_{110,xy}\,. \tag{6.19}$$

For the [111] direction, after the projection of each force constant $k_{111,x}$, $k_{111,y}$ in [110] direction, the two new projections are connected in series to each other. The new force constant $k^*_{111,xy}$, which is coming from these two force constant projections, is parallel to the force constant $k_{111,xy}$. Therefore, the sum of the force constants $k_{111,xy}$ and $k^*_{111,xy}$ is required and its result is called $k_{111,xy,tot}$. To have the projection of the force constant $k_{111,xy,tot}$ in the [111] direction, its values must be multiplied by $\sqrt{2}/\sqrt{3}$. Now, this projected force constant is connected in series to the projection of the force constant $k_{111,z}$ in the [111] direction. Below, the total force constant k_{111} in [111] direction is calculated as described above. The calculated force constants for each direction for niobium are given in table 20.

$$k_{111,x} \text{ projected in [110] direction} \quad \rightarrow \quad \frac{\sqrt{2}k_{111,x}}{2}\,, \tag{6.20}$$

$$k_{111,y} \text{ projected in [110] direction} \quad \rightarrow \quad \frac{\sqrt{2}k_{111,y}}{2}\,, \tag{6.21}$$

$$k^*_{111,xy} = \left(\left(\frac{\sqrt{2}k_{111,x}}{2}\right)^{-1} + \left(\frac{\sqrt{2}k_{111,y}}{2}\right)^{-1}\right)^{-1}\,, \tag{6.22}$$

$$k_{111,xy,tot} = k^*_{111,xy} + k_{111,xy}\,, \tag{6.23}$$

$k_{111,xy,tot}$ projected in [111] direction → $\frac{\sqrt{2}k_{111,xy,tot}}{\sqrt{3}}$, (6.24)

$k_{111,z}$ projected in [111] direction → $\frac{\sqrt{2}k_{111,z}}{2}$, (6.25)

$$k_{111} = \frac{\sqrt{2}k_{111,z}}{2} + \frac{\sqrt{2}k_{111,xy,tot}}{\sqrt{3}} \ . \quad (6.26)$$

Force constant	[N/m]
k_{100}	13.330
k_{110}	2.127
k_{111}	4.647

Table 20: The calculated force constants for each direction in the unit cell of niobium.

6.2.2 Calculation of Coulomb Forces

As for aluminium, the three equivalent directions [100], [010] and [001] for the movement of the electron have been considered to calculate the Coulomb forces on each ion in the unit cell (figure 26). As explained in the previous chapter, there are two electrons in the unit cell of niobium. In order to have two electrons in the unit cell moving in the [100] direction, one electron must move in each of the (001), (010), (002) and (020) planes (only 1/2 of each electron in the planes belongs to the unit cell; therefore, there is a total of two electrons in the unit cell). The coordinate $\mathbf{r_{e,j}}(t)$ of electron j calculated in a similar manner to aluminium, resulting in table 21.

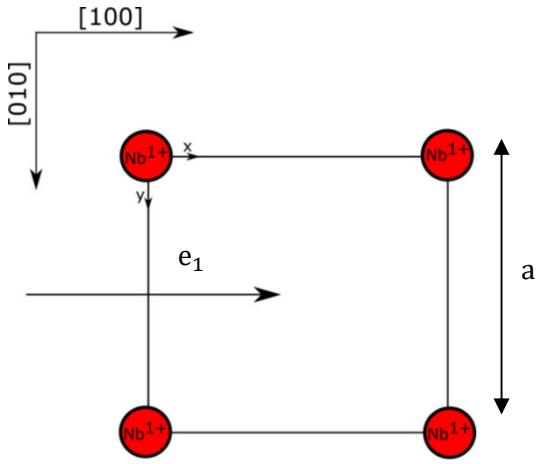

Figure 26: Path of the electron moving in the (100) plane in the unit cell of niobium.

$\mathbf{r_{e,j}}(t)$	Coordinate	Moving plane Moving direction
$\mathbf{r_{e,1}}(t)$	$(30a - tv_e, \frac{a}{2}, 0)$	(001) [100]
$\mathbf{r_{e,2}}(t)$	$(30a - tv_e, \frac{a}{2}, a)$	(002) [100]
$\mathbf{r_{e,3}}(t)$	$(30a - tv_e, 0, \frac{a}{2})$	(010) [100]
$\mathbf{r_{e,4}}(t)$	$(30a - tv_e, a, \frac{a}{2})$	(020) [100]

Table 21: Coordinates of the electrons in the different planes and directions of niobium.

Now, since the distance between the Fermi electron and each ion (equation 6.11) depends on the Fermi velocity, so do the Coulomb forces as well. In table 18, there are three Fermi velocities for the three types of Fermi electrons and there is an average Fermi velocity for the Fermi electrons in table 17. The Coulomb force can be calculated like aluminium. However, equation 6.13 must be rewritten for four electrons, because the total Coulomb force between each ion in the unit cell and the four electrons must be calculated as follows:

$$F_i(t) = \sum_{j=1}^{4} F_{i,j} \ . \qquad (6.27)$$

6.2.3 Simulation of the Attractive Potential Energy V_0 and the Binding Energy Δ

As described for aluminium, the amount of each ion belonging to the unit cell is required in order to calculate the total attractive potential energy V_0. There are 8 ions on the corners and an ion in the middle of the unit cell. 1/8 of each ion located on the corner belongs to the unit cell. The attractive potential energy of each ion $V_{0,i}$ is given by equation 6.14; for the total attractive potential energy equation 6.15 must be rewritten for eight ions on the corners and an ion in the middle of the unit cell which results equation 6.28. As described for aluminium in chapter 6.1.3 it must be noted that the total attractive energy V_0 must be divided by four because it should be calculated only for one electron.

$$V_0 = \sum_{i=1}^{9} a_i V_{0,i} \qquad a_i = \frac{1}{8} \text{ or } 1 \ . \qquad (6.28)$$

The simulation has been carried out for each of the three types of Fermi electrons to find its corresponding potential energy (table 22). The attractive potential energy $V_{0,OCT}$ belonging to the OCT type is very low due to its high Fermi velocity (there is no enough time for the ions to feel the Coulomb forces because of its high Fermi velocity). Therefore, the electron pairing can only occur among the two other types of Fermi electrons (ELL and Jung) due to their higher attractive potential energies $V_{0,ELL}$ and $V_{0,Jung}$. The total binding energy Δ_t and the total superconducting constant c_t are given in table 23 and are calculated by equation 2.58 and 2.59 respectively. The value of 0.632 for the total superconducting constant c_t is much smaller than the given value of 3.8 given in Ref. [8]. Therefore, the simulation was performed once again

for the average Fermi velocity and density of states from the Ref. [20] which is given in table 17. The results are given in table 24. The calculated value for the superconducting constant c coming from the electron properties of Ref. [20] is 2.36 which is not far from 3.8. However, it must be noted that these values for the Fermi velocity and the density of states are only theoretically calculated. It's not expected for them to correspond exactly to reality, which can account for the difference between the calculated values (Δ and c) and 3.8.

According to the results obtained from the simulation of the two conventional superconductors Al and Nb, the finite element method can also be used to calculate the binding energy Δ and the superconducting constant c for other superconductors to investigate whether these superconductors can be explained by the BSC theory.

type	$v_e\left[\frac{m}{s}\right]/10^6$	$D(E_f)[\frac{1}{eV}]$	$V_0[eV]$	Δ [meV]	c
ELL	0.35	2.5	0.056	0.000016	0.00004
OCT	0.81	1.09	0.011	9.49×10^{-74}	2.38×10^{-73}
Jung	0.28	3.15	0.091	0.02	0.05

Table 22: Attractive potential energy V_0, binding energy Δ and superconducting constant c for the three types of Fermi electrons with electrical properties according to **[31]**.

$\sum D(E_f)V_0$	Δ_t [meV]	c_t
0.438	0.25	0.632

Table 23: Total binding energy Δ_t and total superconducting constant c_t for Fermi electrons.

$v_e\left[\frac{m}{s}\right]/10^6$	$D(E_f)[\frac{1}{eV}]$	$V_0[eV]$	Δ [meV]	c
0.273	6.62	0.09	0.94	2.36

Table 24: Attractive potential energy V_0, binding energy Δ and superconducting constant c for Fermi electrons with average electrical properties according to **[20]**.

6.3 Sr_2RuO_4

Sr2RuO4 exhibits spin-triplet superconductivity (spin-triplet: two electrons in an electron pair have the same spin +1/2 and +1/2 and so the total electron spin number is 1. The degeneracy equals 2S+1, where S is the total spin number. The degeneracy of this pair is 3 and, therefore, it is called spin triplet. Unconventional superconductors indicate spin-triplet pairing) and consequently, it is an unconventional superconductor with the critical temperature T_c= 1.5 K [33]. It has a tetragonal structure with I4/mmm symmetry and lattice parameters a, b = 3.87 Å and c = 12.7 Å [14]. There are two chemical formulas in the unit cell of Sr2RuO4. An undistorted octahedral RuO6 can be found in its middle (figure 18). It seems that the RuO_2 planes play an important role regarding superconductivity [34]. Its Debye temperature is about 312 K [13]. The electronic band structure of Sr_2RuO_4 is quasi-two-dimensional because of its layered structure, which prevents the overlap of the orbitals along the c-axis [35]. Its Fermi surface consists of three sheets corresponding to three different types of Fermi electrons: α, β and γ (figure 27). It is believed that the γ electrons are responsible for the superconductivity [36, 37]. The β electrons are also relevant. Ref. [38] gives binding energies of Δ_β= 0.045 meV and Δ_γ= 0.15 meV for the β and γ electrons. According to Ref. [39], the binding energy of Δ_γ is 0.14 meV, which corresponds to the BCS theory. A range for the superconducting constant c between 6.2 and 8 has been measured, whereby the superconductivity of Sr_2RuO_4 exhibits an anisotropic behaviour (with the average superconducting constant being c_{av}= 5.5) [40].

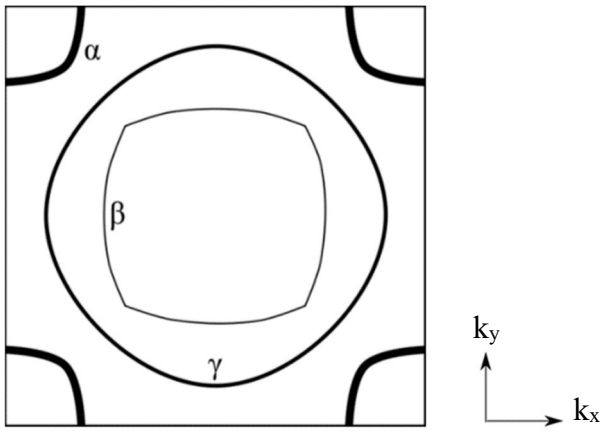

Figure 27: The Fermi surface of Sr_2RuO_4 with three different sheets α, β and γ. k_x and k_y are the wave vectors in x and y direction.

Sr_2RuO_4	$k_f(Å^{-1})$	m_{eff}/m_e	$v_e\left[\frac{m}{s}\right]/10^6$	$D_{2D}(E_f)[\frac{1}{eV}]$
α-type	0.302	1.1	0.318	0.69
β-type	0.621	2.0	0.359	1.24
γ-type	0.750	2.9	0.299	1.80

Table 25: The three types of the Fermi electrons α, β and γ and their electrical properties in Sr_2RuO_4 **[26]**.

6.3.1 Calculation of Force constants

The force constants for some ionic pairs in the unit cell of Sr_2RuO_4 have been calculated from Raman spectroscopy in Ref. [41]. To get other force constants in the unit cell, a calculation with the potential theory (chapter 2.4.1) is required. To do that, the potential parameters, the charge of each component and spring constant between the shell and the core of an ion are needed, as which are given in table 26 and 27. OI stands for the oxygen ion located in the RuO_2 plane whereas the OII is the apical oxygen ion in the unit cell (figure 18).

Pair	A[eV]	ρ[Å]	$A[eV/Å^6]$
Sr-OI	1825	0.318	
Sr-OII	2250	0.318	
Ru-OI	2999	0.260	
Ru-OII	3874	0.260	
OI-OI	2000	0.284	-100
OI-OII	2000	0.284	-100
OII-OII	2000	0.284	-100

Table 26: The potential parameters for each ionic pair **[42]**.

Ion	Z	q_{shell}	k[N/m]
Ru	2.58	0.47	8000/2000
Sr	2	5.86	3600
OI	-1.52	-3.25	1800
OII	-1.77	-2.77	1800

Table 27: The charge of the shell q_{shell} and the total ion charge Z and the inner spring constant for each ion **[42]**.

Due to the fact that only the value of the equilibrium distance between the whole ions of each ionic pair is available, only the Coulomb interaction between the whole ions can be considered instead of the Coulomb interactions between all components of ions (shells and cores). Therefore, equations 2.60, 2.61 and 2.62 must be rewritten only for two whole ions as follows:

$$V_{coul} = \frac{Z_i Z_j}{4\pi\varepsilon_0 r_{ij}} \ , \tag{6.29}$$

$$V_{VW} = -C r_{ij}^{-6} \ , \tag{6.30}$$

$$V_{short} = A \exp\left(-\frac{r_{ij}}{\rho}\right) \ , \tag{6.31}$$

where Z_i and Z_j are the total charges of the ions. The total potential interaction is calculated as the sum of these interactions. Since two whole ions are assumed for the calculation (instead of shells and cores), no polarization can be considered, and the term V_{pol} disappears. Due to the consideration of whole ions ($i = 1$ and $j = 2$) instead of shells and cores, there is only an equilibrium distance r_{eq} between the ions of an ionic pair. Using the equilibrium distance r_{eq} in the second derivative of the total potential interaction with respect to r_{ij} (equation 6.32), the force constants can be calculated with equation 6.33. The results are given in table 28.

$$\frac{\partial^2 V_{tot}}{\partial^2 r_{ij}} = \frac{Z_i Z_j r_{ij}}{2\pi\varepsilon_0 {r_{ij}}^3} - 42C{r_{ij}}^{-8} + \frac{A}{\rho^2}\exp\left(-\frac{r_{ij}}{\rho}\right) \ , \tag{6.32}$$

$$i = 1 \text{ and } j = 2 \ ,$$

$$k_{12}(r_{eq}) = \frac{Z_1 Z_2 r_{eq}}{2\pi\varepsilon_0 {r_{eq}}^3} - 42C{r_{eq}}^{-8} + \frac{A}{\rho^2}\exp\left(-\frac{r_{eq}}{\rho}\right) \ . \tag{6.33}$$

Pair	r_{eq}[Å]	Force constant [N/m]	Ref./Calculated
Sr-OI	2.687	64	Ref. [41]
Sr-OII	2.736	21	Ref. [41]
Ru-OI	a	173	calculated
Ru-OII	a_I	90	calculated
OI-OI	$\sqrt{2}a_I$	57	calculated
OI-OII	$\sqrt{{a_I}^2 + {a_{II}}^2}$	67	calculated
OII-OII	a	21	calculated

Table 28: Equilibrium distance r_{eq}[Å] for each ionic pair and its force constant as calculated with the potential theory as well as taken from Ref. **[41]**. a_I=1.93 Å, a_{II}=2.06 Å and a is the lattice parameter.

6.3.2 Calculation of Coulomb Forces

Because the RuO_2 planes play an important role for the superconductivity, it is assumed that the charge carriers move in this plane. As shown in figure 28, the path of the movement of the electron goes between the O1 and O2 atoms. So, by calculating the distance between the moving electron and each ion in the unit cell, the Coulomb force can be calculated for each ion in the same manner as for Al and Nb in the previous chapters.

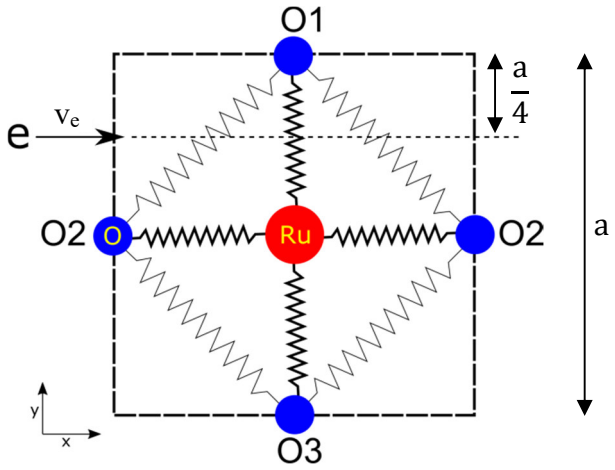

Figure 28: Path of the moving electron in the RuO_2 plane.

6.3.3 Simulation of the Attractive Potential Energy V_0 and the Binding Energy Δ

The simulation is performed for the three different types of Fermi electrons α, β and γ. The results for the attractive potential energies are given in table 29. The fractional volume $\mathrm{Vol_{frac}}$ corresponding to each type in the unit cell is also given in table 29. The amount of each type of Fermi electrons can be considered according to $\mathrm{Vol_{frac}}$. Multiplying $\mathrm{Vol_{frac}}$ with the attractive potential energy caused by each type of Fermi electrons, the amount of the attractive potential energy for each type is determined, which allows the calculation of the binding energy and the superconducting constant for each type. Considering the results for the superconducting constants in table 29, it becomes obvious that the γ type plays the main role regarding superconductivity, since its binding energy and superconducting constant are the greatest. Due to the very small binding energies of the two other types, it can be assumed that the total binding energy and the total superconducting constant are equal to those of the γ electrons. This result coincides with those of Ref. [43] and [44], which state that the γ electrons should be responsible for superconductivity. The binding energy $\Delta_\gamma = 0.16$ meV is close to the measured values of Ref. [45] and [39] (table 30). There are two reasons why the binding energy Δ_γ is larger than the other two in the simulations are the following. Firstly, the Fermi velocity of the γ electrons is lower than that of the α and β electrons, therefore, the acting time of the Coulomb force due to the γ electrons on each ion in the unit cell is larger than for the others, which leads to a larger attractive potential energy V_0. Secondly, the density of states of the γ electrons is larger, increasing the binding energy Δ due to its exponential dependence on the value of $D(E_f)V_0$ (equation 2.57).

Sr_2RuO_4	$v_e\left[\frac{m}{s}\right]/10^6$	$D_{2D}(E_f)[\frac{1}{eV}]$	$\mathrm{Vol_{frac}}$	V_0[eV]	$\mathrm{Vol_{frac}}V_0$[eV]	Δ [meV]	c
α-type	0.318	0.69	0.108	0.03	0.003	1.13×10^{-40}	≈ 0
β-type	0.359	1.24	0.457	0.1	0.046	2.08×10^{-6}	4×10^{-5}
γ-type	0.299	1.80	0.667	0.22	0.147	0.16	2.43

Table 29: Electrical properties, volume fraction $\mathrm{Vol_{frac}}$, simulated attractive potential energy V_0, binding energy Δ_0 and superconducting constant c for each type of Fermi electrons α, β and γ **[26]**.

calculated	Δ_γ= 0.16 meV
Ref. [38]	Δ_γ= 0.15 meV
Ref. [46]	Δ = 0.14 meV

Table 30: Comparison between the calculated and measured binding energy Δ.

6.4 $La_{1.85}Sr_{0.15}CuO_4$ (LSCO)

$La_{1.85}Sr_{0.15}CuO_4$ is one of the high temperature superconductor cuprates, with the critical temperature $T_c = 38$ K, a tetragonal structure with I4/mmm symmetry (figure 19) and lattice parameters a, b $= 3.78$ Å and $c = 13.2$ Å [15]. Its Debye temperature lies around 360 [8]. The unit cell consists of two chemical formulas. La_2CuO_4 is the parent compound that is antiferromagnetic and a semiconductor at low temperatures (to about 30 K) [47]. Its semiconductor properties can be due to the phase transition of the crystal structure to the monoclinic structure that gives rise to an energy gap [47, 48]. To see the superconductivity in La_2CuO_4, this parent compound must be doped by Ba or Sr atoms which bring charged holes into the crystal structure. The critical temperature T_c of the doped structure increases with increasing doping up to an optimal doping amount $x = 0.15$, at which the maximal critical temperature $T_c = 38$ K is reached. By overdoping, the superconductivity disappears. In contrast to Sr_2RuO_4, the octahedral CuO_6 of La_2CuO_4 located in the middle of the unit is distorted. In cuprates, it has been established that the superconductivity is induced by the CuO_2 planes. The physical properties of the cuprates change depending on the number of charge carriers on this plane [34]. It has been found that the doped holes are located in the oxygen-2p orbital in hole-doped cuprates whereas the doped carriers in electron-doped cuprates sit at the cupper-3d orbitals [49]. The calculated values for the density of states $D(E_f)$ and the Fermi velocity v_e for $La_{1.85}Sr_{0.15}CuO_4$ are given in table 3. The different measured superconducting constants, binding energies and critical temperatures are listed in table 31.

T_c[K]	Δ [meV]	c	Ref.	
33		8.9±0.2	[50]	BCS-like
38	2.45 to 4.9	3 to 6	[51]	
38	4	5.2	[52]	BCS-like

Table 31: Critical temperature, superconducting constant and binding energy.

6.4.1 Force Constants

The force constants in the unit cell of $La_{1.85}Sr_{0.15}CuO_4$ have been measured by Raman spectroscopy [28] and are given in table 32.

Pair	Force constant [N/m]
Cu-OI	85
Cu-OII	20
La-OI	160
La-OII *	105
La-OII	50
La-La	30
La-Cu	10
OI-OI	20
OI-OII	4
OII-OII	7

Table 32: Force constants for each ionic pair in $La_{1.85}Sr_{0.15}CuO_4$ **[28]**. *: shifted by (a/2, a/2, c/2).

6.4.2 Calculation of Coulomb Forces

Hole carriers jump from an oxygen 2p orbital to a neighbour orbital in a CuO_2 plane. This displacement of a hole in the plane is equivalent to the movement of an electron in the same plane but in opposite direction. Therefore, an electron has been used instead of a hole to calculate the Coulomb forces. In figure 17, the path for the movement of the electron is shown. By calculating the distance between the moving electron and each ion in the unit cell, the Coulomb forces acting on each ion are determined.

6.4.3 Simulation of the Attractive Potential Energy V_0 and the Binding Energy Δ

The simulation has been performed and the simulated value of V_0 has been used to calculate the binding energy Δ. The calculated values for the binding energy Δ and the superconducting constant c are smaller than the values in table 31. This can be due to the Fermi velocity, the density of states, or the force constants. A small change in the first two of these properties has a strong influence on the results of the simulation. Furthermore, the values used correspond to theoretical calculations [21] instead of measurements. An inaccuracy in the results is, therefore, expected.

Since the potential energy of a simple harmonic oscillator depends on the spring constant, the deformation energy of the unit cell depends on the force constants in the unit cell, too. This means that if the force constants used don't agree with their real values, the deformation energy could differ as well. This could be a reason why the calculated superconducting constant does not coincide with the values from the different references in table 31. Another reason could just as well be that the BCS theory doesn't apply in this case and, if our result for the calculation of the superconducting constant c were correct, there would have to be a second pairing mechanism to overcome the thermal fluctuation energy.

Superconductor	$v_e \left[\frac{m}{s}\right]/10^6$	$D(E_f)[\frac{1}{eV}]$	V_0[eV]	Δ [meV]	c
$La_{1.85}Sr_{0.15}CuO_4$	0.314	2.09	0.31	1.5	0.91

Table 33: Electrical properties, simulated attractive potential energy V_0, binding energy Δ and the superconducting constant c for $La_{1.85}Sr_{0.15}CuO_4$.

6.5 $Bi_2Sr_2CaCu_2O_{8+\delta}$ (Bi2212)

$Bi_2Sr_2CaCu_2O_{8+\delta}$ is one of the high temperature superconductor cuprates, with a critical temperature T_c of about 93 K. It is doped with oxygen atoms. The oxygen atoms are placed in interstitial positions in the crystal structure. The unit cell used for the simulation has a tetragonal structure with lattice parameters $a, b = 3.817$ Å and $c = 30.5$ Å, and two chemical formulas with four CuO_2 planes in the unit cell [16]. However, according to different references, an orthorhombic unit cell with four chemical formulas has been also found [23]. The Fermi velocity v_e, the Fermi wave number k_f and the effective mass m_{eff} from two different references are given in table 34 for optimally doped Bi2212 crystals. The density of states has been calculated from the Fermi wave number and the effective mass is given in table 34 with equation 6.34, where V is the volume of the unit cell [5]:

$$D(E_f) = \frac{m_{eff} k_f}{\hbar^2 \pi^2} V \ . \qquad (6.34)$$

The binding energy Δ for underdoped, optimally doped and overdoped Bi2212 at 4.2 K has been found by use of tunneling current-voltage in Ref. [53]. In this reference, the critical temperature for the overdoped and underdoped probes lies at 83 K whereas for the optimally doped it lies at 95 K. The measured values of the binding energy Δ for the overdoped, optimally doped and underdoped crystal are 26, 37.5 and 45 meV respectively. The corresponding superconducting constants are 7.3, 9.2 and 12.6.

In Ref. [54], four different values of 44, 41.5, 34 and 28 meV for the binding energy Δ have been found for four different doping oxygen amounts from underdoping to overdoping (41.5 corresponding to the optimum). The corresponding critical temperatures are 83, 92, 74.3 and 56 K. In this reference, the values for the superconducting constants 12.3±1 and 8.7±1 are reported for underdoped and overdoped crystal respectively. This reference concludes that superconductivity in Bi2212 does not exhibit BCS-like behaviour.

In Ref. [55], tunneling spectroscopy measurements have been performed on optimally doped and overdoped crystals of Bi2212. The binding energy Δ for the overdoped crystal with $T_c = 89$ K is about 25.8 meV, whereas its average value for the optimally doped crystal with the average critical temperature $T_c = 93.2$ K is about 32.52 meV [55]. The two superconducting constants for overdoped and optimally doped crystal are 7.2 and 8.1 respectively. In general the superconducting constant for overdoped, optimally doped and underdoped crystal lies between 7.0 and 13.0.

$Bi_2Sr_2CaCu_2O_8$	T_c [K]	k_f	$v_e \left[\frac{m}{s}\right]/10^6$	m_{eff}/m_e	$D(E_f)[\frac{1}{eV}]$
Ref. [22]	89	0.71	0.274	3.00	12.57
Ref. [24]	87	0.74	0.250	3.43	14.97

Table 34: Critical temperature T_c, Fermi wave number k_f, Fermi velocity v_e, effective mass m_{eff} and density of states $D(E_f)$ of Bi2212 for optimally doping.

6.5.1 Force Constants

In Ref. [29] the force constants for Bi2212 are calculated from Raman and infrared phonon spectra which are in good agreement with experimental data. In table 35, the force constants for each ionic pair are given.

Pair	Force constant [N/m]
Ca-OI	30
Cu-OI	85
Cu-OII	20
Sr-OI	50
Sr-OII	50
Sr-OIII	80
Bi-OII	105
Bi-OIII	160
Bi-OIII (a)	105
OI-OI	20
OI-OII	10
OII-OIII	35
OIII-OIII (a)	35
Ca-Cu	15
Cu-Sr	15
Sr-Bi	13
Bi-Bi (a)	10

Table 35: Force constants for each ionic pair in Bi2212 **[29]**. (a) for OIII and Bi in adjacent planes. OI, OII, OIII are for oxygen ions located in CuO_2, SrO and BiO planes respectively.

6.5.2 Calculation of Coulomb Forces

To calculate Coulomb forces, the tetragonal structure of Bi2212 has been considered. There are four CuO_2 planes in the unit cell of Bi2212, and none of them lie in the middle of the unit cell (figure 19). To calculate the Coulomb forces, one of the CuO_2 planes closer to the center of the unit cell has been considered as the plane in which the electron moves. Because of its off-center location, the deformation of the unit cell due to the movement of an electron in this plane is not symmetric. The path used for the movement of the electron is the same as for $La_{1.85}Sr_{0.15}CuO_4$. The Coulomb forces between the electron and the ions in the unit cell have been determined as described previously.

6.5.3 Simulation of the Attractive Potential Energy V_0 and the Binding Energy Δ

To simulate the attractive potential energy V_0, the two Fermi velocities from table 34 have been used. Due to the difference in the Fermi velocities, the time in which Coulomb forces act on each ion is different. Therefore, two different values for the attractive potential energy V_0 and binding energy Δ have been simulated, as seen in table 36.

Because the Fermi velocity in Ref. [22] is larger than that from Ref. [24], the corresponding Coulomb forces act over a smaller time interval and, therefore, their attractive potential energy V_0 is lower. This result signifies the importance of the Fermi velocity for the formation of Cooper pairs. It can be seen from table 36 that a decrease of 0.02×10^6 m/s in the Fermi velocity in Ref. [24] can change the superconducting constant c from 3.7 to 6.5. Furthermore, due to the exponential dependence of the binding energy Δ on $D(E_f)V_0$, the different values of the density of states (from both references) influence the calculated values of the superconducting constant c.

According to Refs. [53], [54] and [55] the measured values of the binding energy Δ for overdoped crystals are 26, 28 and 25.8 meV, with a critical temperature of 83 K for the first two and 89 K for the last. The calculated value of Δ using the available data from Ref. [24] is 24.4 meV (table 36). This lies close to the values for overdoping given in Refs. [53], [54] and [55] even though Ref. [24] states that the Fermi velocity and the density of states in table 34 correspond to optimal doping. Due to the crystal structure of optimally doped Bi2212, the critical temperature determined by Ref. [24], in table 34, should be larger than those given in the other three references (92 to 95 K), which is not the case. This all hints to the possibility

that the assertion made in Ref. [24] is not correct and the measured probe may be actually overdoped.

$Bi_2Sr_2CaCu_2O_8$	T_c [K]	$v_e \left[\frac{m}{s}\right]/10^6$	$D(E_f)[\frac{1}{eV}]$	V_0 [eV]	Δ [meV]	c
Ref. [22]	89	0.274	12.57	0.17	14.2	3.7
Ref. [24]	87	0.250	14.97	0.21	24.4	6.5

Table 36: Simulated attractive potential energy V_0, binding energy Δ and superconducting constant c for the Fermi velocity v_e and density of states $D(E_f)$ given by Ref. **[22]** and **[24]**.

6.6 $HgBa_2Ca_2Cu_3O_{8+\delta}$ (Hg1223)

$HgBa_2Ca_2Cu_3O_{8+\delta}$ is another high temperature superconductor cuprate, with a critical temperature T_c = 134 K at its optimally doped oxygen amount and a tetragonal unit cell with lattice parameters a, b = 3.85 Å and c = 16.1 Å [8]. The unit cell contains one chemical formula and three CuO_2 planes. As described in chapter 5.3, its Debye frequency has been calculated as well as measured from heat capacities. Like the Fermi surface of Sr_2RuO_4, the Fermi surface of Hg1223 consists of the three different sheets which correspond to three different types of Fermi electrons [27]. The Fermi velocity and the density of states for each type are calculated for the doped crystal from Ref. [27] and are given in table 37.

The binding energy Δ = 12 meV for Hg1223 with T_c = 133 K has been determined at 4.2 K from tunneling-conductance measurements with a scanning-tunneling microscope [56]. The binding energy $\Delta \approx 14$ meV is also given in Ref. [4]. The corresponding superconducting constants for the two references are 2.44 and 2.51.

$HgBa_2Ca_2Cu_3O_{8+\delta}$	$v_e \left[\frac{m}{s}\right] / 10^6$	$D(E_f)\ [\frac{1}{eV}]$
1-type	0.198	0.75
2-type	0.189	0.84
3-type	0.177	1.75

Table 37: The three types of the Fermi electrons in Hg1223 and their electrical properties **[27]**.

Ref.	T_c [K]	Δ [meV]	c
[56]	133	12	2.44
[4]	133	14	2.51

Table 38: The binding energy Δ and the superconducting constant c.

6.6.1 Calculation of Force Constants

The force constants must be calculated according to the shell model described in chapter 2.4.1 using the quantum mechanics program GULP [12]. For this, potential parameters are needed as given in table 39 and 40 [57]. The results for the force constants calculated by GULP can be seen in table 41. In order to validate the results for the force constants, the elastic constants and the dielectric constants, which are calculated as well with these potential parameters in GULP, must be compared with the components of the fourth-order stiffness tensor and dielectric constants reported in Ref. [57]. In table 42, a very good agreement between the results from GULP and Ref. [57] can be observed. Therefore, the calculated force constants can be used for the simulation of the attractive potential energy V_0.

Pair	A[eV]	ρ[Å]	A[eV/Å^6]
Hg-O	648.5	0.3251	0
Ba-O	2096.8	0.3522	8
Ba-Ba	2663.7	0.3428	0
Ca-O	1228.9	0.3372	0
Cu-O	3860.6	0.2427	0
O-O	22764	0.1490	43

Table 39: Potential parameters of each ionic pair for Hg1223 **[57]**.

Ion	Z	q_{shell}	k [N/m]
Hg	2	1.50	598.0
Ba	2	1.848	29.1
Ca	2	1.26	34.0
Cu	2	1.00	99999
O	-2	-2.389	3.88

Table 40: Total charge of ions (Z) and shells (q_{shell}) and shell model spring constant k for each ion in the unit cell of Hg1223 **[57]**.

Pair	Force constant [N/m]	Pair	Force constant [N/m]
Ba-Ca	37.81	CuI-CuII	28.00
Ba-CuII	76.28	CuI-OI	111.59
Ba-Hg	32.20	CuI-OII	1.93
Ba-OII	18.77	CuII-OI	0.87
BaI-OIII	8.78	CuII-OII	113.37
Ca-Ca	44.14	CuII-OIII	3.35
Ca-CuI	51.93	Hg-OIII	85.42
Ca-CuII	66.19	OI-OII	241.54
Ca-OI	17.30	OII-OII	214.06
Ca-OII	20.15	OIII-OIII	1.18

Table 41: Calculated force constants for each ionic pair in the unit cell of Hg1223. I: ions in the CuO_2 plane in middle of the unit cell, II: ions in other CuO_2 planes, III: apical O between Hg and Cu.

Stiffness tensor components	GULP [GPa]	Ref. [57] [GPa]
C_{11}	289.7	290
C_{12}	119.5	119
C_{13}	42.5	42
C_{33}	199.5	199
C_{44}	14.0	14
C_{66}	124.3	124
Dielectric constants	GULP	Ref. [57]
ϵ_0	10.17	10.18
ϵ_∞	5.56	5.80

Table 42: Elastic and dielectric constants in Hg1223 from GULP as well as Ref. **[57]**.

6.6.2 Calculation of Coulomb Forces

For the calculation of the Coulomb forces, the electron is assumed to move in the CuO_2 plane located in the middle of the unit cell. Its moving path in this CuO_2 plane is the same as for $La_{1.85}Sr_{0.15}CuO_4$. The Coulomb forces have been calculated as explained previously.

6.6.3 Simulation of the Attractive Potential Energy V_0 and the Binding Energy Δ

The simulation has been performed after constructing the unit cell and loading the Coulomb forces on each of its ions. The results for the attractive potential energy V_0, the binding energy Δ and the superconducting constant c for each type are given in table 43. The Fermi velocity of type 3 is lower than that of the two others, consequently, its attractive potential energy is larger. Furthermore, the density of states of type 3 is the largest. Hence its value of $D(E_f)V_0$ is the largest and, due to the exponential dependence of Δ on $D(E_f)V_0$, so is its binding energy Δ as can be observed in table 43.

To calculate the total binding energy and the total superconducting constant, equation 2.58 has been used. From table 44 it can be seen that their values for doped crystals are in very good agreement with the results from Refs. [56] and [4] in table 38.

$HgBa_2Ca_2Cu_3O_{8+\delta}$	$v_e\left[\frac{m}{s}\right]/10^6$	$D(E_f)\ [\frac{1}{eV}]$	V_0[eV]	Δ [meV]	c
1-type	0.198	0.75	0.337	0.04	0.0036
2-type	0.189	0.84	0.346	0.11	0.0099
3-type	0.177	1.75	0.397	6.71	0.5813

Table 43: Electrical properties, simulated attractive potential energy V_0, binding energy Δ and superconducting constant c for each type.

$\sum D(E_f)V_0$	Δ [meV]	c
1.237	13.978	2.42

Table 44: Total binding energy Δ and total superconducting constant c for Hg1223.

6.7 $YBa_2Cu_3O_{7-\delta}$ (YBCO)

$YBa_2Cu_3O_{7-\delta}$ is one of the most important high temperature superconductor cuprates. It has an orthorhombic unit cell with two CuO_2 planes and one CuO chain and lattice parameters a = 3.83 Å, b = 3.88 Å and c = 11.68 Å [8]. Its phase diagram (critical temperature T_c vs. doping amount δ) shows two maxima, one of them at δ = 0.55 with T_c = 57 K, and the other at δ = 0.96 with T_c = 93 K [58]. Below δ = 0.4, superconductivity vanishes and the material becomes an insulator [58].

According to theoretical work from Ref. [59], two superconducting gaps should be present for YBCO: a large one due to electron pairing in the CuO_2 planes and a small one due to the CuO chains. Actual measurements show either two or three band gaps.

Tunneling measurements show three superconducting gaps for two different doped YBCO-samples with T_c = 89 and 91 K (two large gaps for the CuO_2 planes and a small gap for the CuO chains) [60]. The corresponding binding energies are $\Delta_{plane,1}$ = 9.5-10, $\Delta_{plane,2}$ = 15-18 and Δ_{chain} = 2.25-2.75 meV.

According to Ref. [61], two superconducting gaps have been found in optimally doped $YBa_2Cu_3O_{7-\delta}$ which correspond to the CuO chain and the CuO_2 plane. In this reference, the observation of the two superconducting gaps is related to the BCS-like density of states. Values for the binding energies of Δ_{chain} = 0.25-0.75 and Δ_{plane} = 12-14 meV are reported in this reference. A value of about 1.9 for the superconducting constant c is reported in Ref. [62] for doped YBCO with T_c = 90 K. The different binding energies determined by different references are given in table 46.

In Ref. [63], a mean Fermi velocity of $v_e = 0.35\times10^6$ m/s for the charge carriers moving along the chain and in the plane has been calculated for $YBa_2Cu_3O_7$. A mean Fermi velocity of $v_e = 0.25\times10^6$ [m/s] in the a-axis (no chain contribution) is also calculated for $YBa_2Cu_3O_{6.9}$ in Ref. [24], in which a mean binding energy of Δ = 10 meV has been also reported.

The different values of the densities of states at the Fermi level for different doping amounts have been determined in Ref. [64] and are given in table 45. A density of states of $D(E_f)$ = 5.58 [1/meV] and a Fermi velocity of $v_e = 0.34\times10^6$ [m/s] are calculated from the electronic band structure in Ref. [21].

δ	$v_e \left[\frac{m}{s}\right] / 10^6$	$D(E_f)[\frac{1}{eV}]$
0	0.35	5.54
0.1	0.25	4.19
0.2	unkn.	3.59
0.3	unkn.	3.23

Table 45: Density of states $D(E_f)$ for different doping amounts δ in $YBa_2Cu_3O_{7-\delta}$ **[64]**. Fermi velocities are taken from Refs. **[24]** and **[63]**.

Ref.	$\Delta_{plane,1}$ [meV]	$\Delta_{plane,2}$ [meV]	Δ_{chain} [meV]
[24]	10*		
[60]	9.5-10	15-18	2.5-2.75
[61]	12-14**		0.25-0.75

Table 46: The different binding energies of $YBa_2Cu_3O_{7-\delta}$ by Ref. **[60]** and **[61]**. * Only a value of the binding energy has been found by Ref. **[24]**.** Only a superconducting gap related to the CuO_2 has been found by Ref. **[61]**.

6.7.1 Force Constants

The force constants for each ionic pair to construct the unit cell have been determined from Raman spectroscopy data in Ref. [65]. They are given in table 47.

Pair	Force constant [N/m]	Pair	Force constant [N/m]
CuI-OI	152	Ba-OIII	54
CuI-OII	176	Ba-OIIII	54
CuII-OIII	155	Y-OIII	77
CuII-OIIII	149	Y-OIIII	79
CuII-OII	103	CuII-CuII	51
Ba-OI	55	Ba-Ba*	40
Ba-OII	58		

Table 47: Measured force constants for each ionic pair in the unit cell of $YBa_2Cu_3O_7$ **[65]**.*: Force constant for a Ba-Ba pair in $YBa_2Cu_3O_6$. I for ions in the CuO chain, OII is the apical oxygen and CuII, OIII and OIIII are located in the CuO_2 plane (figure 19).

6.7.2 Calculation of Coulomb Forces

To calculate the two binding energies Δ_{chain} and Δ_{plane}, two paths for the movement of the electron, one along the CuO chain and the other in the CuO_2 plane, must be considered. The path in the CuO_2 plane is the same as the one described in previous chapters. But for the electron moving along the CuO chain, the CuO plane on the top or bottom of the unit cell has been used. This path is located between the two chains in the CuO plane (figure 29). The Coulomb forces have been calculated for the two paths, like before.

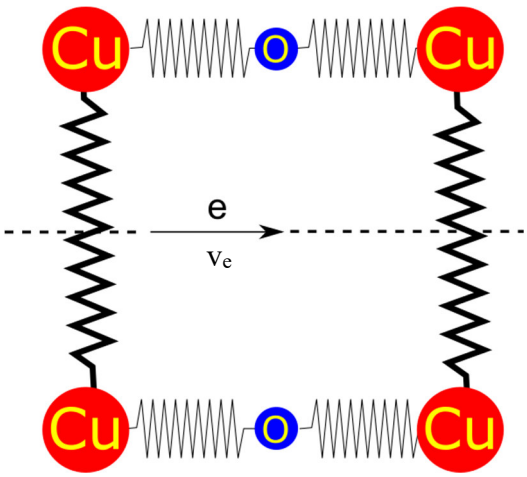

Figure 29: Path for the movement of the electron along the CuO chain in the CuO plane. The red ions are copper and the blue ions are oxygen.

6.7.3 Simulation of the Attractive Potential Energy V_0 and the Binding Energy Δ

$YBa_2Cu_3O_{7-\delta}$ has been simulated to see if the results for a superconductor with two superconducting gaps correspond to the values from the different references. To find the two binding energies Δ_{chain} and Δ_{plane}, two paths for the movement of the electron have been selected, one along the CuO chain and the other in the CuO_2 plane, for the simulation. The Fermi velocities and the density of states have been taken from Refs. [21], [24] and [63]. The simulation has been done for the two different doping amounts δ = 0 and 0.1 and the results are listed in table 48 and 49. The calculated binding energies Δ_{plane} = 12.3 meV for δ = 0.1 are in good agreement with the reported values of $\Delta_{plane,1}$ = 9.5-10 (Ref. [60]), Δ_{plane} = 12-14 (Ref. [61]) and Δ = 10 meV (Ref. [24]), hinting at BCS-like superconductivity. For the two doping amounts, the values of 4.8 and 11 meV for Δ_{chain} are far from the measured values from Refs. [24], [60] and [61]. This is most probably because the same Fermi velocity for both paths (in the CuO_2 plane and along CuO chain) is assumed in the simulation due to the shortage of more specific data. Nevertheless, the superconducting constant c_{chain} of 1.22 for δ = 0 is relatively close to 1.9 from Ref. [62]. The comparison between the results of the calculation and different references are given in table 50 and 51.

For δ = 0, the Fermi velocity is larger, leading to a smaller attractive potential energy V_0 than for δ = 0.1. As a result, the binding energies are also lower for δ = 0 and so is the critical temperature. This can be proven by the results of the simulation in table 48 and 49 for both superconducting gaps (Δ_{plane} and Δ_{chain}). It was not possible to simulate the binding energies for other doping amounts since no values for the corresponding Fermi velocities are published. The simulation results show that superconductivity in YBCO can behave as the same way in the conventional BCS-superconductors.

δ	T_c[K]	$v_e\left[\frac{m}{s}\right]/10^6$	$D(E_f)[\frac{1}{eV}]$	T_D[K]	$V_{0,chain}$[eV]	Δ_{chain} [meV]	c_{chain}
0	90	0.35	5.54	437	0.165	4.8	1.22
0.1	93.6	0.25	4.19	437	0.32	11	2.71

Table 48: Electrical properties, simulated attractive potential energy V_0, binding energy Δ and superconducting constant c for the movement of the electron along the CuO chain in the unit cell of $YBa_2Cu_3O_{7-\delta}$.

δ	T_c[K]	$v_e \left[\frac{m}{s}\right]/10^6$	$D(E_f)[\frac{1}{eV}]$	T_D[K]	$V_{0,plane}$[eV]	Δ_{plane} [meV]	c_{plane}
0	90	0.35	5.54	437	0.17	5.1	1.31
0.1	93.6	0.25	4.19	437	0.34	12.3	3.04

Table 49: Electrical properties, simulated attractive potential energy V_0, binding energy Δ and superconducting constant c for the movement of the electron in the CuO_2 plane in the unit cell of $YBa_2Cu_3O_{7-\delta}$.

$\delta = 0.1$	Δ_{plane} [meV]
calculated	12.3
Ref. [24]	10
Ref. [60]	9.5-10
Ref. [61]	12-14

Table 50: Comparison between the binding energy from calculation and references for $YBa_2Cu_3O_{7-\delta}$ with $\delta = 0.1$.

$\delta = 0$	c_{chain}
calculated	1.2
Ref. [62]	1.9

Table 51: Comparison between the superconducting constant from calculation and Ref. **[62]** for $YBa_2Cu_3O_{7-\delta}$ with $\delta = 0$.

6.8 Results and Discussion

According to the results from the simulation, the Fermi velocity v_e of the superconductors plays an important role regarding the appearance of superconductivity. The lower the Fermi velocity is, the larger the attractive potential energy V_0, because the time during which the Coulomb forces act on each ion in the unit cell reduces. A larger V_0 leads to a larger binding energy Δ. On the other hand, the density of states $D(E_f)$ decreases with a reduction in the Fermi velocity, and decreasing $D(E_f)$ yields to lower binding energies. The overall effect of a decrease in the Fermi velocity can be either an increase or a decrease of the binding energy, depending on the values of V_0 and $D(E_f)$.

Superconductivity in HTSCs only occurs in the so-called superconductivity dome in their phase diagram (critical temperature T_c vs. doping amount δ). In this region, there is always an optimal doping amount δ_{opt} for which the critical temperature T_c is a maximum. The Fermi velocity v_e is directly proportional to the doping amount. This means that the responses of the attractive potential energy V_0 and the density of states $D(E_f)$ to a change in the doping amount δ, are qualitatively the same as a change in the Fermi velocity v_e. According to the simulation results, V_0 and $D(E_f)$ exhibit opposite responses to a changing Fermi velocity or doping amount δ. Due to these responses and to the fact that the binding energy is directly related to both (being dependent on the product $V_0 D(E_f)$), it is then clear that an optimal doping amount must exist at which the binding energy is maximum. At the maximum value of the binding energy the critical temperature reaches its maximum value. The critical temperature decreases for δ smaller or larger than δ_{opt}. Therefore, a dome with a maximum must be found in the phase diagram (T_c vs. δ).

In Ref [4] a linear relationship, which is described by the BCS theory, between the width of the superconducting gap 2Δ and the critical temperature T_c has been found for high temperature superconductor cuprates. This relationship (shown in figure 30) can be expressed as $2\Delta = 2.214T_c$. It was not possible to conduct simulations of the attractive potential energy V_0 for all superconductors covered in the reference because the required force constants, Fermi velocities, densities of states and Debye temperatures could not be found in the available literatures. Therefore, the most important superconductors have been taken. The simulation results for the width of the superconducting gap 2Δ vs. the critical temperature T_c are shown in figure 31. The difference between this and figure 30 is that the latter only shows results for HTCS-cuprates, whereas in figure 31, the results are for conventional, unconventional superconductors and HTCS-cuprates. In figure 30 the binding energy Δ for the optimally doped Bi2212 is about 15 meV, which does not correspond to the results of Refs. [53], [54] and [55]. According to the simulation results for $Bi_2Sr_2CaCu_2O_{8+\delta}$ in table 36, a binding energy Δ of 14.2 meV has been calculated for the Fermi velocity $v_e = 0.25\times10^6$ as well. This shows once again the importance of the Fermi velocity for calculating the exact value of the binding energy, because for $Bi_2Sr_2CaCu_2O_{8+\delta}$ a decrease of 9.6% for the Fermi velocity yields a large increase of 41% for the binding energy.

Figure 31 shows the results from the simulation for the superconductors considered in this work. The two values of the binding energy for $Bi_2Sr_2CaCu_2O_{8+\delta}$ (table 36) have been considered in this figure. The two solid lines (1) and (2) are fitted to the simulation results to compare their equations with the relationship $2\Delta = 2.214T_c$ given in Ref. [4]. For line (1) the Fermi velocity

of $Bi_2Sr_2CaCu_2O_{8+\delta}$ is 0.274×10^6, whereas it is 0.25×10^6 for line (2). Line (1) has a slope of 2.865, which is close to the slope of 2.214 in Ref. [4].

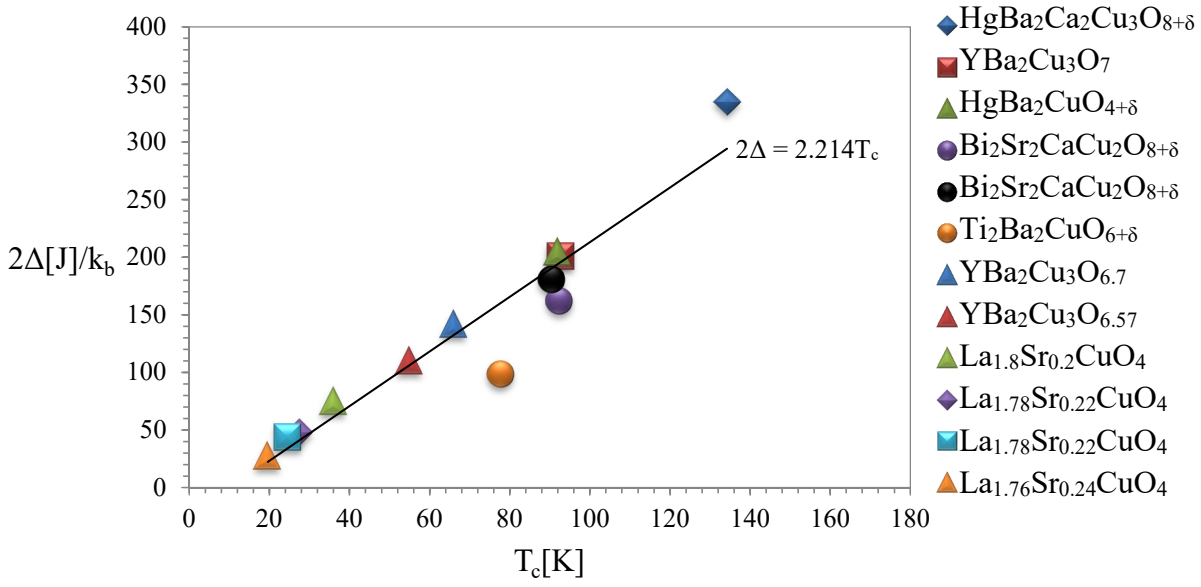

Figure 30: Superconducting gap 2Δ vs. critical temperature T_c. The solid line is for the relationship $2\Delta=2.214T_c$ from Ref **[4]**. k_b is the Boltzmann constant.

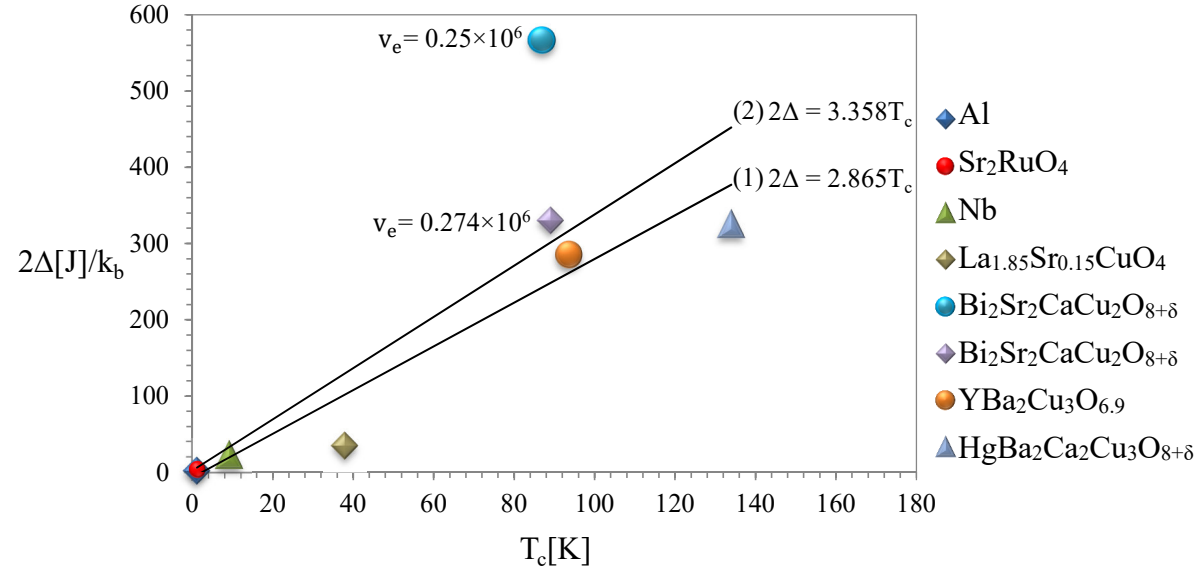

Figure 31: Calculated superconducting gap 2Δ vs. critical temperature T_c for some high temperature, conventional and unconventional superconductors. The solid lines (1) and (2) are fitted lines on data. The Fermi velocity of $Bi_2Sr_2CaCu_2O_{8+\delta}$ considered for the line (1) is 0.274×10^6 and 0.25×10^6 for the line (2). k_b is the Boltzmann constant.

The simulations for the two superconductors Sr_2RuO_4 and $La_{1.85}Sr_{0.15}CuO_4$ were of particular interest since they have the same crystal structure. However, their electronic band structures are not similar, therefore, their Fermi velocities and densities of states are different. Other differences lie in the charges and masses of the ions in the unit cell, which influence the attractive potential energy V_0. The simulation then leads to different attractive potential energies for the unit cells, different binding energies Δ and different critical temperatures T_c. For example, in Sr_2RuO_4, it has been assumed that the electron or the charge carriers move in the RuO_2 plane, in which there are one ruthenium ion with charge 4+ and two oxygen ions each with 2-. On the other hand, there is a copper ion with charge 2+ in the CuO_2 plane of $La_{1.85}Sr_{0.15}CuO_4$. As a result, the Coulomb force acting on the ruthenium ion is twice larger than that on the copper ion. Furthermore, the mass of the two ions must be considered to calculate their displacement.

From table 1, it can be observed that the Debye temperatures of these two superconductors are different. Due to the dependence between the Debye temperature and the force constants, a difference in the force constants is expected, which can be seen from the comparison between the force constants from table 28 and 32. This difference causes different values for the attractive potential energy of both superconductors.

The results for the superconducting constants in the bottom table point out that the superconductivity in Sr_2RuO_4 exhibit BCS-like behaviour. In case of $La_{1.85}Sr_{0.15}CuO_4$, superconductivity could also correspond to the BCS theory, but it might be possible that it arises through another, as yet unknown second pairing mechanism.

Superconductors	c
Sr_2RuO_4	2.43
$La_{1.85}Sr_{0.15}CuO_4$	0.91

Table 52: Calculated superconducting constant c in Sr_2RuO_4 and $La_{1.85}Sr_{0.15}CuO_4$.

7 Summary

Using the BCS theory, superconductivity in conventional superconductors can be explained. According to it, the phenomenon appears below the critical temperature T_c when two electrons form a so-called Cooper pair, for which an attractive potential interaction V_0 is required. In this work, this attractive potential energy is calculated analytically and also simulated using the finite element method. With the results for the attractive potential energy, the binding energy Δ for Cooper pairs can be calculated.

Two conventional superconductors Al and Nb, four high temperature superconductor cuprates ($La_{1.85}Sr_{0.15}CuO_4$, $Bi_2Sr_2CaCu_2O_{8+\delta}$, $HgBa_2Ca_2Cu_3O_{8+\delta}$ and $YBa_2Cu_3O_{7-\delta}$) and one unconventional superconductor Sr_2RuO_4 have been investigated. For comparison and ultimately motivation, the attractive potential energy of each superconductor has been calculated analytically by a simplified model. The calculation of the attractive potential energy of Al and Nb is relatively simple due to their simple unit cell. Due to the complex unit cell of cuprates and Sr_2RuO_4, only the attractive potential energy of the CuO_2 and RuO_2 planes was calculated. The attractive potential energy determines the binding energy according to the BCS theory. Hence, the obtained values are far from the corresponding experimental measurement as a result of the simplifications necessary for an analytical calculation. Nevertheless, the expected, increasing trend for the critical temperature vs. the calculated binding energy was found. Therefore, the finite element method has been used to obtain more exact values of the attractive potential energy.

The attractive potential energy of each superconductor has been simulated to calculate the corresponding binding energy. For Al and Nb, the [100] direction has been taken as the direction of movement for the Fermi electrons. For cuprates it is assumed that the electrons move on the CuO_2 plane (or also along CuO chains in the case of $YBa_2Cu_3O_{7-\delta}$) in the [100] direction, since it has been found that the charge carriers are doped into this plane. For Sr_2CuO_4, the RuO_2 plane in the middle of the unit cell has been chosen in an analogous way.

The simulation results show that the Fermi velocity v_e is one of the most important electrical properties regarding superconductivity. The Fermi velocity influences the binding energy through the density of states $D(E_f)$ and the attractive potential energy V_0.

According to the simulation results, the attractive potential energy V_0 varies inversely on the Fermi velocity whereas the density of states $D(E_f)$ is proportional to the Fermi velocity. Because of this and the dependence of the binding energy on the product $D(E_f)V_0$, a maximum for the binding energy at an optimal Fermi velocity must be mathematically found at which the critical temperature is maximum. In high temperature superconductor cuprates, the critical

temperature T_c changes with the doping amount δ. Due to the direct proportionality of the Fermi velocity on the doping amount, the critical temperature is proportional to the Fermi velocity as well. This dependence of the critical temperature on the Fermi velocity or the doping amount was proven by the simulation results for two values of the doping amount in $YBa_2Cu_3O_{7-\delta}$.

A linear relationship between the width of the superconducting gap 2Δ and the critical temperature ($2\Delta = 2.865T_c$) was found, which corresponds to the experimentally determined relationship $2\Delta = 2.214T_c$ [4].

It was interesting to perform the simulations for the two superconductors Sr_2RuO_4 and $La_{1.85}Sr_{0.15}CuO_4$, since they have the same crystal structure. It was found that the difference in the electrical properties, the charges and masses of the ion in the unit cell and the force constants can be a reason for the different critical temperatures in both superconductors. The results for their superconducting constants point out that the superconductivity in Sr_2RuO_4 could be BCS-like whereas the superconductivity in $La_{1.85}Sr_{0.15}CuO_4$ could also correspond to the BCS theory or perhaps to an as yet unknown second pairing mechanism.

8 Bibliography

[1] W. P. Czaja, The Finite Element Method Applied to, Drexel University, May 2010.

[2] A. S. Sehra, Finite Element Analysis of the Schrödinger Equation, Singleton Park Swansea: University of Wales Swansea, 17 April 2007.

[3] Q. Du, Finite element methods for the time-dependent Ginzburg-Landau model of superconductivity, Carnegie Mellon University, 1993.

[4] C. Panagopoulos and T. Xiang, "Relationship between the Superconducting Energy Gap and the Critical Temperature in High-Tc Superconductors," Phys. Rev. Lett., pp. Vol. 81, No. 11, pp. 2336, 14 September 1998.

[5] R. E. Hummel, Electronic Properties of Materials, New York: Springer, 2001.

[6] W. Buckel and R. Kleiner, Supraleitung, Grundlagen und Anwendungen, Weinheim.

[7] K. Hock, "7a. Superconductivity - The Nature of the Cooper pair," University of Liverpool, 2010-2011.

[8] Charles P. Poole, Jr., Horacio A. Farach and Richard J. Creswick, Superconductivity, The Netherlands: ELSEVIER, 2007.

[9] M. Reichenbächer and J. Popp, Challenges in Molecular Structure Determination, Chapter 2: Vibrational Spectroscopy, Springer, 2012.

[10] G. P. Nikishkov, Introduction to The Finite Element Method, Aizu-Wakamatsu 965-8580, Japan: University of Aizu, 2004.

[11] ANSYS, Inc. Documentation for Release 15.0.

[12] J. D. Gale, "General Utility Lattice Program Version 4.0," Nanochemistry Research Institute, Department of Chemistry, Curtin University, P.O. Box U1987, Perth, WA 6845, Australia.

[13] S. A. Carter , B. Batlogg , R. J. Cava and J. J. Krajewski , "Mechanism for the metal-insulator transition in Sr2Ir1−xRuxO4," Phys. Rev. B, pp. Vol. 51, No. 23, pp. 17184-17187, 15 June 1995.

[14] Q. Huang, J. L. Soubeyroux, O. Chmaissem and I. Natali Sora, "Neutron Powder Diffraction Study of the Crystal Structures of Sr2RuO4 and Sr2IrO4 at Room Temperature and at 10 K," Journal of Solid State Chemistry, pp. Vol. 112, Issue 2, pp. 355-361, October 1994.

[15] M. Decroux, A. Junod, A. Bezinge and D. Cattani, "Structure, Resistivity, Critical Field, Specific-Heat Jump at Tc, Meissner Effect, a.c. and d.c. Susceptibility of the High-Temperature Superconductor La2-xSrxCuO4," Europhysics Letters, pp. Vol. 3, No. 9, pp. 1035-1040, 1 May 1987.

[16] J. M. Tarascon, Y. L. Page, P. Barboux, B. G. Bagley, L. H. Greene, W. R. McKinnon, G. W. Hull, M. Giroud and D. M. Hwang, "Crystal substructure aud physical properties of the supercouductiug phase Bi4(Sr,Ca)6Cu4O16+x," Physical Review B, pp. Vol. 37, No. 16, 1 June 1988.

[17] H. Ledbetter, M. Lei and S. Kim, "Elastic constants, debye temperatures, and electron-phonon parameters of superconducting cuprates and related oxides," Phase Transitions, pp. Vol. 23, pp. 61-70 , 6 March 1990.

[18] H. Roeser, D. Haslam, J. López, M. Stepper, M.F. von Schoenermark, F. Huber and A. Nikoghosyan, "Electronic Energy Levels in High-Temperature Superconductors," J. Supercond. Nov. Magn., pp. Vol. 24, pp.1443–1451, 24 September 2010.

[19] Y.-M. Juan and E. Kaxiras, "Application of gradient corrections to density-functional theory for atoms and solids," Phys. Rev. B, pp. Vol. 48, No. 20, pp. 14944, 15 November 1993-II.

[20] H. R. Kerchner, D. K. Christen and S. T. Sekula, "Critical fields Hc and Hc2 of superconducting niobium," Phys. Rev. B, pp. Vol. 24, No. 3, 1 August 1981.

[21] P. B. Allen, W. E. Pickett and H. Krakauer, "Anisotropic normal-state transport properties predicted and analyzed for high-Tc oxide snpercondnctors," Phys. Rev. B, pp. Vol. 37, No. 13, 1 May 1988.

[22] L. B. Rigal, D. C. Schmadel, H. D. Drew, B. Maiorov, E. Osquiguil, J. S. Preston, R. Hughes and G. D. Gu, "Magneto-optical Evidence for a Gapped Fermi Surface in UnderdopedYBa2Cu3O6+x," Phys. Rev. Lett., pp. Vol. 93, No. 13, pp. 137002, 23 September 2004.

[23] W. E. Pickett, "Electronic structure of the high-temperature oxide superconductors," in Complex Systems Theory Branch, Condensed Matter and Radiation Sciences Division, Naval Research Laboratory, Washington, O. C 20975-5000.

[24] M. Chiao, R. W. Hill, C. Lupien, L. Taillefer, P. Lambert, R. Gagnon and P. Fournier, "Low-energy quasiparticles in cuprate superconductors: A quantitative analysis," Phys. Rev. B., pp. Vol. 62, No. 5, pp. 3554, 1 August 2000-I.

[25] H. Krakauer, W. E. Pickett and R. E. Cohen, "Analysis of electronic structure and charge density of the high-temperature superconductor YBa2Cu3O7," Journal of Superconductivity, pp. Vol. I, No. 1,, 1988.

[26] A. P. Mackenzie, S. R. Julian, A. J. Diver and G. J. McMullan, "Quantum Oscillations in the Layered Perovskite Superconductor Sr2RuO4," Phys. Rev. Lett., pp. Vol. 76, No. 20, pp. 3786-3789, 13 May 1996.

[27] D. Novikov and A. Freeman, "Van Hove singularities and the role of doping in the stabilization, synthesis and superconductivity of HgBa2Ca2Cu3O8.37," Physica C, pp. Vol. 216, pp. 273-283, 9 August 1993.

[28] T. Brun, M. Grimsditch, K. E. Gray and R. Bhardra, "Phonon dispersion curves for La1.85Sr0.15CuO4," Phys. Rev. B, pp. Vol. 35, No. 16, pp. 8837-8839, 1 June 1987.

[29] S. J. CHUN and S. Z. WU, "Calculation of Zone Center Phonon Modes of Bi2Sr2CaCu2O8," phys. stat. sol. (b), pp. Vol. 163, K49-K59, 1 January 1991.

[30] G. GILAT and R. M. NICKLOW, "Normal Vibrations in Aluminum and Derived Thermodynamic Properties," Phys. Rev., pp. Vol. 143, No. 2, March 1966.

[31] G. W. Crabtree, D. H. Dye, D. P. Karim and D. D. Koelling, "Anisotropic Many-Body Effects in the Quasiparticle Velocity of Nb," Phys. Rev. Lett., pp. Vol. 42, No. 6, 5 February 1979.

[32] F. Giithoffti, B. Hemion, C. Herzig, W. Petryll, H. R. Schober and J. Trampenaull, "Lattice dynamics and self-diffusion in niobium at elevated temperatures," J. Phys.: Condens. Matter, pp. Vol. 6, pp. 6211-6220., 5 April 1994.

[33] K. Ishida, H. Mukuda, Y. Kitaoka and K. Asayama, "Spin-triplet superconductivity in Sr2RuO4 identified by 17O Knight shift," Nature, pp. 396, pp. 658-660, 20 August 1998.

[34] K. H. Bennemann and J. B. Ketterson, "Electronic Theory for Superconductivity in High-Tc Cuprates and Sr2RuO4," in Superconductivity, Novel Superconductors, Heidleberg, Springer, 2008.

[35] C. Bergemann, A. P. Bergemann and S. Julian, "Quasi-two-dimensional Fermi liquid properties of the unconventional superconductor Sr2RuO4," Advances in Physics, pp. Vol. 55, pp. 639-725, 2003.

[36] T. M. Riseman, P. G. Kealey, E. M. Forgan and A. P. Mackenzie, "Observation of a square flux-line lattice in the unconventional superconductor Sr2RuO4," Nature, pp. Vol. 396, pp. 242-245, 19 November 1998.

[37] M. E. Zhitomirsky and T. M. Rice, "Interband Proximity Effect and Nodes of Superconducting Gap in Sr2RuO4," Phys. Rev. Lett., pp. Vol. 87, No. 5, pp. 057001-1, 11 July 2001.

[38] P. L. Contreras, "Electronic heat transport for a multiband superconducting gap in Sr2RuO4," Revista Mexicana de Fisica, pp. Vol. 57, No. 5, pp. 395-399, October 2011.

[39] H. Suderow, V. Crespo, I. Guillamon and S. Vieira, "A nodeless superconducting gap in Sr2RuO4 from tunneling spectroscopy," New J. Phys. , pp. Vol. 11, pp. 093004, 2 September 2009.

[40] M. D. Upward, L. P. Kouwenhoven, A. F. Morpurgo and N. Kikugawa, "Direct observation of the superconducting gap of Sr2RuO4," Phys. Rev. B , pp. Vol. 65, pp. 220512(R), 14 June 2002.

[41] M. Udagawa, T. Minami, N. Ogita and Y. Maeno, "Phonon Raman scattering of Sr2RuO4," Physica B, pp. Vol. 219-220, pp. 222-224, 1 April 1996.

[42] M. Braden, W. Reichardt, Y. Sidis and Z. Mao, "Lattice dynamics and electron-phonon coupling in Sr2RuO4: Inelastic neutron scattering and shell-model calculations," Phys. Rev. B, pp. Vol. 76, pp. 014505, 11 July 2007.

[43] T. M. Riseman, P. G. Kealey, E. M. Forgan and A. P. Mackenzie, "Observation of a square flux-line lattice in the unconventional superconductor Sr2RuO4," Nature, pp. 396, pp. 242-245, 19 November 1998.

[44] M. E. Zhitomirsky and T. M. Rice, "Interband Proximity Effect and Nodes of Superconducting Gap in Sr2RuO4," Phys. Rev. Lett., pp. Vol. 87, pp. 087001, 11 July 2001.

[45] P. L. Contreras, "Oriented matroid theory and loop quantum gravity in (2+2) and eight dimensions," Revista Mexicana de Fisica, pp. Vol. 57, pp. 395-399, 9 August 2011.

[46] H. Suderow, V. Crespo, I. Guillamon and S. Vieira, "A nodeless superconducting gap in Sr2RuO4 from tunneling spectroscopy," New J. Phys., pp. Vol. 11, pp. 093004, 2 September 2009.

[47] R. V. Kasowski, W. Y. Hsu and F. Herman, "Electronic properties of oxygen vacancies in La2CuO4−y," Phys. Rev. B, pp. Vol. 36, No. 13, pp. 7248(R), 1 November 1987.

[48] G. Y. Guo, W. M. Temmerman and G. M. Stocks, "On the metal-semiconductor transition and antiferromagnetism in La2CuO4," J. Phys. C: Solid State Phys., pp. Vol. 21, No. 6, pp. L103-L108., 29 February 1988.

[49] K. H. Bennemann and J. B. Ketterson, Superconductivity, Berlin, Germany: Springer, 2008.

[50] T. Ekino, T. Doukan, H. Fujii and F. Nakamura, "Superconducting energy gap of La1.85Sr0.15CuO4 single crystals from break-junction tunneling," Physica C, pp. Vol. 263, Issues 1-4, pp. 249-252, May 1996.

[51] P. Leiderer, R. Feile, B. Renker and D. Ewert, "Tunneling and point contact investigations of La1.85Sr0.15CuO4," Z. Phys. B, pp. Vol. 67, Issue 1, pp. 25-29, March 1987.

[52] T. Sato, T. Yokoya, Y. Naitoh and T. Takahashi, "Pseudogap of Optimally Doped La1.85Sr0.15CuO4 Observed by Ultrahigh-Resolution Photoemission Spectroscopy," Phys. Rev. Lett., pp. Vol. 83, No. 11, pp. 2254-2257, 13 September 1999.

[53] N. Miyakawa, P. Guptasarma, J. F. Zasadzinski, D. G. Hinks and K. E. Gray, "Strong Dependence of the Superconducting Gap on Oxygen Doping from Tunneling Measurements on Bi2Sr2CaCu2O8−δ," Phys. Rev. Lett., pp. Vol. 80, No. 1, pp. 157, 5 January 1998.

[54] C. Renner, B. Revaz, J. -Y. Genoud, K. Kadowaki and Fischer, "Pseudogap Precursor of the Superconducting Gap in Under- and Overdoped Bi2Sr2CaCu2O8+δ," Phys. Rev. Lett., pp. Vol. 80, No.1, pp. 149, 5 January 1998.

[55] V. M. Krasnov, A. Yurgens, D. Winkler, P. Delsing and T. Claeson, "Evidence for Coexistence of the Superconducting Gap and the Pseudogap in Bi-2212 from Intrinsic Tunneling Spectroscopy," Phys. Rev. Lett., pp. Vol. 84, No. 25, pp. 5860, 19 June 2000.

[56] A. Schilling, O. Jeandupeux, S. Büchi, H. R. Ott and C. Rossel, "Physical properties of HgBa2Ca2Cu3O8 with Tc ≈ 133K," Physica C, pp. Vol. 235-240, pp. 229-232, December 1994.

[57] M. S. Islam and L. J. Winch, "Defect chemistry and oxygen diffusion in the HgBa2Ca2Cu3O8+δ superconductor: A computer simulation study," Phys. Rev. B, pp. Vo. 52, No. 14, pp. 10510, 1 October 1995-II.

[58] H. P. Roeser, F. Hetfleisch, F. M. Huber, M. F. von Schoenermark, M. Stepper, A. Moritz and A. S. Nikoghosyan, "A link between critical transition temperature and the structure of superconducting YBa2Cu3O7−x," Acta Astronautica, pp. Vol. 62, pp. 733-736, 10 April 2008.

[59] V. Z. Kresin and S. A. Wolf, "Induced superconducting state and two-gap structure: Application to cuprate superconductors and conventional multilayers," Phys. Rev. B, pp. Vol. 64, pp. 6458-6471, 1 September 1992-II.

[60] A. Mourachkine, "The MCS Model of the Superconductivity in Hole-Doped Cuprates: An Experimental Evidence," Journal of Superconductivity: Incorporating Novel Magnetism, pp. Vol. 13, No. 3, 2000.

[61] B. A. Aminov, M. A. Hein, G. Müller, H. Piel, D. Wehler, Y. G. Ponomarev, K. Rosner and K. Winzer, "Two-Gap Structure in Yb(Y)Ba2Cu3O7-x Single Crystals," Journal of Superconductivity, pp. Vol. 7, No. 2, 1994.

[62] J. Schützmann, W. Ose, J. Keller, K. F. Renk, B. Roas, L. Schultz and G. Saemann-Ischenko, "Far-Infrared Reflectivity and Dynamical Conductivity of an Epitaxial YBa2Cu307-x Thin Film.," Europhys. Lett., pp. Vol. 8 (7), pp. 679-684, 1 April 1989.

[63] H. Romberg, N. Nücker, J. Fink, T. Wolf, X. X. Xi, B. Koch, H. P. Geserich, M. Dürrler, W. Assmus and B. Gegenheimer, "Dielectric function of YBa2Cu3O7-δ between 50 meV and 50 eV," Zietschrift für Physik B- Codensed Matter, pp. Vol. 78, pp. 367-380, 1990.

[64] H. Krakauer, W. E. Pickett and R. E. Cohen, "Analysis of Electronic Structure and Charge Density of the High-Temperature Superconductor YBa2Cu307," Journal of Superconductivity, pp. Vol. 1, No. 1, 1988.

[65] F. E. Bates, "Normal modes of tetragonal YBa2Cu306 and orthorhombic YBa2Cu307," Physical Review B, pp. Vol. 39, No. 1, 1 January 1989.

[66] C. Bergemann, A. P. Bergemann and S. Julian, "Quasi-two-dimensional Fermi liquid properties of the unconventional superconductor Sr2RuO4," Advances in Physics, pp. Vol. 52, No. T, pp. 639-725, 3 September 2003.

[67] S. A. Carter , B. Batlogg , R. J. Cava and J. J. Krajewski , "Mechanism for the metal-insulator transition in Sr2Ir1−xRuxO4," Phys. Rev. B, pp. Vol. 51, No. 23, pp.17184-17187, 15 June 1995.

[68] Q. Huang, J. L. Soubeyroux, O. Chmaissem and I. Natali Sora, "Neutron Powder Diffraction Study of the Crystal Structures of Sr2RuO4 and Sr2IrO4 at Room Temperature and at 10 K," Journal of Solid State Chemistry, pp. Vol. 112, pp. 355-361, 20 January 1994.

[69] M. Udagawa, T. Minami, N. Ogita and Y. Maeno, "Phonon Raman scattering of Sr2RuO4," Physica B, pp. Vol. 219&220, pp. 222-224, 1996.

[70] J. VALLIN, M. MONGY, K. SALAMA and O. BECKMAN, "Elastic Constants of Aluminum," JOURNAL OF APPLIED PHYSICS, pp. Vol. 35, No. 6, June 1964.

[71] R. S. Puche, "Magentic properties of metallic La2CuO4," Materials Research Bulletin, pp. Vol. 17, Issue 11, No. 1982, pp. 1429–1435, 1982.

[72] S. J. Chun and S. Z. Wu, "Calculation of Zone Center Phonon Modes of Bi2Sr2CaCu2O8," phys. stat. sol. (b), pp. Vol. 163, K49 (1991), 1991.

[73] J. Halbritter, "Pair weakening anti tunnel channels at cuprate interfaces," Phys. Rev. B, pp. Vol. 46, No. 22, pp. 14862-14872, 1 December 1992-II.

[74] K. Ishida, H. Mukuda, Y. Kitaoka and K. Asayama, "Spin-triplet superconductivity in Sr2RuO4 identified by 17O Knight shift," Nature, pp. Vol. 396, pp. 658-660, 21 october 1998.

[75] M. Chiao, R. W. Hill, C. Lupien, L. Taillefer, P. Lambert, R. Gagnon and P. Fournier, "Low-energy quasiparticles in cuprate superconductors: A quantitative analysis," Physical Review B, pp. Vol. 63, No. 5, pp. 3554, 1 August 2000-I.

[76] M. D. Upward, L. P. Kouwenhoven, A. F. Morpurgo and N. Kikugawa, "Direct observation of the superconducting gap of Sr2RuO4," Phys. Rev. B, pp. Vol. 65, pp. 220512(R), 14 June 2002.

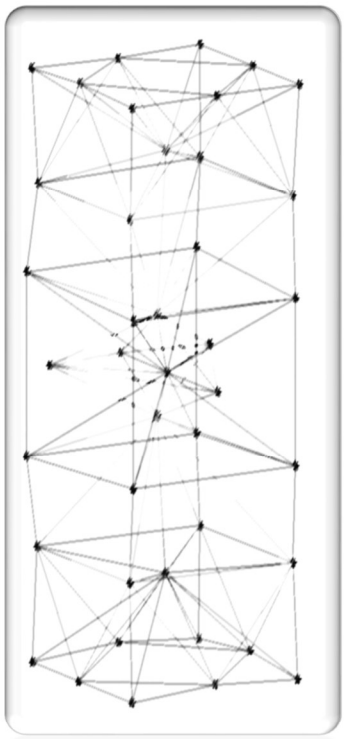

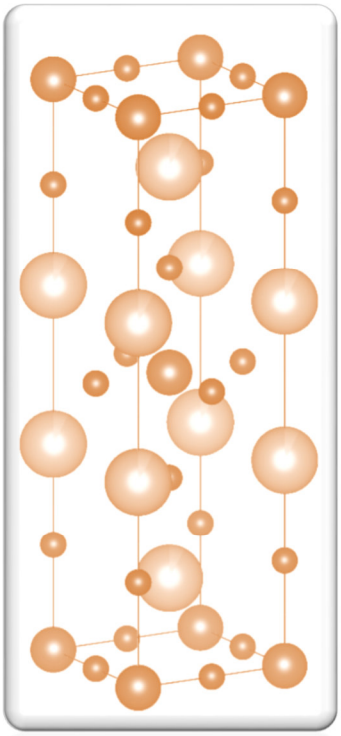

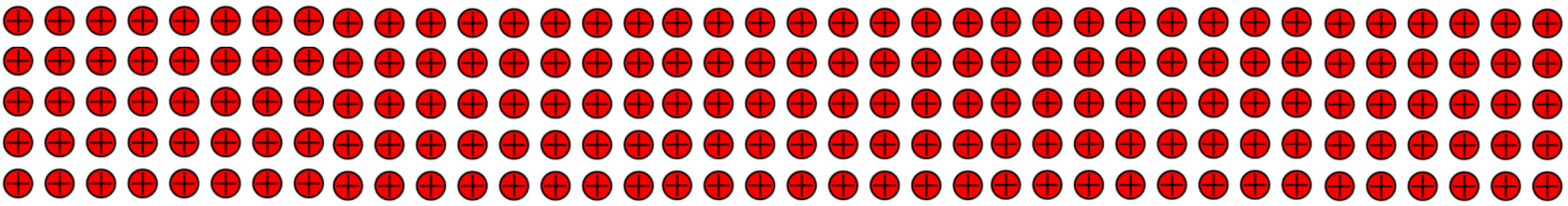

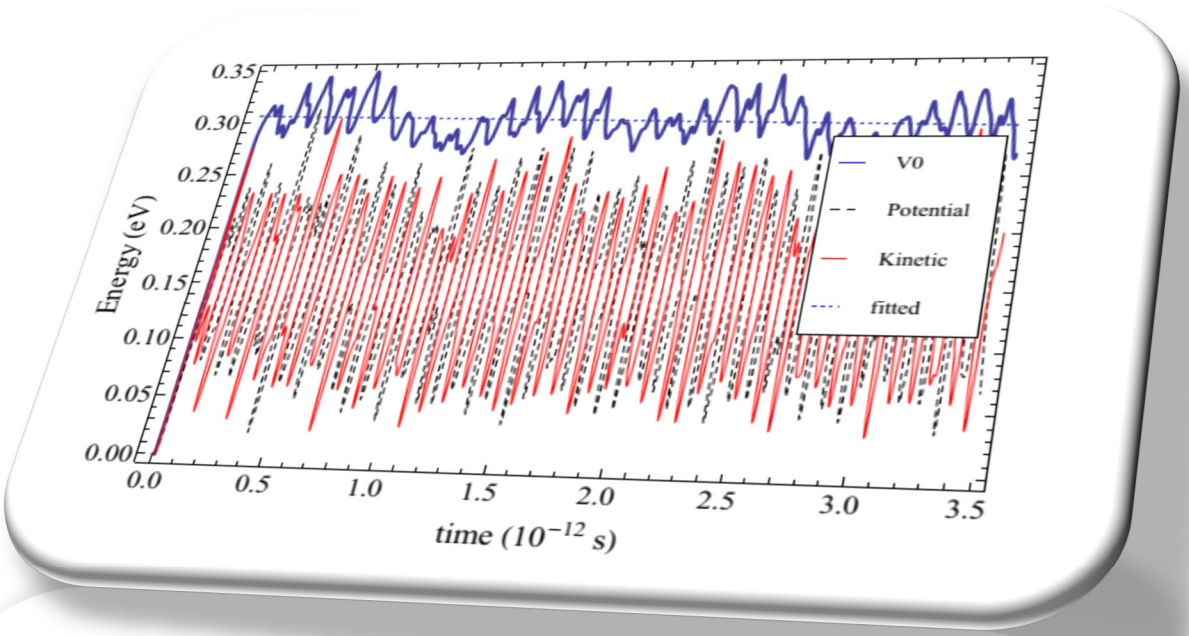
0.35
0.30
0.25
0.20
0.15
0.10
0.05
0.00
Energy (eV)
0.0
0.5
1.0
1.5
2.0
2.5
3.0
3.5
time (10^{-12} s)
V0
Potential
Kinetic
fitted